VGI

Österreichische Zeitschrift für

# Vermessung & Geoinformation

84. Jahrgang 1996 Heft 3/96

Organ der Österreichischen Gesellschaft für Vermessung und Geoinformation und der Österreichischen Geodätischen Kommission


## AUSTRIAN CONTRIBUTIONS

to the

XXI. General Assembly of the
International Union of Geodesy and Geophysics
July 2-14, 1995 in Boulder, Colorado

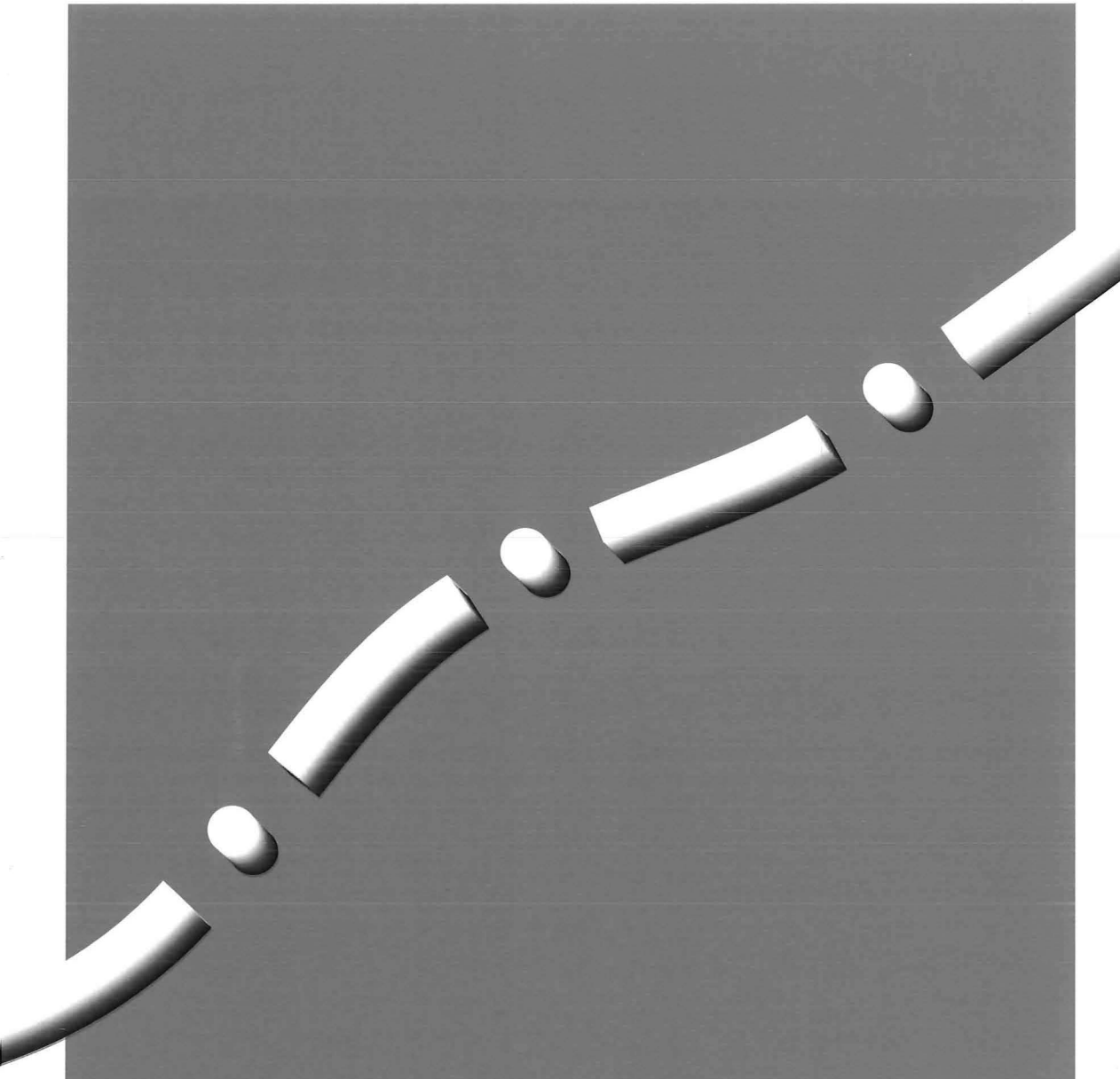

**Gruppe Landesaufnahme**
1080 Wien, Krotenthallerg. 3 Tel.: +43-1-401 46/460
Fax: +43-1-406 99 92 e-mail: rkilga@bev.gv.at

BEV

VGI

Österreichische Zeitschrift für
VERMESSUNG & GEOINFORMATION

84. Jahrgang 1996
vormals ÖZ

Heft 3/1996

**Schriftleiter:** **Dipl.-Ing. Reinhard Gissing**
**Stellvertreter:** **Dipl.-Ing. Wolfgang Gold**
**Dipl.-Ing. Bernhard Jüptner**
A-1025 Wien, Schiffamtsgasse 1–3

Organ der Österreichischen Gesellschaft für Vermessung und Geoinformation und der Österreichischen Geodätischen Kommission

**Special Issue**
**XXI. General Assembly of the International Union of Geodesy and Geophysics**
**July 2–14, 1995 in Boulder, Colorado**
**AUSTRIAN CONTRIBUTIONS**

CONTENTS



# Transponders for Altimeter Calibration and Height Transfer

*Peter Pesec, Hans Sünkel, Nadja Fachbach, Graz*

**Abstract**

Transponders receive altimeter signals and return them, after amplification, to the altimeter satellite. They provide a well-defined reflexion surface of some square-decimeters which replaces the sea surface at virtually any arbitrary point on mainland. As each radar pulse can be detected individually no averaging is required which leads to a significant increase of the precision of the measurements. Applications are manifold leading from altimeter calibration and orbit control to the determination height differences and of very accurate absolute geoid profiles along the ground track of the satellite. The report summarizes the activities of the Graz group and its future plans.

**Zusammenfassung**

Transponder empfangen Altimeter Radarpulse und senden diese verstärkt an das Satellitenaltimeter zurück. Im Gegensatz zu Anwendungen der Altimetrie über Meeresflächen ist die reflektierende Fläche von einigen Quadratdezimetern exakt definiert und der Einsatzbereich für beinahe beliebige Punkte am Festland gegeben. Nachdem jeder Radarpuls eindeutig aufgelöst werden kann, kann auf Mittelungsmethoden verzichtet und die Meßgenauigkeit erheblich gesteigert werden. Die Anwendungsbereiche sind vielfältig, sie erstrecken sich von Altimeter-Kalibrierungen über Beiträge zur Bahnbestimmung von Altimetersatelliten bis zu exakten Höhenübertragungen zwischen der Meeresoberfläche und dem Festland sowie zwischen Punkten am Festland. Aus letzteren können sehr genaue absolute Geoidprofile entlang der Bahnprojektion abgeleitet werden. Der vorliegende Beitrag faßt die bisherigen und geplanten Arbeiten der Grazer Gruppe in diesem Bereich zusammen.

## 1. Introduction

A transponder is a "simple" electronic device which receives satellite altimeter signals and returns them, after amplification, to the signal source.

Unlike the sea surface the reflecting surface is a precisely defined point target which produces, like corner reflectors in satellite laser ranging, unambigous returns. No averaging procedure of different reflection points is required, the returns detected by the altimeter satellite during the transponder's stay in the foot-print show a nice parabolic shape (slant range as a function of time). The value of the slant range at the vertex of the parabola gives the shortest distance between the satellite and the transponder, which is roughly the height of the satellite above the transponder ($\pm$ 7 mm) if the transponder is located within 100 m of the ground track.

Additional informations can be extracted which are correlated to the along track component of the satellite position. It is a straight-forward matter to measure the time of the received pulses with respect to an external time-reference (e.g. the one per second clock pulse of a GPS-receiver) with an accuracy of $\pm$ 5 microseconds. In order to identify the epoch times of the continuous pulse flow hitting the transponder some pulses are suppressed in a systematic way by switching off the transponder for definite periods (like in old optical satellite geodesy) and recording the suppressing times.

The identification of the vertex of the parabola from a large number of measurements (altimeter waveforms) significantly reduces the noise of the altimeter. Variations of the fit procedure show a very stable behaviour of the vertex (some millimetres). It can be emphasized that, currently, transponders introduce errors of below 1 cm in the range and some microseconds in the pulse-timing equivalent to about 10 to 70 cm of the satellite along-track component.

Without going into more details about the reduction of the altimeter data (see e.g. [4]) it is obvious that the determined height is not a true geometrical height but affected by ionosphere and troposphere. To reduce the measured height to a "vacuum" value the total electron content along the signal and the tropospheric zenith delay have to be estimated. As the measurement itself takes only some seconds and is confined to one single frequency, a careful monitoring of the matter between the transponder and the satellite is required in order not to water down the transponder accuracy.

## 2. Ionospheric and Tropospheric Corrections

The height of the altimeter satellite above ground (the transponder reflecting surface) is only biased by signal propagation delays and the altimeter itself.

Informations on the ionosphere are globally available (NNSS, IGS, ionosondes, geostationary satellites, seasonal models) and can be estimated for the particular transponder position by carrying out simultaneous GPS-measurements and mapping the ionospheric component (L4) of each GPS-satellite to the zenith direction. The situation is facilitated by the fact that the influence of the GPS-derived ionospheric parameters on altimeter measurements is reduced by a factor of 50 due to the different wavelengths, but complicated because GPS-derived values determine the total ionospheric delay for a distance of 20.000 km above the earth's surface [1]. The portion of the delay affecting the measurements to e.g. ERS-1/2 at a height of 700 km is difficult to estimate. In summary, we believe that ionospheric delays can be estimated with accuracies of better than $\pm$ 10 mm.

On the other hand the means to monitor the tropospheric delay are very cumbersome as in most cases the simple modelling of the troposphere via measured ground-data does not work for the wet part of the partial water vapour pressure. The employment of water vapour radiometers (WVR) combined with informations from weather baloons and distributed ground meteo-data seems to be a prerequisite for keeping the accuracy of transponder derived heights at the level of below $\pm$ 20 mm.

## 3. Possible Applications

The employment of transponders for supporting altimetry missions is obvious. The well-defined reflecting surface of the transponder allows for a pulse per pulse analysis of the reflected data as opposed to the averaging procedure applied for "diffuse" surfaces like oceans, ice, or other flat areas. It further enables the use of altimeters in areas of rough topography, virtually in any locality as long as the transponder can be situated along the satellite ground track and no other reflecting surfaces exist in the close vicinity. It operates in a quasi-passive mode, the active components being limited to the signal amplification procedure and the pre-setting of operation-windows to reduce power consumption. In this mode transponders can operate fairly unattended as long as power can be supplied; data accumulation is confined to the source as long as the timing feature is disabled.

The following scenario indicates the possible applications:

Two transponders are situated along the ground track of an altimeter satellite. Their positions are computed by GPS-methods in a global reference frame ITRF (eventually supplemented by SLR). The corrected heights of the satellite above the transponders and eventually above a nearby sea surface are measured by altimetry. The satellite orbit is determined via SLR, PRARE, GPS in the same ITRF. This system defines a closed loop where the misclosures are a measure of the sum of errors introduced by the different procedures (see Fig. 1). If this system covers only a local region some of the quantities are correlated and the errors reduced by forming differences. Dependent on which part of this closed system is examined the following applications can be seen (see also [2]):

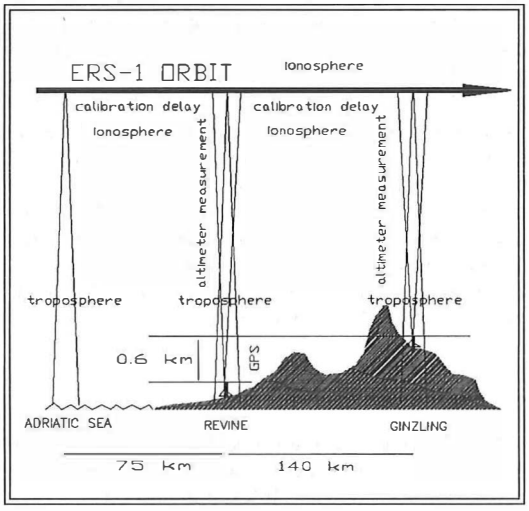


*Fig. 1: Closed self-controlling measurement system realized during the transponder campaign COMPASS II.*

### *3.1 Altimeter Calibration*

If the height of the satellite above the transponder is determined by independent means (SLR, PRARE) transponder measurements can be used for the calibration of the on-board altimeter. A transponder deployment close to a SLR site and tied to this site by GPS removes part of the orbital errors and contributes to the verification and comparison of the altimeter

range biases of ERS-1 and ERS-2 simply by comparing laser- and radar-derived distances. Costly arrangements like the "Venice Tower" are superfluous, the transponder behaves like a reference target replacing the sea surface in the gulf of Venice by a considerably more accurate reference surface.

### *3.2 Orbit Determination and Control*

The orbit of ERS-1 is currently determined by combining an accurate model of the gravitational and non-conservative forces acting on the satellite with the somewhat sparse laser ranging data provided by the world-wide network of SLR stations. This situation was improved for ERS-2 by the PRARE tracking system. Transponders tied to ITRF by GPS contribute, point by point, to orbit determination by giving estimates of the radial component (rms about $\pm$ 2 cm) and the along-track component (rms about $\pm$ 30 cm) independent of weather conditions. Although this method is relatively cost-effective it provides an independent check and assessment of the quality of the global orbital model.

### *3.3 Height Transfer*

Transponders are suitable for providing extremely precise targets for altimeter measurements in a rough topography. If the satellite orbit is precisely known, with exception of a translation, this orbit can be used to "transfer" the height of a terrestrial transponder site to another transponder site. In addition, transponders provide a link between the coastland and the mean (averaged) sea surface (playing the role of a tide-gauge for the time of the overpass). It is evident that uncertainties in the orbit play a secondary role the shorter the "transfer distance" is. Likewise, a considerable part of the atmospheric delays is cancelled, leaving the problem to model local effects. Altimeter measurements are only subject to zenith delays, the high frequency band damps ionospheric delays, they provide an independent, nearly model-free method to complement and verify GPS height determination on mainland.

### *3.4 Monitoring of Uplifts and Subsidences*

Transponders allow the automatic collection of data in unattended mode for long time periods. Although the data-rate is pretty low (10 datasets per year for a 35-days repeat orbit) it is sufficient to monitor vertical displacements, especially in perilous environment like near volcaneous or on ice caps.

### *3.5 Absolute Geoid Profiles*

All applications discussed so far are based on purely geometrical considerations (apart from orbit modelling and the definition of the sea surface). Earth physics comes into play when deploying several transponders along a ground track, combining SLR orbit determination, altimetry and orthometric height control, and comparing it with GPS + orthometric height derived geoid heights.

## 4. Experiences in Height Transfer

Based on an idea of R.J. Powell [3] two transponders (NORDA, ESTEC) were deployed along the Venice arc during the calibration phase of ERS-1 and the following month (COMPASS II) in order to demonstrate the efficiency of transponders as altimeter targets on mainland using the concept of height transfer. Utmost care was taken to monitor atmospheric conditions during the overpasses and to tie the transponder locations at Revine (Italy) and Oberböden (Austria) by GPS. Relevant details are reported in [4], a further joint report will be published this year by P. Cross, University of Newcastle upon Tyne.

Altogether five common ERS-1 overpasses could be detected, the final result for the "height-misclosures" was shown to be

$$2.8 \text{ cm} \pm 2.6 \text{ cm}$$

indicating that in spite of the various error sources the applied method leads to very satisfactory results.

In view of this promising result ISRSG Graz purchased a newly designed transponder version including the timing option for monitoring the along-track component of the satellite orbit (see Fig. 2). As a pilot project, the demonstration of the transponder technique for monitoring the height of the SHELL oil platform Brent (160 km north-east of Shetland Islands) by height transfer to Schindlet (near Zurich) was conducted using the ERS-1 overpass on Sunday, July 10, 1994 at 21.20 UT. The new Graz transponder was deployed at Schindlet. After a quick-look analysis of the altimeter data carried out by Rutherford Appleton Lab. the results for the Graz transponder suggest an uncertainty of $\pm$ 1 mm in the vertical and $\pm$ 40 cm for the along-track which confirms the expected specifications. The final results [5] show that the precision of altimeter de-

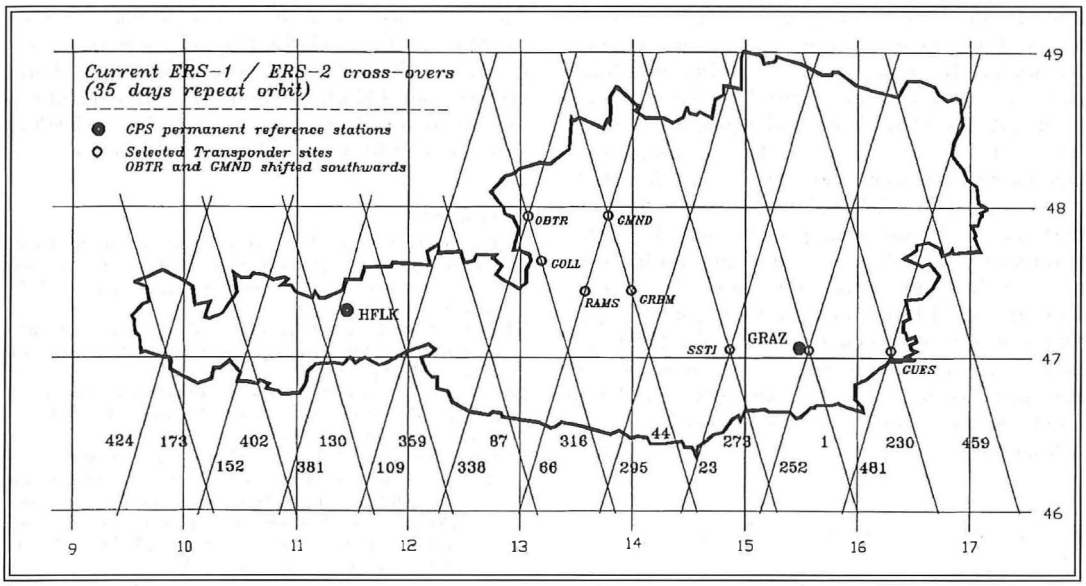


*Fig. 2: ERS-1/2 Subtracks in Austria (35 days repeat orbit)*

rived height differences is in the order of ± 3 cm, consistent with COMPASS II.

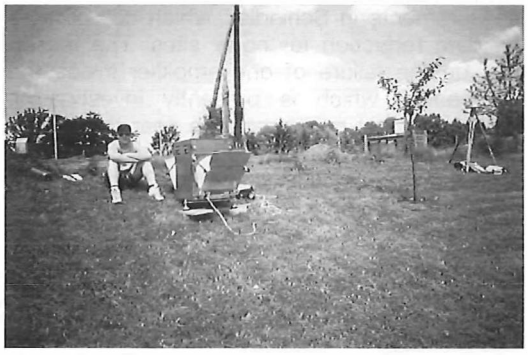

*Fig. 3: Graz Transponder deployed at LASS (near Lustbühel)*

## 5. ERS-2 Altimeter Calibration and Orbit Determination

In response to the ESA Announcement of Opportunity for ERS-1/ERS-2 a common project "The Use of Transponders with ERS-1 and ERS-2 Altimeters" was worked out by Rutherford Appleton Laboratory (Didcot, UK), Geodetic Institute of the University of Newcastle upon Tyne (UK), Royal Greenwich Observatory (Cambridge, UK), Geophysical Department of the University of Copenhagen (Denmark), and Institute for Space Research (Graz, Austria). Special emphasis was laid on the role of transponders (4 of them are presently available in Europe) for the calibration of the ERS-2 altimeter and a direct comparison with ERS-1, which are presently operating in a tandem-mode (identical 35-days repeat orbits with 1 day separation).

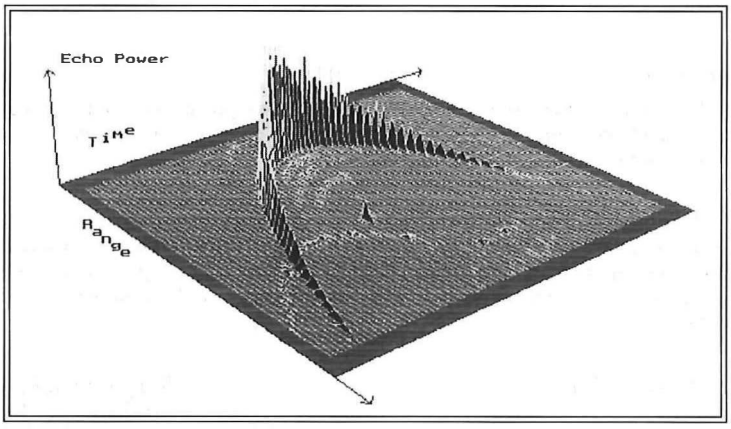


*Fig. 4: Radar altimeter returns for ERS-1 pass <26.08.1995> at Ramsau/Dachstein.*

The transponder measurements were originally planned to be carried out at five cross-over points (intersec-

tion of north- and south-going passes) displayed in Fig. 3. Two of them showed too many local reflections to be of any further use, therefore three new sites were defined along the particular subtracks. As an example the radar altimeter returns for an ERS-1 overpass at RAMS (Ramsau / Dachstein) are shown in Fig. 4. All sites were connected to the International Terrestrial Reference Frame by preceding or on-site GPS-measurements, the latter also being used for the estimate of the ionospheric corrections. Special attention is paid to the cross-over point LASS, situated in the near vicinity of the Graz laser station (7 km) for which altimeter derived heights and laser distances are highly correlated and can be used for a direct calibration of the ERS-2 altimeter.

## 6. Current Status and Future Plans

The recent measurements have shown a substantial decrease of the power of the emitted return pulses by a factor of 8 compared to the first measurements in Schindlet, which complicates the data reduction for noisy sites. The reason may be the failure of one amplifier inside the transponder which is presently investigated. After some test-measurements near the observatory Lustbühel it is planned to repeat the measurements in Austria for a further 70 days period. After that the Graz transponder will be employed, together with the Copenhagen transponder, for a dedicated mission which aims at the connection of North Sea and the Adriatic on the one hand and the connection of the individual sea surfaces to the coastland on the other.


**References:**

[1] *Leitinger R., P. Pesec:* Ionospheric Corrections for the Land-Based Altimetry Campaign. In: Proc. of Symp. on Refraction of Transatmospheric Signals in Geodesy; The Hague, Netherlands, 1992.

[2] *Pesec P., H. Sünkel, N. Windholz:* The Use of Transponders in Altimetry; In: IAG Symposia No. 113 (Gravity and Geoid), Springer Verlag, 1995.

[3] *Powell R.J:* Relative Vertical Positioning Using Ground-Level Transponders with the ERS-1 Altimeter; IEEE Trans. Geoscience and Remote Sensing, GE24, 1986.

[4] *Denys P.H., A.R. Birks, P.A. Cross, R.J. Powell:* Precise Height determination using the ERS-1 Radar Altimeter and Active ground Based Transponders, Central Europe, August-November 1991; Final report prepared for the European Space Agency, Dept. of Surveying, UNoT and RAL, Didcot. UK. Final Report Version 4.0, 1993.

[5] *Denys P.H., A.R. Birks, P.A. Cross, R.J. Powell:* The Brent Alpha Transponder Altimetry Trial North Sea - Switzerland; Report prepared for Shell UK Exploration and Production. Final report Version 3.0, 1995.



*Address of the authors:*

Dr. Peter Pesec, o. Univ.-Prof. Dipl-Ing. Dr. Hans Sünkel., Dipl.-Ing. Nadja Fachbach: Department of Satellite Geodesy, Institute for Space Research, Austrian Academy of Sciences, Lustbühelstraße 46, A-8042 Graz.


# On the Separation of Gravitation and Inertia in the Case of Free Motion


*Wenbin Shen, Helmut Moritz, Graz*



**Abstract**

The authors explored the possibility of separating gravitation from inertia in the case of free motion according to general relativity, proposed a general method of determining the relativistic gravity field of the earth, and put forward and proved two important statements.

**Zusammenfassung**

Die Verfasser untersuchten die Möglichkeit der Trennung von Gravitation und Trägheit in dem Fall der freien Bewegung gemäß der allgemeinen Relativitätstheorie. Es wurde eine allgemeine Methode zur Berechnung des relativistischen Gravitätsfeldes der Erde vorgeschlagen. Weiters wurden zwei wichtige Theoreme aufgestellt und bewiesen.


## 1. Introduction

Quite a few geodesists paid attention to relativistic effects in geodesy [2, 5, 7, 8, 12]. It is generally agreed that, if an order $10^{-8}$–$10^{-9}$ or a higher accuracy requirement is needed, the relativistic effects should be considered.

When a particle is in the state of motion in a gravitational field, it experiences some forces, which generally include gravitational andinertial forces. Some forces may be balanced by each other, and others may not. In the special case that the particle is moving freely in the gravitational field, the nature of the particle is very important. In this case, the particle will not sense any force or the forces it senses are completely balanced so that it senses a resultant zero, because of *Einstein's equivalence principle,* which states that *the gravitational mass is equivalent to the inertial mass,* and later generalized as follows: *in a closed freely falling system, one cannot find out whether the system is in the state of free fall in a gravitational field or in the state of uniform motion or at rest far away from any matter sources* [16]. Hence, generally it is believed that gravitation and inertia are not distinguishable. But this belief is correct only if one considers the force at one point only. In a finite region however, gravitation and inertia can be separated, at least in principle, because the gravitational field is essentially different from the "inertial field". Roughly speaking, the inertial field is smoother and more regular than the gravitational field, so that we can find some kind of quantity which is sensitive only to the gravitational effects. This quantity is the Riemann tensor, which has an absolute character. We can conclude that there is a gravitational field or none, according as the Riemann tensor does not vanish or vanishes. In the case of free motion, if we can find a way to determine the Riemann tensor, then we have separated gravitation from inertia, and in this sense, gravitation and inertia are absolutely distinguishable. This conclusion was first pointed out by Synge [14], and later followed a detailed study emphasizing the application in geodesy by Moritz [7]. However, unfortunately, we have not yet reached a final confirmation. The key problem is: is it possible to find the Riemann tensor in a closed local reference system, no matter what methods one applies, without exchanging signals with the external world? The answer is positive. In the following, we will explore this problem.

## 2. The Geodesic Deviation Equation

Let us choose a co-moving proper reference frame, an orthonormal tetrad, which consists of four mutually orthonormal base vectors, with the fourth vector coinciding with the unit tangent vector of the worldline (it is the geodesic in our present case). In this case, the tetrad is *parallelly transported* [6, 13, 14]. The four mutually orthornormal base vectors can be expressed as [6, 12]:

$$e_{(\alpha)} = \lambda^{\beta}_{(\alpha)} \frac{\partial}{\partial x^{\beta}} \tag{1}$$

where $\lambda^{\beta}_{(\alpha)}$ are the coefficients to be chosen. We note that, in this paper, *Einstein's summation convention* and *the light unit system* ($c \equiv 1$) are adopted; and furthermore, for Greek indices, the summation covers 0, 1, 2, 3; for Latin indices 1, 2, 3.

The orthonormality of a tetrad is given by the following condition

$$g^{\mu\nu} e_{(\alpha)\mu} e_{(\beta)\nu} = \eta_{(\alpha\beta)} \equiv \eta_{\alpha\beta} \tag{2}$$

where the index $(\alpha)$ denotes a specific vector (or tensor) and the index $\mu$ denotes the component with respect to coordinates $x^{\mu}$, $g^{\mu\nu}$ is the inverse of $g_{\mu\nu}$, which is the general metric tensor and reduces to the Minkowsky tensor $\eta_{\mu\nu} = diag(-1,1,1,1)$ if the spacetime becomes flat.

The general expression of the geodesic deviation can be written as follows [14, 15]:

$$a^{\mu} \equiv \frac{D^2 X^{\mu}}{Dt^2} = - R_{\lambda\alpha\sigma}{}^{\mu} T^{\lambda} X^{\alpha} T^{\sigma} \tag{3}$$

where $D$ is *the covariant differential operator,* $T^{\lambda}$ is *the tangent vector* to the geodesic, $X^{\mu}$ and $a^{\mu}$ denote *the diplacement vector* and the relative acceleration between two neighbouring geodesics, $R_{\lambda\alpha\sigma}{}^{\mu}$ is the Riemann tensor. Equation (3) gives the relativistic generalization of *the Newtonian tidal equation.*

With respect to the co-moving proper reference tetrad $e^{\mu}_{(\alpha)}$, the geodesic deviation equation can be expressed as [14,15]

$$\frac{d^2 X^{(\alpha)}}{dt^2} + \eta^{(\alpha\beta)} R_{(\varepsilon\rho\delta\beta)} T^{(\varepsilon)} X^{(\rho)} T^{(\delta)} = 0 \tag{4}$$

where

$$R_{(\varepsilon\rho\delta\beta)} = R_{\lambda\nu\sigma\mu} e^{\lambda}_{(\varepsilon)} e^{\nu}_{(\rho)} e^{\sigma}_{(\delta)} e^{\mu}_{(\beta)} \tag{5}$$

and

$$T^{(\lambda)} = \frac{dx^{(\lambda)}}{dt} \tag{6}$$

is the particle's 4-velocity observed in the chosen tetrad.

Equation (4) is similar to equation (3). The advantage of equation (4) is in that this equation is measurable in practice, at least partly. To confirm this conclusion, let us further investigate this equation.

## 3. The Determination of Riemannian Components

Suppose we use a gradiometer to measure the relative acceleration of two neighbouring geodesics, and let the gradiometer be at rest relative to the satellite, then, in the co-moving local reference frame, equation (4) becomes:

$$\frac{d^2X_{(0)}}{dt^2} = 0 \tag{7}$$

$$\frac{d^2X_{(i)}}{dt^2} + R_{(0j0l)}X^{(l)} = 0 \tag{8}$$

On the right hand side of equation (8), the first term is interpreted as the relative acceleration of the two proof masses and can be measured by gradiometers [1,4,6,9]. Equation (8) has the same form as the *tidal equation* expressed in the frame of Newtonian mechanics [8,9]

$$f_i = \frac{d^2\xi_i}{dt^2} = \frac{\partial^2 V}{\partial x^i \partial x^j}\,\xi^j$$

where $f_i$ is the *tidal force*, $d^2\xi_i/dt^2$ is the relative acceleration (in the sense of Newtonian mechanics) of the two proof masses, and $\xi^j$ is the distance between the two proof masses. This equation has been applied extensively in *satellite gradiometry* [5,10]. It can be shown that the equation (8) reduces to the above classical tidal equation under the Newtonian limit.

By appropriate orientations (puting the proof masses in the directions of $e_{(i)}$ respectively), we can make $R_{(0i0j)} = 0 (i \neq j)$ [6]. In this case, equation (8) becomes

$$\frac{d^2X_{(i)}}{dt^2} + R_{(0i0l)}X^{(i)} = 0 \quad \textit{(no sum over i!)} \tag{9}$$

where the relation

$$X^{(i)} = \eta^{(ij)}X_{(j)} = X_{(i)}$$

has been introduced. Hence, from (9) we can find the Riemannian components $R_{(0i0l)}$:

$$R_{(0i0l)} = -\left(\frac{d^2X_{(i)}}{dt^2}\right)/X^{(i)} \quad \textit{(no sum over i!)} \tag{10}$$

and the remaining components $R_{(0i0l)} = 0 (i \neq j)$.

To find the Riemann tensor $R_{\lambda\nu\sigma\mu}$, we should apply equation (4), from which, noticing the orthonormality of the tetrad $e^{\lambda}_{(\alpha)}$:

$$e^{\lambda}_{(\alpha)}\, e^{(\alpha)}_{\beta} = \delta^{\lambda}_{\beta} \tag{11}$$

by multiplying both sides of the equation (5) with $e^{(\xi)}_{\xi} e^{(\rho)}_{\eta} e^{(\delta)}_{\theta} e^{(\beta)}_{\tau}$, we get:

$$R_{\mu\nu\alpha\beta} = R_{(\xi\eta\rho\sigma)}\, e^{(\xi)}_{\mu} e^{(\eta)}_{\nu} e^{(\rho)}_{\alpha} e^{(\sigma)}_{\beta} \tag{12}$$

We are most interested in $R_{0i0j}$, i.e.,

$$R_{0i0j} = R_{(\xi\eta\rho\sigma)}\, e^{(\xi)}_{0} e^{(\eta)}_{i} e^{(\rho)}_{0} e^{(\sigma)}_{j} \tag{13}$$

Suppose we can choose such a tetrad $e^{(\alpha)}$, so that the $\mu$ components $e^{(\alpha)}_{\mu} = 0$, if $\alpha \neq \mu$. Then, we have

$$R_{0i0j} = R_{(0i0j)} e^{(0)}_{0} e^{(i)}_{i} e^{(0)}_{0} e^{(j)}_{j} \quad \textit{(no sum over i, j!)} \tag{14}$$

Since gradiometers have been appropriately oriented ($R_{(j0j0)} = 0$, $i \neq j$, [6]), we have

$$R_{0i0j} = 0, \textit{ if } i \neq j \tag{15}$$

$$R_{0i0i} = R_{(0i0j)} e^{(0)}_{0} e^{(i)}_{i} e^{(0)}_{0} e^{(j)}_{i} \quad \textit{(no sum over i!)} \tag{16}$$

From (10), we can see that $R_{(0i0j)}$ are the quantities measured by gradiometers which are fixed on a satellite. Then, from (15) and (16), we can find $R_{0i0j}$, which are independent of the coordinate system. In this way, the gravitational effects are separated from inertia, at least partly. We should keep in mind that, according to the equivalence principle, in a freely moving elevator (or satellite), one can not tell whetherone is in the state of free fall or the state of uniform motion or at rest, no matter what method one uses, provided one does not exchange signals with the world outside the elevator. However, by some kinds of devices (such as gradiometers), one finds that the devices can "feel" the action of the gravitation (even if in a very small region provided the device can be made as small as possible). This conclusion is very attractive and it means that in a strict sense Einstein's equivalence principle is correct only at one point. Extending to any finite region, even if very small, the equivalence principle holds no more.

Now, let us explore how to determine $R_{0i0j}$ from equation (16) or (13) in practice. In a general curved spacetime (four dimensional manifold), it is not easy to determine the base vectors of the orthonormal tetrad. However, with some kind of approximation, it becomes easier.

Let us introduce the standard PPN *coordinate induced tetrad* (at rest with respect to the coordinates) [12]:

$$e_{(t)} = \eta + \frac{\partial}{\partial t}, \quad e_{(i)} = \eta - \frac{\partial}{\partial x^i} \tag{17}$$

with

$$\eta \pm = 1 \pm \frac{GM}{r} \tag{18}$$

where $G$ is the gravitational constant and $M$ is the earth's mass. Suppose we have chosen the spherical polar coordinate grid ($t$, $r$, $\theta$, $\lambda$) with its origin at the earth's center, where $r$ is the distance between the origin and the field point, $\theta$ is the polar angle, and $\lambda$ is the longitude. The tan-

gent vectors to the coordinate lines of the coordinate grid $(t, r, \theta, \lambda)$ are respectively

$$\partial/\partial t,\ \partial/\partial r,\ \partial/\partial\theta,\ \partial/\partial\lambda$$

Although the above tetrad is orthogonal, it is not parallelly transported (in general case). In fact, it is at rest with respect to the global coordinates $(t, r, \theta, \lambda)$. At every point $P$ passed by the satellite, there exists a coordinate induced tetrad $e^{\mu}_{(\alpha)}$. However, in order to correlate the Riemann tensor with the measured quantities, we need to find the parallelly transported tetrad $e'^{\mu}_{(\alpha)}$, which is a proper reference frame of the satellite. For this purpose, we need to know the velocity of the satellite. Fortunately, in this case, the velocity is known.

Let us use $\vec{v}$ to denote the ordinary 3-velocity of the satellite observed in the geocentric star-fixed coordinate system (GSS). Then, the comoving parallelly transported tetrad $e'^{\mu}_{(\alpha)}$ can be obtained by a Lorentz transformation $\Lambda^{(\alpha)}_{(\beta)}$, i.e.,

$$e^{(\alpha)} = \Lambda^{(\alpha)}_{(\beta)} e^{(\beta)} \tag{19}$$

where

$$\begin{aligned} \Lambda^{(0)}_{(0)} &= 1 + \frac{1}{2}\upsilon^2 \\ \Lambda^{(i)}_{(0)} = \Lambda^{(0)}_{(i)} &= -\upsilon^i \equiv -\upsilon_i, \\ \Lambda^{(j)}_{(i)} &= \delta^j_i + \frac{1}{2}\upsilon^j \upsilon_i \end{aligned} \tag{20}$$

With the above tetrad, equation (12) or (13) should be used. In this case, we cannot find $R_{\mu\nu\alpha\beta}$ or $R_{0i0j}$, because only some components of $R_{(\xi\eta\rho\sigma)}$ have been measured. Hence, we need to apply an approximate method, with which the Riemann tensor can be found, and as a result the earth's gravitational field can be determined.

## 4. The Determination of the Gravitational Field

In the spacetime considered in section 3, suppose we have chosen a global spherical polar coordinate grid $(t, r, \theta, \lambda)$. In this case, at every fixed spacetime point $P$, there exists a *coordinate induced tetrad* $e^{(\alpha)}_{\mu}$ [12], which is given by expression (17).

It should be pointed out here that in general case one cannot find exact solution for determining a gravitational field. One must use anapproximate method. In our present case, if we use *the Post-Newtonian Approximation* [16], we will find that only five potential quantities need to be determined, where four of them can be calculated by a normal model (a uniform sphere) and the fifth is connected to the measured Riemannian components $R_{(0i0j)}$.

With the Post-Newtonian Approximation, the metric tensor $g_{\mu\nu}$ can be expressed as [16]

$$g_{00} = -1 - 2\phi - 2\phi^2 - 2\psi \tag{21}$$

$$g_{0j} = \zeta_j \tag{22}$$

$$g_{ij} = \delta_{ij} - 2\delta_{ij}\phi \tag{23}$$

where $\phi$, $\psi$, $\vec{\zeta}$ (which are on the orders $\upsilon^2$, $\upsilon^3$, $\upsilon^4$) are the *first Newtonian potential, second Newtonian potential,* and *vector potential,* respectively.

The Riemannian components can be expressed as follows [16]:

$$\begin{aligned} R_{0i0j} &= \phi_{ij} + 3\phi_i\phi_j + 2\phi\phi_{ij} - \delta_{ij}(\nabla\phi)^2 + \psi_{ij}, \\ R_{0ijk} &= \frac{1}{2}(\partial_i\partial_j\zeta_k - \partial_i\partial_k\zeta_j) - \partial_t(\delta_{ij}\phi_k - \delta_{ik}\phi_j), \\ R_{ijkl} &= \delta_{ik}\phi_{jl} - \delta_{il}\phi_{jk} - \delta_{jk}\phi_{il} + \delta_{jl}\phi_{ik} \end{aligned} \tag{24}$$

where $\partial_i \equiv \partial/\partial x^i$, $\partial_t \equiv \partial/\partial t$, $\phi_i \equiv \partial_i\phi$, $\phi_{ij} \equiv \partial_i\partial_j\phi$, etc.

To determine the potential $\phi$, we first establish the connection between $R_{\mu\nu\alpha\beta}$ and $R_{(\xi\eta\rho\sigma)}$. The connection between $R_{\mu\nu\alpha\beta}$ and $R_{(\xi\eta\rho\sigma)}$ can be easily established through the Lorentz transformation $\Lambda^{\mu\nu\alpha\beta}_{(\xi\eta\rho\sigma)}$:

$$R_{(\xi\eta\rho\sigma)} = \Lambda^{\mu\nu\alpha\beta}_{(\xi\eta\rho\sigma)} R_{\mu\nu\alpha\beta} \tag{25}$$

where

$$\Lambda^{\mu\nu\alpha\beta}_{(\xi\eta\rho\sigma)} \equiv \Lambda^{\mu}_{(\xi)}\Lambda^{\nu}_{(\eta)}\Lambda^{\alpha}_{(\rho)}\Lambda^{\beta}_{(\sigma)} \tag{26}$$

and $\Lambda^{\mu}_{(\xi)}$ is given by equation (20). Then, from the above two equations we have:

$$R_{(0i0j)} = R_{\mu\nu\alpha\beta}\Lambda^{\mu}_{(0)}\Lambda^{\nu}_{(i)}\Lambda^{\alpha}_{(0)}\Lambda^{\beta}_{(j)} \tag{27}$$

From (20) and (27), accurate to $\upsilon^4$, we find that the following connection holds:

$$\begin{aligned} R_{(0i0j)} = R_{0i0j}(1+\upsilon^2) - \frac{1}{2}R_{0i0k}\upsilon^k\upsilon_j \frac{1}{2} - R_{0k0j}\upsilon^k\upsilon_i \\ - R_{0ikj}\upsilon^k - R_{0jki}\upsilon^k + R_{kimj}\upsilon^k\upsilon^m \end{aligned} \tag{28}$$

If substituting (24) into (28), we find that equation (28) connects the measured quantities $R_{(0i0j)}$ with the potentials $\phi$, $\zeta_i$ and $\psi$. Obviously, it is impossible to find the potentials by using the measured quantities $R_{(0i0j)}$ at only one point. However, by using a lot of sets of quantities $R_{(0i0j)}$ (observed in one or more satellite orbits) it may be possible to determine the potentials. To confirm this conclusion, let us first consider the Newtonian limit: accurate to $\upsilon^2$. In this case, from (28) and the first equation of (24) we get

$$R_{0i0j} = R_{(0i0j)} = \phi_{ij} \tag{29}$$

Now since the components $R_{0i0j}$ have been found, we can use the conventional method [10] to determine the first Newtonian potential $\phi$. The basic idea is as follows:

Set

$$V = -\phi \tag{30}$$

in agreement with the common concept of the potential used in geodesy. Combining (29) and (30) we get

$$\partial_i\partial_j V = -R_{(0i0j)} \tag{31}$$

Suppose that in the region where the mass density $\rho$ vanishes the potential $V$ can be expressed as a *spherical harmonic expansion* [10]:

$$V = C + C_i x^i + \frac{GM}{R}\sum_{n=0}^{N}\sum_{m=0}^{n}\sum_{\alpha=0}^{1} C_{nm\alpha}\left(\frac{R}{r}\right)^{n+1} Y_{nm\alpha}(P) \tag{32}$$

where $C$ and $C_i$ are constants to be determined (if only considering the earth's potential, $C$ and $C_i$ are equal to zero), $C_{nm\alpha}$ are unknown potential coefficients to be determined, $N$ is a large enough possitive integer (depending on the accuracy required), and

$$\begin{aligned} Y_{nm0}(P) &= P_{nm}(\cos\theta)\cos(m\lambda), \\ Y_{nm1}(P) &= P_{nm}(\cos\theta)\sin(m\lambda) \end{aligned} \tag{33}$$

are fully normalized spherical harmonics of degree $n$ and order $m$.

Substituting equation (32) into (31) we get

$$\frac{GM}{R}\sum_{n=0}^{N}\sum_{m=0}^{n}\sum_{\alpha=0}^{1} C_{nm\alpha}\partial_i\partial_j\left[\left(\frac{R}{r}\right)^{n+1} Y_{nm\alpha}(P)\right] = -R_{(0i0j)} \tag{34}$$

Note that point $P$ is on the trajectory (orbit) of the satellite. With equation (34), in principle, the coefficients $C_{nm\alpha}$ can be determined, provided sufficiently many sets of the Riemannian components $R_{0i0j}$ are observed. (For practical reasons, greater and well determined coefficients, corresponding to a reference gravity field, should be taken out first.)

Suppose we have determined all the coefficients $C_{nm\alpha}$ from equation (34), then, from equation (32) we know that the potential $V$ has been determined up to four constants $C$ and $C_i$. These four constants cannot be determined by the Riemannian components $R_{0i0j}$. However, in the case of determining the gravity field of the earth, we require that the potential $V$ approaches zero with $P$ tending to *infinity;* then, $C = C_i = 0$. In this sense, the potential $V$ is completely determined [10].

Now we aim at the accuracy of $v^4$. From (28) and (24) we get:

$$V_{ij} \equiv -\phi_{ij} = -R_{(0i0j)} + Q_{ij} \tag{35}$$

where

$$\begin{aligned} Q_{ij} = \{&[3U_iU_j + 2UU_{ij} - \delta_{ij}(\nabla U)^2 + \psi_{ij}] \\ &-[2U_{ij}v^2 - \frac{3}{2}U_{ik}v^k v_j - \frac{3}{2}U_{kj}v^k v_i + \delta_{ij}U_{km}v^k v^m] \\ &+[\partial_i\partial_j\zeta_k - \frac{1}{2}\partial_i\partial_k\zeta_j - \frac{1}{2}\partial_j\partial_k\zeta_i]\} \end{aligned} \tag{36}$$

$U$ (the normal spherical potential) as well as $\zeta_i$ and $\psi$ are calculated by a normal spherical model [11]. In this sense, $V_{ij}$ have been determined as the measured quantities.

Substituting equation (32) into (35), we get a relativistic model of satellite gradiometry (accurate to the order of $v^4$)

$$\frac{GM}{R}\sum_{n=0}^{N}\sum_{m=0}^{n}\sum_{\alpha=0}^{1} C_{nm\alpha}\partial_i\partial_j\left[\left(\frac{R}{r}\right)^{n+1} Y_{nm\alpha}\right] = -R_{(0i0j)} + Q_{ij} \tag{37}$$

which is a generalization of the Newtonian model (34).

## 5. Proofs of Two Statements

Now, we put forward the following two statements:

1. *In the case of using gradiometers on a satellite, with some kind of approximation, the Riemann tensor $R_{\mu\nu\alpha\beta}$ can be found.*
2. *In the case of free motion, if the measured Riemannian components $R_{(0k0l)}$ are always equal to zero, then, accurate to $v^2$, the whole Riemann tensor $R_{\mu\nu\alpha\beta}$ equals zero.*

Let us first prove the second statement. Suppose

$$R_{(0k0l)} = 0 \tag{38}$$

From (34) and (38), the potential coefficients $C_{nm\alpha}$ must be equal to zero:

$$C_{nm\alpha} = 0 \tag{39}$$

Then, from equation (32) we have

$$V = C + C_i x^i$$

This potential denotes a global uniform gravitational field. However, in reality, no global uniform gravitational field exists; hence we have

$$V = C$$

or without loss of generality, we choose $C = 0$, i.e.

$$\phi = -V = 0 \tag{40}$$

This equation means that there exists no mass sources in our spacetime. Consequently we have

$$\phi = 0,\ \vec{\zeta} = 0,\ \psi = 0 \tag{41}$$

In this case, we can choose a global coordinate system in which the metric tensor is the Minkowsky metric $\eta_{\mu\nu} = diag(-1,1,1,1)$. In this coordinate system, the Riemann tensor $R\mu\nu\alpha\beta$ is equal to zero:

$$R_{\mu\nu\alpha\beta} = 0 \tag{42}$$

Since any tensor is invariant under coordinate transformations, the above equation holds in any coordinates, i.e., the Riemann tensor $R_{\mu\nu\alpha\beta}$ is always equal to zero. This completes the proof of the second statement.

To prove the first statement, we need only to prove that the metric tensor $g_{\mu\nu}$ can be determined with the aid of the Post-Newtonian Approximation. In fact, we have shown (see section 4) that the first Newtonian potential $\phi$ can be determined provided that as many sets of the Riemannian components $R_{(0k0l)}$ as possible are observed. As a result. equations (21), (22) and (23) tell us that the metric tensor $g_{\mu\nu}$ can be determined. Once $g_{\mu\nu}$ is determined, $R_{\mu\nu\alpha\beta}$ is also determined. This completes the proof.

## 6. Discussion

In principle, the relativistic gravity field can be determined strictly by satellite gradiometry. The method is very general. First, we determine $\phi$, $\psi$ and $\zeta_i$ by measuring as many sets of the components $R_{(0k0l)}$ as possible. Now $\phi$, $\psi$ and $\zeta_i$ are connected with $R_{\mu\nu\alpha\beta}$ by equation (24) and $R_{\mu\nu\alpha\beta}$ is connected with $R_{(0k0l)}$ through Lorentz transformations; hence $\phi$, $\psi$ and $\zeta_i$ (using spherical harmonic expansion forms) are connected with $R_{(0k0l)}$. In this way, $\phi$, $\psi$ and $\zeta_i$ can be determined and consequently $g_{\mu\nu}$ can be found by equations (21), (22) and (23). Once the metric tensor $g_{\mu\nu}$ is determined, as a result the (relativistic) gravitational field expressed in the geocentric star-fixed system (GSS) is determined. This field, in essence, is just the gravity field expressed in the geocentric earth-fixed system (GES). To transform the expression from GSS to GES is straightforward.

**Acknowledgment**

This research program is supported by ÖAD Foundation.

**References**

[1] *Bell C. C., Forward R. L., Williams H. P.* (1970), Simulated Terrain apping with the Rotating Gravity Gradiometer, in Advances in Dynamic Gravimetry. Instrument Society of America, Pittsburgh, pp. 115–129.

[2] *Bjerhammar A.* (1985), On a Relativistic Geodesy. Bull. Geod., V.59, pp. 207–220.

[3] *Fock V.* (1961), The Theory of Space, Time, and Gravitation (N.Kemmer tran. from the Russian publ. 1955). Bergamon Press (2nd rev. ed 1966, repr. 1969, 1976).

[4] *Forward R. L.* (1972), Geodesy with Orbiting Gravity Gradiometers, in The Use of Artificial Satellite for Geodesy. Geophysical Monograph, V.15, pp. 239–243 (American Geophysical Union).

[5] *Koop R.* (1993), Global Gravity Field Modelling Using Satellite Gravity Gradiometry. Netherland Geodesic Commission, Number 38.

[6] *Misner C. W., Thorne K. S., Wheeler J. A.* (1973), Gravitation. W.H. Freeman and Company, San Francisco.

[7] *Moritz H.* (1968), Kinematical Geodesy. Publications of the German Geodesic Commission, Reihe A: Höhere Geodäsie–Heft Nr. 59.

[8] *Moritz H., Hofmann-Wellenhof B.* (1993), Geometry, Relativity, Geodesy. Wichmann, Karlsruhe.

[9] *Ohanian H. C.* (1976), Gravitation and Spacetime. W.W. Norton and Company, Inc.

[10] *Rummel R., Colombo O. L.* (1985), Gravity Field Determination from Satellite Gradiometry. Bull. Geod., V. 59, pp. 233–246.

[11] *Shen W., Moritz H.* (1996), The Separation of Gravitation and Inertia in Airborne Gradiometry. Boll. Geod. Sci. Affini, V.54, N.2 (accepted).

[12] *Soffel M. H.* (1989), Relativity in Astrometry, Celestial Mechanics and Geodesy. Springer-Verlag, Berlin.

[13] *Stephani H.* (1982), General Relativity: An introduction to the theory of the gravitational field. Cambridge University Press, Cambridge.

[14] *Synge J. L.* (1960), Relativity: The General Theory. North-Holland Publishing Company, Amsterdam (fourth printing 1971).12

[15] *Wald R. M.* (1984), General Relativity. The University of Chicago Press, Chicago.

[16] *Weinberg S.* (1972), Gravitation and Cosmology. John Wiley & Sons, New York.

*Address of the authors:*

Wenbin Shen, Univ.Prof. Dr. Helmut Moritz, Graz University of Technology, Section of Physical Geodesy, Steyrergasse 30, A-8010 Graz, Austria


# Radially Symmetric Zero-Potential Densities for the Solution of Gravitational Inverse Problems

*Sylvia Krappmann, Helmut Moritz, Graz*

**Abstract**

There are infinitely many density distributions that are compatible with a given external potential *(gravitational inverse problem).* This non-uniqueness is best expressed by the possibility to add arbitrary *zero-potential densities* which change the mass distribution without affecting the external potential. The present paper investigates special *radially symmetric* zero-potential densities, which can be used as some kind of *spline functions* for approximating more general zero-potential densities.

**Zusammenfassung**

Ein gegebenes Außenraumpotential kann durch unendlich viele Dichteverteilungen erzeugt werden *(inverses gravimetrisches Problem).* Diese Mehrdeudigkeit wird am besten dadurch ausgedrückt, daß man beliebige *Nullpotentialdichten* addieren kann, die zwar die Massenverteilung verändern, aber keine Wirkung auf das Außenraumpotential ausüben. Im vorliegenden Artikel werden spezielle *radialsymmetrischen* Nullpotentialdichtenuntersucht, die für die Approximation allgemeinerer Nullpotentialdichten als eine Art *Spline-Funktionen* verwendet werden können.

## 1. Introduction

The gravitational potential $V$ of a body is given by the well-known Newton integral

$$V(P) = G \iiint_v \frac{\rho(Q)}{l_{PQ}} dv_Q, \qquad (1)$$

where $P$ denotes the point at which $V$ is to be computed and $Q$ is the variable integration point to which the density $\rho$ and the volume element $v$ refer; $l_{PQ}$ is the distance between $P$ and $Q$; the gravitational constant is denoted by $G$ as usual.

It is an essential point that the potential $V$ is *linear* in the density $\rho$, cf. [4]. Thus we can write

$$V = N\,\rho, \qquad (2)$$

where $N$ defined by the integral (1) denotes the linear *Newtonian operator.* If the external potential $V$ is given, we solve the *gravitational inverse problem* by inverting (2)

$$\rho = N^{-1}\,V, \qquad (3)$$

which provides us an opportunity to determine the unknown density $\rho$. But the operator $N^{-1}$ is a nonunique quantity and this is the reason why (3) has infinitely many solutions for the density $\rho$.

The general solution of the inhomogeneous equation (2) is obtained as the sum of the *uniquely defined harmonic density* $\rho_H$, which satisfy Laplace's equation $\Delta\rho_H = 0$, and *the set of zero-potential densities* $\rho_0$, cf. [4],

$$\rho = \rho_H + \rho_0. \qquad (4)$$

The set of zero-potential densities $\rho_0$ comprises all density distributions within the surface $S$ which produces zero external potential

$$N\,\rho_0 = V_0 = 0. \qquad (5)$$

The result of (5) is nonunique. Thus the ambiguity of the general solution (4) is expressed by the set of possible zero-potential densities $\rho_0$. The condition of zero external potential is the absence of gravitational attraction outside the body and this will only be satisfied if the *total mass of the body is zero.* Therefore the densities $\rho_0$ must be alternatively positive and negative. But physically there are no negative densities, so the "densities" $\rho_0$ represent *density anomalies* and the potentials $V_0$ are the corresponding *potential anomalies.*

In the following sections we shall examine special *radially symmetric* zero-potential densities. We suppose that the boundary surface $S$ of the body is a sphere. In many cases the sphere represents a sufficient approximation to the earth as far as *potential anomalies* are concerned.

## 2. Radially Symmetric Zero-Potential Densities

As a preparation for the approximation of more general zero-potential densities, let us expand a *radially symmetric* zero-potential density function

$\rho_0(\bar{r})$ into a normalized (division of $\bar{r}$ by $R$) polynomial which is restricted to even powers, cf. [2],

$$\rho_0(\bar{r}) = \sum_{k=0}^{N} a_k \left(\frac{\bar{r}}{R}\right)^{2k}, \qquad (6)$$

where $a_k$ denote constant coefficients. Now the following question arises: What condition must the constant coefficients $a_k$ satisfy to produce zero-potential densities $\rho_0$? The condition for zero-potential densities is that the *total mass* of the body becomes zero. Therefore the linear dependence of the constant coefficients ($a_0$, $a_1$,..., $a_N$) can be derived as follows.

The total mass $M$ of a sphere, cf. [4], which has to be zero in this case, can be determined by

$$M = 4\pi \int_{\bar{r}=0}^{R} \rho_0(\bar{r})\bar{r}^2 \, d\bar{r} = 0. \qquad (7)$$

Replacing $\rho_0(\bar{r})$ by the definition (6), the solution of (7) gives the general condition of the constant coefficients ($a_0$, $a_1$,..., $a_N$) of $\rho_0$:

$$\sum_{k=0}^{N} \frac{a_k}{2k+3} = 0, \qquad (8)$$

to be satisfied by zero-potential densities (6).

To determine an explicit solution for zero-potential densities, we extend the polynomial (6) to sixth-order, which means $N = 3$. Setting $a_0 = a$, $a_1 = b$, $a_2 = c$ and $a_3 = d$, we obtain for the unit sphere ($R = 1$) by (6)

$$\rho_0(\bar{r}) = a + b\bar{r}^2 + c\bar{r}^4 + d\bar{r}^6. \qquad (9)$$

As we have seen above, the constant coefficients ($a$, $b$, $c$, $d$) must satisfy the necessary condition of zero-potential density (8). Besides we require that the function (9), together with its first derivative, must be zero at the boundary. In addition we normalize $a = 1$. Taking all these conditions into account, we finally get *one* of the infinitely many zero-potential density distributions as

$$\rho_0(\bar{r}) = 1 - 5\bar{r}^2 + 7\bar{r}^4 - 3\bar{r}^6. \qquad (10)$$

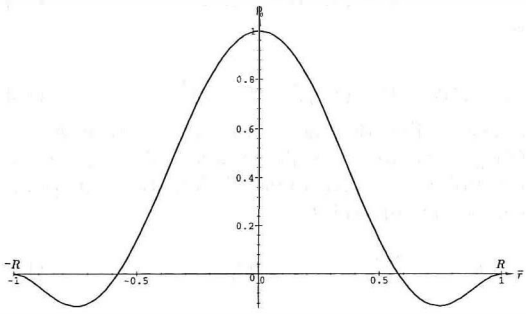


*Fig. 1: A zero-potential density function $\rho_0(\bar{r})$ for one dimension*

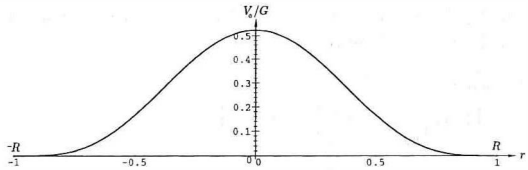


*Fig. 2: The zero-potential distribution $V_0(\bar{r})/G$ corresponding to Fig.1*

Figure 1 shows the zero-potential density distribution (10), for one dimension. As we can see in this figure, the function $\rho_0(\bar{r})$ has positive and negative values and is continuous and differentiable everywhere (also on the surface $S$). The next figure, Fig. 2, illustrates the corresponding zero-potential distribution (divided by the gravitational constant $G$). The potential inside the sphere is determined by the well-known Lauricella's second theorem, cf. [4] and [2].

## 3. Zero-Potential Splines

Now we try to approximate arbitrary zero-potential density distributions $\rho_0$ by a linear combination of *zero-potential splines,* in analogy to the approximation of potentials by discrete point masses.

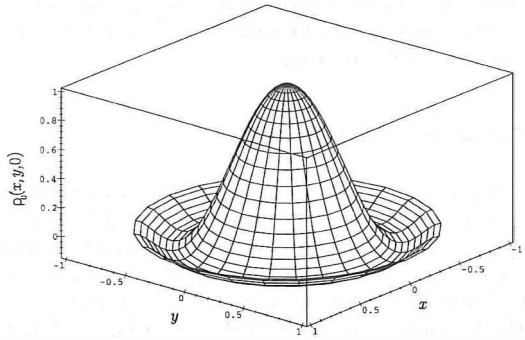


*Fig.3: The spline function $s(\bar{r}_i, R)$ for two dimensions: $R = 1$*

*Zero-potential splines* are defined in the following way, cf. [2]. Assume that there are $N$ spheres of the same radius $R$ = *const.*, of centres $M_i$ ($1 \leq i \leq N$), and of radially symmetric zero-potential density distributions $\rho_0(\bar{r}_i, R)$ according to (10), see also Fig. 3,

$$\rho_0(\bar{r}_i, R) = 1 - 5\left(\frac{\bar{r}_i}{R}\right)^2 + 7\left(\frac{\bar{r}_i}{R}\right)^4 - 3\left(\frac{\bar{r}_i}{R}\right)^6 \qquad (11)$$

where $\bar{r}_i$ *is the distance from the centre* $M_i$ to point $Q$ at which the density should be determined. But also any multiple of this function gives a possible solution. Thus we introduce a

"weight factor" $\alpha_i$ which can be prescribed rather arbitrarily and gives us

$$\rho_{0,i}(\bar{r}_i, R) = \alpha_i\, s(\bar{r}_i, R) = \\ = \alpha_i \left[1-5\left(\frac{\bar{r}_i}{R}\right)^2+7\left(\frac{\bar{r}_i}{R}\right)^4-3\left(\frac{\bar{r}_i}{R}\right)^6\right]. \quad (12)$$

The function $s(\bar{r}_i, R)$ is called *zero-potential spline,* since it has the character of a spline function in the following sense. It is a *finite function* which means that its support is finite. The support of a function is the region in which the function is different from zero. Obviously, in our case the support of the spline function is a sphere of radius $R$.

Now we want to know the density $\rho_0$ at an arbitrary point $Q$. For this purpose we approximate the unknown density $\rho_0\,(Q)$ by a linear combination of the given splines:

$$\rho_0\,(Q) = \sum_{i=1}^{N} \alpha_i\, s(\bar{r}_i, R). \quad (13)$$

The summation takes all $N$ splines $s(\bar{r}_i, R)$ into account, but note: If $\bar{r}_i > R$), the value of the spline is zero, which means no effect of the corresponding spline exists. Only if $0 \le \bar{r}_i \le R$) is satisfied, the corresponding spline is used for the approximation of the unknown density $\rho_0$ at the special point $Q$, but this depends on the geometric situation. In the following sections different simple models will be investigated in three-dimensional space, in order to get a first understanding of the method.

## 4. Models with 27 Spheres

Let us put $N$ spheres (centres $M_{ijk}$, radius $R$) in a cube of length $L$. Place the centres $M_{ijk}$ of the spheres at the nodes of a cubical grid inside the cube. The mesh width of the grid is denoted by $h$, being the same in each direction of the axes. The configuration of the nodes $M_{ijk}$ of the cubical grid should be symmetric with respect to the origin $O$ (centre of the cube ($L$)). Symmetric with respect to the origin $O$ means that each point $M_{ijk}$ has an opposite point in the direction of the origin $O$, which is the centre of the distance between such a pair of points. Therefore the centre of the cubical grid must be the origin $O$. Further the outer spheres should touch the boundary of the cube ($L$), see also Figure 4 and 6.

So the basic configuration has been fixed, but we can still choose the number of the spheres $N = n^3$ ($n$ = positive integer), the radius $R$ which is the same for all spheres, and the mesh width $h$ of the centres $M_{ijk}$ of the spheres. Since the outer spheres should touch the boundary of the cube, the length $L$ of the cube can be determined by

$$L = 2R + nh. \quad (14)$$

Remark: In this paper the name of a vector (small letter) and of a matrix (capital letter) is written in boldface, and a three-dimensional tensor is represented by an *underlined* boldface letter.

Now let us consider an example for $n = 3$. In this case we get $N = 3 \times 3 \times 3 = 27$ spheres of constant radii $R$. The distance $h$ can be prescribed arbitrarily. Different distances $h$ give different lengths $L$ of the cube (14).

To get more symmetry, let the indices $i$ ($x$-direction), $j$ ($y$-direction), and $k$ ($z$-direction) run from –1 to 1. Consider the following tensor $\underline{\mathbf{M}}$ with ist centre-elements $M_{ijk}$

$$\underline{\mathbf{M}} = \left[\begin{bmatrix} M_{-1,-1,1} & M_{-1,0,1} & M_{-1,1,1} \\ M_{0,-1,1} & M_{0,0,1} & M_{0,1,1} \\ M_{1,-1,1} & M_{1,0,1} & M_{1,1,1} \end{bmatrix} \begin{bmatrix} M_{-1,-1,0} & M_{-1,0,0} & M_{-1,1,0} \\ M_{0,-1,0} & M_{0,0,0} & M_{0,1,0} \\ M_{1,-1,0} & M_{1,0,0} & M_{1,1,0} \end{bmatrix} \begin{bmatrix} M_{-1,-1,-1} & M_{-1,0,-1} & M_{-1,1,-1} \\ M_{0,-1,-1} & M_{0,0,-1} & M_{0,1,-1} \\ M_{1,-1,-1} & M_{1,0,-1} & M_{1,1,-1} \end{bmatrix}\right] \quad (15)$$

Comparing (15) with Fig. 4, we see that the tensor reflects the geometrical situation of the centres $M_{ijk}$. Index $k$ is equivalent to the number of the corresponding plane.

Now, at any centre there is a corresponding spline function $s(\bar{r}_{ijk}, R)$. Since $R$ is constant, we can write

$$s(\bar{r}_{ijk}, R) = s(\bar{r}_{ijk}) = s(M_{ijk}, Q) = s_{ijk}(Q), \quad (16)$$

which is defined by analogy to (11) as

$$s_{ijk}\,(Q) = \begin{cases} 1-5\left(\dfrac{\bar{r}_{ijk}}{R}\right)^2+7\left(\dfrac{\bar{r}_{ijk}}{R}\right)^4-3\left(\dfrac{\bar{r}_{ijk}}{R}\right)^6 \\ \\ 0 \text{ on and outside } S \end{cases} \quad (17)$$

where

$$\bar{r}_{ijk} = \sqrt{(x-\bar{x}_i)^2 + (y-\bar{y}_j)^2 + (z-\bar{z}_k)^2} \quad (18)$$

denotes the distance from the centre $M_{ijk} = M(\bar{x}_i, \bar{y}_j, \bar{z}_k)$ to an arbitrary point $Q(x, y, z)$. Then the unknown zero-potential density $\rho_0$ at point $Q(x, y, z)$ is given by

$$\rho_0(Q) = \sum_{k=-1}^{1} \sum_{j=-1}^{1} \sum_{i=-1}^{1} \alpha_{ijk}\, s_{ijk}(Q), \quad (19)$$

a superposition of spline functions $s_{ijk}$ with different scales $\alpha_{ijk}$, according to (13).

Originally we have 27 $\alpha_{ijk}$, which can be chosen arbitrarily. On the other hand they can be determined by prescribing definite values of $\rho_0$ at data points $Q_{ijk}$. We thus assume our zero-potential densities to be the result of the superposition of splines given at special points $Q_{ijk}$. Then the following question arises: Which coefficients $\alpha_{ijk}$ produce the given values at $Q_{ijk}$?

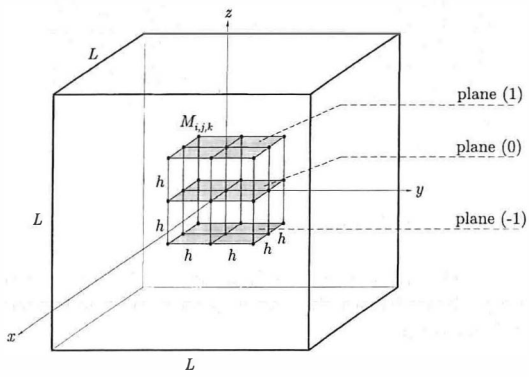


*Fig. 4: Positions of the centres $M_{ijk}$ of the spheres (R) inside the cube (L)*

Generally we need values at 27 points $Q_{ijk}$ to determine the 27 unknown $\alpha_{ijk}$. Let these values be summarized in vectors **l** and **a**

$$\mathbf{l} = \begin{pmatrix} \rho_0(Q_{-1,-1,-1}) \\ \rho_0(Q_{-1,-1,0}) \\ \vdots \\ \rho_0(Q_{1,1,1}) \end{pmatrix} \qquad \mathbf{a} = \begin{pmatrix} \alpha_{-1,-1,-1} \\ \alpha_{-1,-1,0} \\ \vdots \\ \alpha_{1,1,1} \end{pmatrix}.$$

Note that the indices of the points $Q_{ijk}$ do not refer to the positions of these points, since $Q_{ijk}$ can lie almost everywhere inside the cube (L), but the indices refer to the centres $M_{ijk}$ of the splines in the sense that we need a value $\rho_0$ at a point $Q_{ijk}$ for each unknown $\alpha_{ijk}$ of the corresponding sphere centered at $M_{ijk}$. According to (19), we obtain

$$\mathbf{l}^T = \mathbf{a}^T \mathbf{B}, \tag{20}$$

where the matrix **B** ($27 \times 27$) consists of the spline elements $s_{ijk}$ ($Q_{ijk}$). Note that the coefficient vector **a** is constant whereas the spline function matrix **B** depends on the variable points $Q_{ijk}(x, y, z)$, see (17) and (18). Thus the coefficients $\alpha_{ijk}$ can be determined by inversion of matrix **B**

$$\mathbf{a}^T = \mathbf{l}^T \mathbf{B}^{-1}. \tag{21}$$

In order to understand a method, it is frequently useful to *apply it to a very simple but very extreme case.* Therefore let us introduce some simplifications. Firstly, assume that the result of the superposition is symmetric with respect to the origin O, and the data points $Q_{ijk}$ should correspond to nodes of a cubical grid in the middle of the cube (L). The mesh width is denoted by $\bar{h}$ ($0 < \bar{h} < L/2$) being the same in each direction of the axes.

Considering the 27-point cube of length $2\bar{h}$, we notice that the points can be divided into 4 kinds (0,...,3) on the basis of the 4 different kinds of diagonals regarding the origin O (Fig. 5). Each point of *one* kind has the same distance to the origin O whereas points of *different* kinds belong to different kinds of diagonals regarding the origin O. Taking *one* point of *each* kind, i.g.

$$\tilde{Q}_0 = Q_{0,0,0}(0,0,0) \quad \tilde{Q}_2 = Q_{0,1,1}(0, \bar{h}, \bar{h})$$
$$\tilde{Q}_1 = Q_{0,0,1}(0,0,\bar{h}) \quad \tilde{Q}_3 = Q_{1,1,1}(\bar{h}, \bar{h}, \bar{h}) \tag{22}$$

we obtain 4 points $\tilde{Q}_m \in Q_{ijk}$ ($m = 0,...,3$).

Secondly, we assume that *the values at the points of one kind $\tilde{Q}_m$ are the same.* Then we obtain a result of zero-potential density distribution, which is completely symmetric with respect to the origin O. But further this means that also the data $\alpha_{ijk}$ have to be symmetric with respect to the origin O.

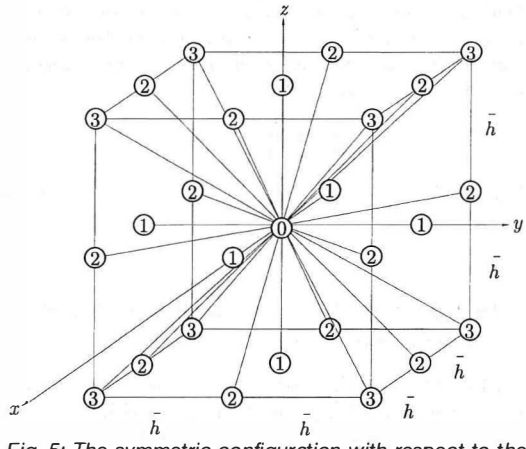


*Fig. 5: The symmetric configuration with respect to the origin O*

In this sense we have only 4 different unknown coefficients ($\tilde{\alpha}_0$, $\tilde{\alpha}_1$, $\tilde{\alpha}_2$, $\tilde{\alpha}_3$) according to Fig. 5. The coefficient $\tilde{\alpha}_0$ occurs once, $\tilde{\alpha}_1$ 6 times, $\tilde{\alpha}_2$ 12 times and $\tilde{\alpha}_3$ 8 times. For better understanding see the following symmetric tensor $\underline{\mathbf{A}}$:

$$\underline{\mathbf{A}} = [\alpha_{ijk}] = \left[ \begin{bmatrix} \tilde{\alpha}_3 & \tilde{\alpha}_2 & \tilde{\alpha}_3 \\ \tilde{\alpha}_2 & \tilde{\alpha}_1 & \tilde{\alpha}_2 \\ \tilde{\alpha}_3 & \tilde{\alpha}_2 & \tilde{\alpha}_3 \end{bmatrix} \begin{bmatrix} \tilde{\alpha}_2 & \tilde{\alpha}_1 & \tilde{\alpha}_2 \\ \tilde{\alpha}_1 & \tilde{\alpha}_0 & \tilde{\alpha}_1 \\ \tilde{\alpha}_2 & \tilde{\alpha}_1 & \tilde{\alpha}_2 \end{bmatrix} \begin{bmatrix} \tilde{\alpha}_3 & \tilde{\alpha}_2 & \tilde{\alpha}_3 \\ \tilde{\alpha}_2 & \tilde{\alpha}_1 & \tilde{\alpha}_2 \\ \tilde{\alpha}_3 & \tilde{\alpha}_2 & \tilde{\alpha}_3 \end{bmatrix} \right] . \quad (23)$$

Taking the symmetric situation into account, we also need only values summarized in vector $\tilde{\mathbf{l}}$ at *one* point of *each* kind to determine these 4 different coefficients of vector $\tilde{\mathbf{a}}$

$$\tilde{\mathbf{l}} = \begin{pmatrix} \rho_0(\tilde{Q}_0) \\ \rho_0(\tilde{Q}_1) \\ \rho_0(\tilde{Q}_2) \\ \rho_0(\tilde{Q}_3) \end{pmatrix} \in \mathbf{l} \qquad \tilde{\mathbf{a}} = \begin{pmatrix} \tilde{\alpha}_0 \\ \tilde{\alpha}_1 \\ \tilde{\alpha}_2 \\ \tilde{\alpha}_3 \end{pmatrix} \in \mathbf{a}.$$

By analogy to (20) we get

$$\tilde{\mathbf{l}}^T = \tilde{\mathbf{a}}^T \tilde{\mathbf{B}}. \quad (24)$$

Thus $\tilde{\mathbf{a}}$ is obtained by inversion of $\tilde{\mathbf{B}}$

$$\tilde{\mathbf{a}}^T = \tilde{\mathbf{l}}^T \tilde{\mathbf{B}}^{-1} \quad . (25)$$

and the 4 coefficients ($\tilde{\alpha}_0$, $\tilde{\alpha}_1$, $\tilde{\alpha}_2$, $\tilde{\alpha}_3$) of $\tilde{\mathbf{a}}$ can be substituted into (23).

At the next stage we put the above assumptions in concrete form. The 27 points $Q_{ijk}$ should correspond to the 27 centres $M_{ijk}$ of the spline functions and *all values at these points should be the same,* namely 1:

$$Q_{ijk} = Mijk \qquad \mathbf{l} = \begin{pmatrix} 1 \\ 1 \\ \vdots \\ 1 \end{pmatrix} . \quad (26)$$

Thus we have the same situation as described above only with $\tilde{h} = h$.

Models with different mesh widths $h$ are investigated in [2]. Using small mesh widths, a very surprising result appears which will be described now.

For the following concrete calculation we introduce the unit sphere ($R$ = 1). In order to illustrate the zero-potential density distribution inside the cube ($L$) graphically we cut the cube by the plane $z$ = 0. The point $Q$ varies all over this plane inside the cube. Let the mesh width $h$ be $R/4$. The geometrical situation is seen in Fig. 6.

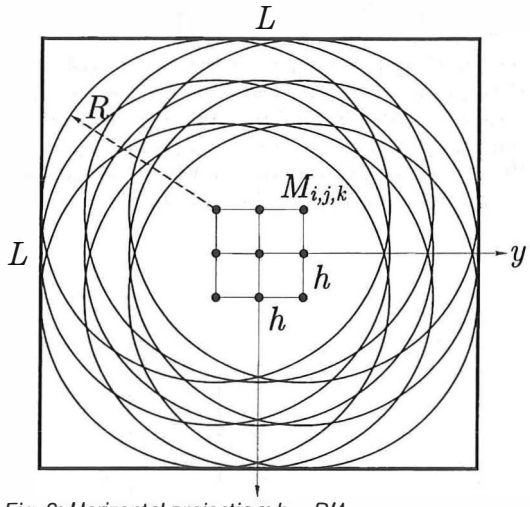


*Fig. 6: Horizontal projection: h = R/4*

We determine the coefficients $\alpha_{ijk}$ by inversion (25). Substituting the result into (23), our tensor $\underline{\mathbf{A}}$ becomes

$$\underline{\mathbf{A}} = [\alpha_{ijk}] = -\frac{1}{144\, h^6} \left[ \begin{bmatrix} 1 & -2 & 1 \\ -2 & 4 & -2 \\ 1 & -2 & 1 \end{bmatrix} \begin{bmatrix} -2 & 4 & -2 \\ 4 & -8 & 4 \\ -2 & 4 & -2 \end{bmatrix} \begin{bmatrix} 1 & -2 & 1 \\ -2 & 4 & -2 \\ 1 & -2 & 1 \end{bmatrix} \right] . \quad (27)$$

In Fig. 7 we see the superposition of the corresponding zero-potential splines.

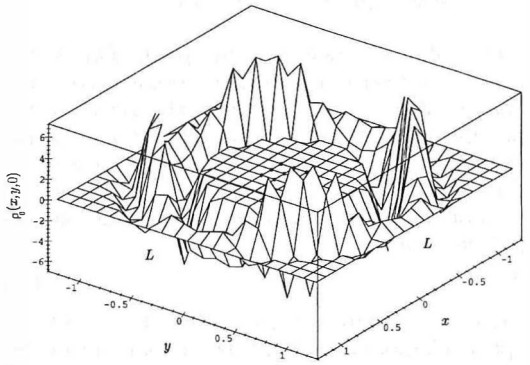


*Fig. 7: Superposition (h = R/4)*

Now two interesting questions arise in an almost miraculous way:

**Miracle 1:** Why is the result in the middle area of Fig. 7 a large *plane* at a height of 1?

**Miracle 2:** Why are the coefficients ($\tilde{\alpha}_0$, $\tilde{\alpha}_1$, $\tilde{\alpha}_2$, $\tilde{\alpha}_3$) of (27) multiples (–8, 4, –2, 1) of the factor $1/(-144h^6)$?

The configuration of the centres $M_{ijk}$ in Fig. 6 has an special property: All centres $M_{ijk}$ lie in a region (intersection of volume), called *"critical region"*, where all 27 spline functions $s_{ijk}$, restricted to their corresponding supports (spheres), are superimposed that is, they are polynomials $\not\equiv 0$. *The plane at a height of 1 is bounded by this "critical region".* (The "critical region" is the plateau in the central part of Fig. 7.) This special configuration of the centres $M_{ijk}$ is always satisfied if the space diagonal of the grid ($M_{ijk}$) is not greater than the radius $R$ of the spheres, which gives the condition $0 \leq h \leq R/2\sqrt{3}$. Whenever $h$ lies in this region, the two miracles described above occur.

It is miraculous indeed that the superposition of zero-potential splines, which are polynomials of higher order, should give an exact plane, which represents a linear function. That the plane is really exact, can be shown by direct computation using (19). Equation (19) can also be written as

$$\rho_0(Q) = \mathbf{a}^T \mathbf{b} = \underline{\mathbf{A}} \odot \underline{\mathbf{B}} \equiv 1, \tag{28}$$

where the tensor $\underline{\mathbf{B}}$ reflects the geometric situation of its element $s_{ijk}$ determined by substituting (18) into (17), cf. also (15). The sign $\odot$ in (28) is defined as the summation over all products of matrices (tensors) – elements with equivalent indices.

Note once more the result is the constant value 1 *identically in the whole "critical region"* defined above, not only at the given data points $Q_{ijk}$!

The fact that the zero-potential density function corresponds to a plane throughout the "critical region" ("Miracle 1"), is so surprising that one is very eager to find an explanation. Perhaps Miracle 1 can be explained by Miracle 2?

We know that the discretization of a differential operator lead to matrices which are quite similar to the matrices occurring in (27). This will be considered now.

## 5. Difference Operators for Approximation of Differential Operators

The approximation of partial derivatives by finite differences is discussed in [1]. As a matter of fact, the derivative of a function with respect to $x$, $y$, or $z$ can be approximated by a difference of values of this function at discrete points. In this section *only one spline function of a unit sphere* ($R = 1$) whose centre corresponds to the origin $O$ of the coordinate-axes is considered and can be denoted by $s_0(x, x, z)$ since

$$s(\bar{r}) = s(M, Q) = s(O, Q) = s_{0,0,0}(Q) = s_0(Q) = s_0(x, y, z). \tag{29}$$

Substituting $\bar{r}$ which is the distance from the centre $O(0,0,0)$ to the variable point $Q(x, y, z)$

$$\bar{r} = \sqrt{x^2 + y^2 + z^2} \tag{30}$$

into (17) we obtain the spline function depending on the position $(x, y, z)$ of point $Q$.

Let us consider only the case if point $Q$ lies inside the range $0 \leq \bar{r} \leq R$. Assume that we introduce a symmetric cubical grid around point $Q$ so that point $Q(x, y, z)$ corresponds to the central node $D_{0,0,0}(x, y, z)$ of the grid. The point $Q$ is not necessarily equal to the origin $O$! The mesh width denoted by $h$ is the same in each direction of the axes. Now the 27 nodes of the grid $D_{ijk}$ (1 central node, 26 outer nodes) should be the discrete points for the approximation. Our aim is to use central differences (differences between outer nodes and the central node) to approximate derivatives of the spline function $s_0(x, y, z)$ at the central node $D_{0,0,0}(x, y, z) = Q(x, y, z)$.

Now let us regard the mixed square derivative of a single spline function $s_0(x, y, z)$ (29) which gives

$$\left(\frac{\partial^6 s_0}{\partial x^2\, \partial y^2\, \partial z^2}\right)_Q = -144, \tag{31}$$

identically for *all* points $(x, y, z)$ in the region $0 \leq \bar{r} \leq R$. At the next stage we replace the mixed square derivative (31) by a difference operator with $0 < h \leq R/2\sqrt{3}$. Using the approximate representation by finite differences, cf. [1], we obtain

$$\left(\frac{\partial^6 s_0}{\partial x^2\, \partial y^2\, \partial z^2}\right)_Q \cong \left(\frac{\partial^6 s_0}{\partial x^2\, \partial y^2\, \partial z^2}\right)^*_Q = \frac{1}{h^6}\,(\underline{\mathbf{A}}^* \odot \underline{\mathbf{B}}^*) = \frac{1}{h^6}\,(-144h^6) = -144, \tag{32}$$

where the difference operator $\underline{\mathbf{A}}^*$ is equal to $-144h^6\,\underline{\mathbf{A}}$ of (27) and tensor $\underline{\mathbf{B}}^*$ reflects the geometric situation of the elements $s_0(D_{ijk})$. By direct computation we see that tensor $\underline{\mathbf{B}}^*$ is identical to $\underline{\mathbf{B}}$ of (28). The sign $\cong$ means: "has the discrete approximation" and $(\,)^*$ denotes the difference expression. Equation (32) holds for a single zero-potential spline $s_0(x, y, z)$. Now a truly remarkable fact appears: *The result (32) is independent of the mesh width h* (gives a constant) and equals the result of the mixed square derivative by the difference operator (31).

Analyzing the results, our basic superposition (28) started from the assumption that the value of the zero-potential density $\rho_0$ is generated by a superposition of 27 spline functions $s_{ijk}$ summarized in tensor **B**. Why is this superposition identically constant in the "critical region" (sec. 4)?

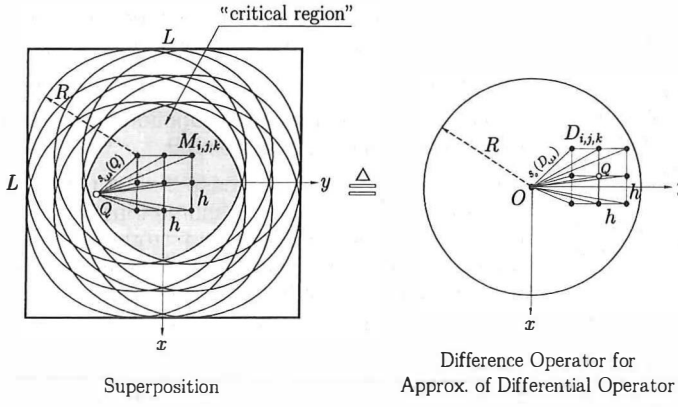


*Fig. 8: Superposition ≙ Approximation by Difference Operator*

The reason is that our superposition is equivalent to an approximation of our operator by finite differences, cf. Fig. 8. This would not yet be spectacular if the result would essentially depend on $h$ (not only as an inessential scale factor). Since (32) is independent of $h$, the result of the *difference operator* is identical to the result of the *corresponding differential operator* since we may let $h \to 0$.

Thus the reason why the superposition (28) gives a constant value is the fact that the differential operator (31) naturally gives a constant value (32).

superposition (28) =
= difference operator result (32) =
= differential operator result (31) =
= **const.**

The crucial point in this argument is that (32) is independent of $h$ so that $h \to 0$ does not change anything.

It is proved that the result of a difference operator, which can be written as a three-dimensional tensor, can always be reproduced by superposition in the "critical region".

## 6. Conclusions

The splines (17) are our basic building blocks for a *practical approximation* of zero-potential densities. Given values at certain data points (e.g. a cubical grid $3 \times 3 \times 3$ points), our spline approximation furnishes the values of a zero-potential density function at any other point in the region under consideration.

The second problem attacked in this paper is of a purely *theoretical significance*. In order to understand a method, it is frequently useful to test it in simple but extreme situations which may be completely unrealistic. (We torture, so to speak, the method in order to force it to show its real character...) Thus we have considered the cubical grid $3 \times 3 \times 3$ and have assumed the data values *equal to 1 at every point of the grid*. This is the "extreme situation" just mentioned and, in fact, it gives the expected unusual behavior which, however, is very instructive: The zero-potential density is identically 1 not only at the data points, but throughout a certain region around them, called "critical region". The result graphically resembles a perfectly smooth plane plateau bounded by wild precipices and jagged mountains.


**References**

[1] *Ghali A., Neville A.M. (1978):* Structural Analysis. A Unified Classical and Matrix Approach. Chapman and Hall, London, New York, pp. 472–475.

[2] *Krappmann S. (1994):* thesis: Nullpotentialdichten als Hilfsmittel für die Lösung inverser gravimetrischer Probleme. TU Graz.

[3] *Krappmann S., Moritz H. (1995):* paper: Radially Symmetric Zero-Potential Densities as a Device for the Solution to Gravitational Inverse Problems, IUGG 1995, Boulder, USA.

[4] *Moritz H. (1990):* The Figure of the Earth. Wichmann, Karlsruhe, pp. 17–24, 183–216.



*Address of the authors:*

Dipl.-Ing. S. Krappmann and Prof. Dr. H. Moritz, Graz University of Technology, Section of Physical Geodesy, Steyrergasse 30, A-8010 Graz, Austria, E-mail: krappmann@ftug.tu-graz.ac.at

# Monitoring Earth Orientation Variations at the Center for Orbit Determination in Europe (CODE)

*Robert Weber, Vienna*

**Abstract**

Since June 1992 the CODE Analysis Center of the International GPS Service for Geodynamics (IGS) has contributed to the International Earth Rotation Service (IERS) series of polar motion parameters $x_p$, $y_p$ as well as length of day (LoD) estimates. The present accuracy of these LoD estimates amount to about 0.03 msec/day. Additionally and because of the special importance of global campaigns including different observation techniques (VLBI, GPS, SLR, LLR) the period of the CONT94-campaign was covered by CODE with a special LoD and polar motion data set of subdiurnal resolution.

The parameters $x_p$, $y_p$ locate the Celestial Ephemeris Pole (CEP) in the terrestrial reference frame, whereas the position of the CEP in Inertial Space is defined by the IAU 1980 Theory of Nutation. Offsets relative to the CEP position as defined above have been detected by VLBI observations since 1986. Since January 1, 1994 we have determined at CODE the first derivative of these CEP offsets ($\Delta\delta\varepsilon$, $\Delta\delta\psi$) with an accuracy of 0.3 mas/day. This is a valuable contribution of the GPS to the monitoring of high frequency variations of the CEP.

This paper discusses the time development of the CODE $x_p$, $y_p$ series over an interval of about 3 years and puts special emphasis on GPS-derived earth rotation parameter variations covering the CONT94 campaign. Finally first results of a spectral analysis of the $\Delta\delta\varepsilon$, $\Delta\delta\psi$ values are presented.

**Zusammenfassung**

Das CODE Analyse Zentrum des Internationalen GPS Dienstes für Geodynamik (IGS) ermittelt seit dem Juni 1992 täglich einen Satz von Erdrotationsparametern (ERP). Diese Serien von Polkoordinaten ($\sigma = \pm 0.2$ mas) und Schätzungen der Tageslänge (LoD, $\sigma = \pm 0.03$ m sec/Tag) werden in erster Linie dem Internationalen Erdrotationsdienst (IERS) zur Verfügung gestellt. Daneben wird vorallem internationalen Kampagnen, welche den Vergleich der Ergebnisse verschiedener Beobachtungstechniken (VLBI, GPS, SLR, LLR) erlauben, eine starke Bedeutung zugemessen. Aus diesem Grund wurde für die Dauer der im Jänner 1994 durchgeführten CONT94-Kampagne zusätzlich ein spezieller ERP-Datensatz erstellt.

Die Polkoordinaten $x_p$, $y_p$ legen den Celestial Ephemeris Pole (CEP) im terrestrischen Referenzrahmen fest. Seine Lage im inertialen Raum wird durch die Nutationstheorie IAU 1980 definiert. Abweichungen von dieser vordefinierten Lage können bereits seit 1986 durch VLBI-Beobachtungen nachgewiesen werden. Seit 1. Jänner 1994 wird nun am CODE-Analysezentrum die erste Ableitung dieser CEP-Abweichungen ($\Delta\delta\varepsilon$, $\Delta\delta\psi$) mit einer Genauigkeit von 0.3 mas/Tag geschätzt. Dies stellt einen bedeutenden Beitrag von GPS zur Überwachung hochfrequenter CEP-Bewegungen dar.

Der vorliegende Artikel beschreibt die Entwicklung einer aus GPS-Beobachtungen abgeleiteten 3-jährigen Serie von Polkoordinaten und diskutiert anschließend ausführlich den für die CONT94-Kampagne erstellten Datensatz hochauflösender ERP-Schätzungen. Abschließend werden die vorläufigen Ergebnisse einer Spektralanalyse der bislang verfügbaren $\Delta\delta\varepsilon$, $\Delta\delta\psi$ - Serien präsentiert.

## 1. The International GPS Service for Geodynamics

In June 1992 a global GPS test campaign was started in order to prove the concept for an International Global Positioning System Service for Geodynamics (IGS). The campaign lasted for three months and was immediately followed by a pilot service which continued until the end of 1993. On January 1, 1994 the IGS took up its routine activities as an official Service of the International Association of Geodesy and later on as a member of the Federation of Astronomical and Geophysical Data Analysis Services (FAGS). The primary objective of the IGS is to provide a service which supports geodetic and geophysical research activities through GPS data products [1].

These data products like satellite ephemeris, earth rotation parameters and station coordinates were based by the end of 1992 on 28 permanent GPS monitor stations [10]. Up to now the network has grown substantially and consisted of more than 60 tracking sites in May 1995 (Fig. 1). This extension of the network goes together with an evolving importance of

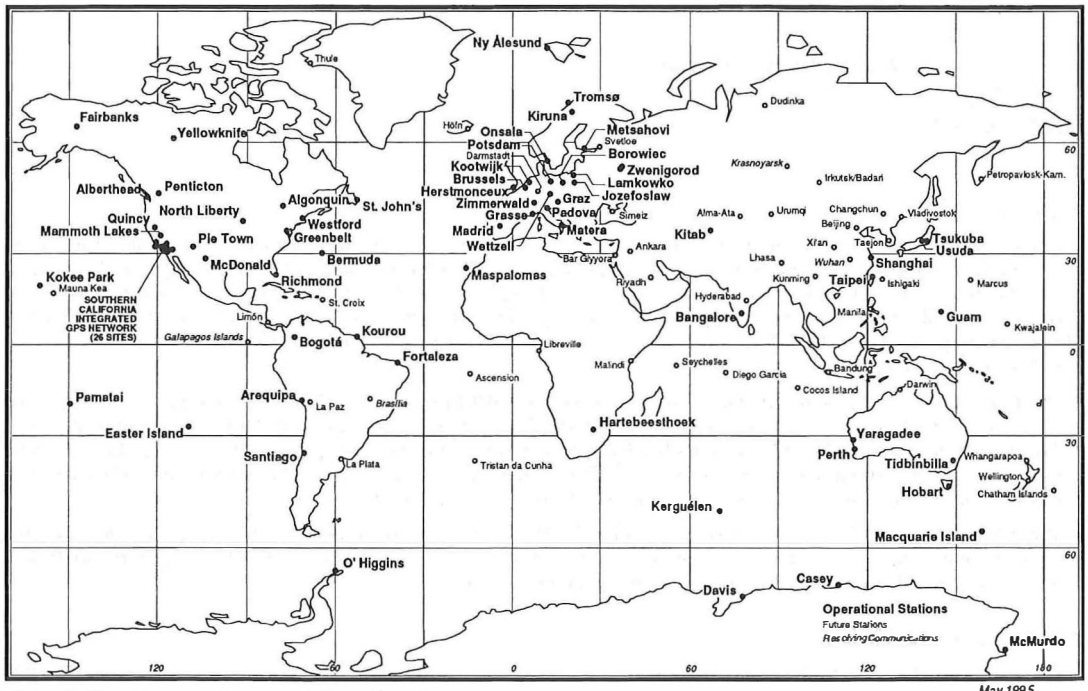


*Fig. 1: IGS network of permanent tracking sites*

the IGS as a provider of data sets useful for geophysical or geodynamical interpretion. Thus, GPS data is for example used nowadays to extract ionospheric information or to support the weather forecast with almost real-time tropospheric delays.

Besides the tracking stations the IGS consists of a considerable number of data- and analysis centers which are responsible for data managment and evaluation of the IGS products. Most of the results discussed in the subsequent chapters were obtained at the Center for Orbit Determination in Europe (CODE, located at the University of Berne), which acts as one (among seven) of these global analysis centers.

## 2. Earth Orientation Parameters

Generally the term 'Earth Orientation Parameter' (EOP) comprises a set of 5 parameters which describe the rotation of the ITRS (International Terrestrial Reference System) in the ICRS (International Celestial Reference System) in conjunction with the conventional Precession-Nutation model. On the other hand, the so-called 'Earth Rotation Parameters' (ERP) characterize a 3-parameter-subset of the EOP, namely the coordinates x and y of the CEP in the terrestrial reference frame (polar motion) and the difference UT1-UTC (respectively UT1-TAI, TAI=International Atomic Time) giving access to the direction of the IERS Reference Meridian in the Celes-

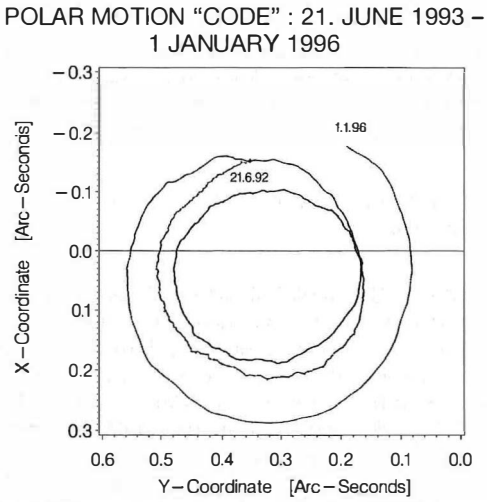


*Fig. 2: Polar motion as produced by the CODE Analysis Center of the IGS*

tial Reference Frame. For detailed information, see [2], [13].

The main components of polar motion are a free oscillation with a period of 1.2 years (Chandler wobble) and an oscillation which is forced by seasonal mass redistribution in the atmosphere and oceans. This variation is superimposed by a slow drift towards the west. In figure 2 GPS-based polar motion series covering a period of more than 3 years are shown. The oldest estimates date back to the start of the IGS-testcampaign in June 1992. Since then we have recognized an obvious improvement in the accuracy of the estimates. Today the accuracy of the CODE pole coordinates is believed to be of the order of about 0.2–0.3 mas.

We conclude that the GPS is very well suited to determine polar motion, provided that the terrestrial reference frame is well defined by means of the coordinates of the tracking stations.

The difference between the astronomically determined duration of the day and $86400^s$ atomic time is called length of day (LoD). The difference $\Delta UT1 = UT1 - TAI$ can easily be obtained by adding up LoD estimates since a change in $\Delta UT1$ is related to a change in LoD by integration (see below).

$$\Delta LoD(t) / LoD_0 = - d(UT1 - TAI) / dt \qquad (1)$$

Unfortunately, the GPS is not capable of providing absolute estimates of $\Delta UT1$. The reason is the correlation between $\Delta UT1$ and the right ascension of the ascending node of the satellite orbits. On the other hand it should be possible to solve for a drift in $\Delta UT1$ by adopting a linear model of the type

$$\Delta UT1(t) = \Delta UT1(t_0) + d(\Delta UT1) / dt \cdot (t - t_0) \qquad (2)$$

This demonstrates that the LoD may be estimated very well with the GPS. Of course, the drift parameter in (2) would be correlated again with the first derivative of the ascending node but under the assumption of a known force model, there is no need to solve for this derivative.

Figure 3 shows the LoD estimates after removal of the terms due to the fixed body tides with periods up to 35 days. These series are furthermore subject to seasonal variations mainly due to atmospheric circulation [4]. The IERS integrates the individual LoD-series (made available by different GPS-Analysis Centers) and produces a combined GPS-solution which finally effects the behaviour of the resulting IERS UT1-UTC series, especially in the high frequency range (periods shorter than about 30 days).

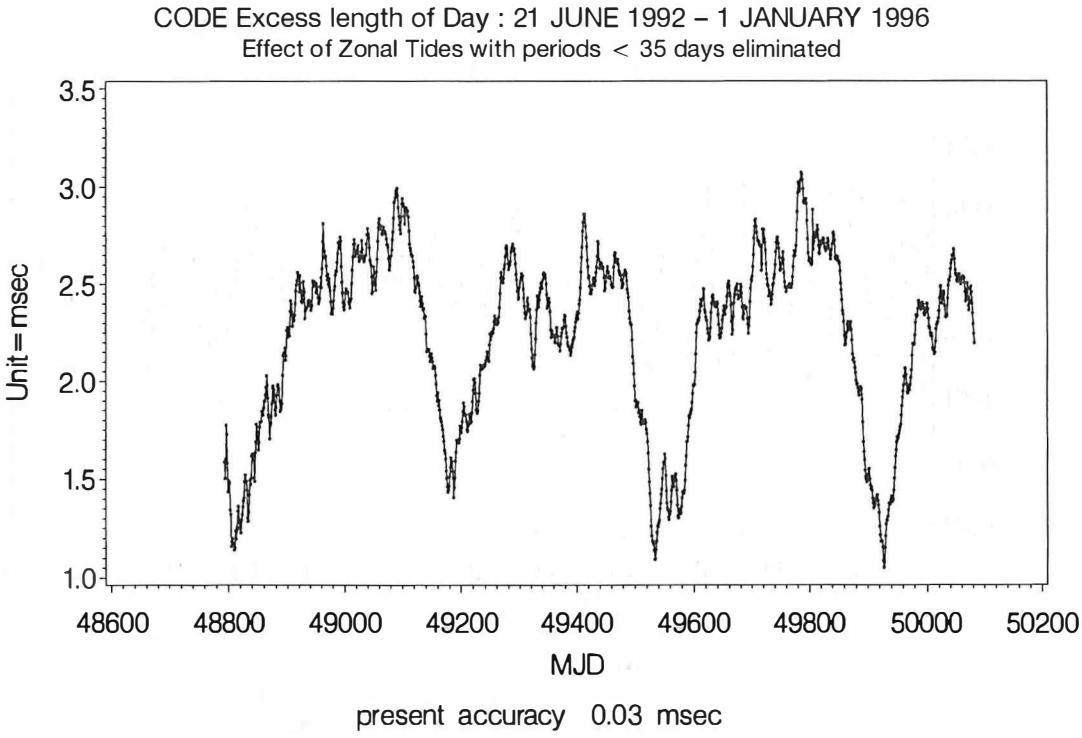


*Fig. 3: CODE LoD-estimates after removal of zonal tides*

### 3. The CONT94 Campaign

In August 1991 the International Union of Geodesy and Geophysics recognized the importance of the determination of rapid Earth rotation variations and its implication for geodynamics through a union resolution. As a result, a major campaign, called SEARCH'92 (Study of Earth-Atmosphere Rapid Changes), for subdaily measurements of Earth rotation was held in summer 1992. Measurements were performed by GPS, VLBI, SLR and LLR in order to analyze subsequently the results of the different techniques. Of course, we have to mention that high-frequency ERP-results based on GPS observations dating from 1992 suffered remarkably due to an incomplete status both of the space segment and the tracking network. Nevertheless, the outcome was really promising and a detailed description can be found in [Dickey, Feissel, 1994].

Another intensive VLBI observation campaign, lasting about 2 weeks, was performed in January 1994. This campaign was intended to serve as continuation of SEARCH'92 and was therefore called CONT94. CONT94 provided the scientific community with hourly Earth orientation measurements and a set of UT1-variations deduced from them [5]. At the CODE Analyses Center the same period was covered with GPS-based estimates of LoD and polar motion coordinates with subdiurnal resolution. First of all we used the official IGS precise ephemeris as a priori information in order to compute and save a set of daily normal equations. Afterwards these normal equations were combined to overlapping 7-day arcs and UT1 (respectively LoD) was estimated every 2 hours. Finally the results obtained from the middle days of the various arcs (Arc 1 – Arc 6) were concatenated to cover the whole period. Figure 4 shows the outcome of this procedure after the removal of lower frequencies.

A closer look at figure 4 tells us that the time series are dominated by diurnal and semidiurnal terms. There is no doubt that the oceanic tidal angular momentum can be considered to be the primary cause for these variations in the earth's rotational rate. Since, in the absence of external torques, the angular momentum of the ocean-solid earth system is conserved, changes in the ocean tidal angular momentum must be accompanied by changes in the angular momentum of the solid earth, thereby leading to changes in the solid earth's rotation. Furthermore figure 4 compares our $\Delta$UT1 estimates with predictions obtained from two well-known tide models. The

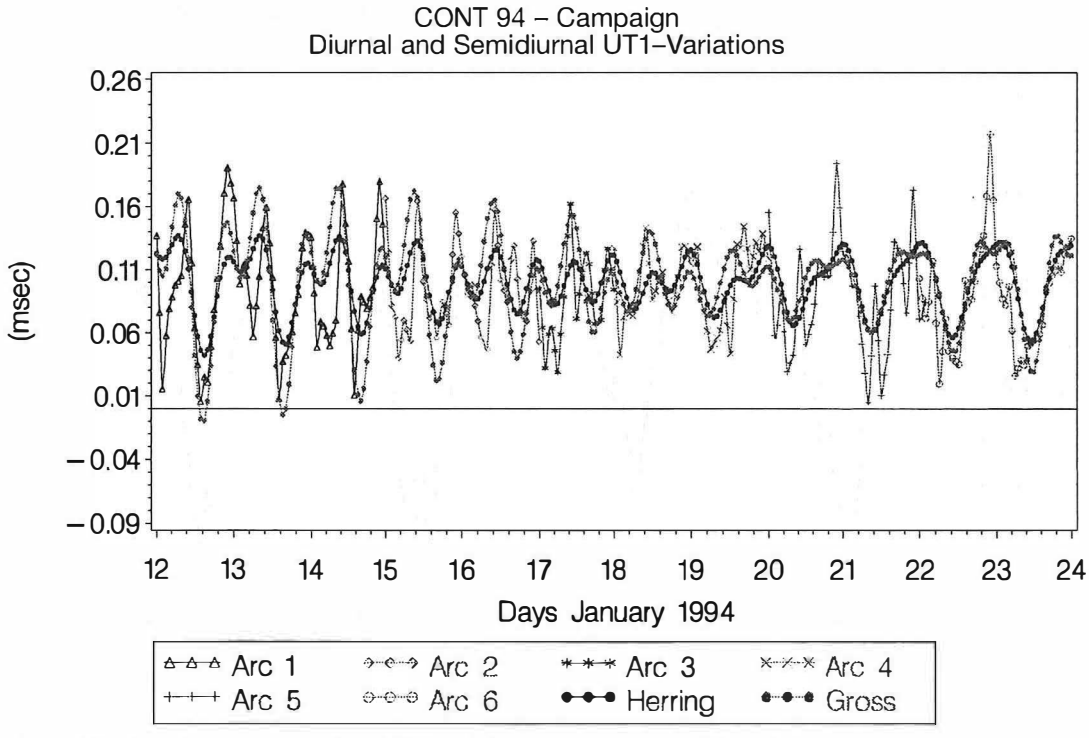


*Fig. 4: Estimated diurnal and semidiurnal UT1-variations compared to model predictions*

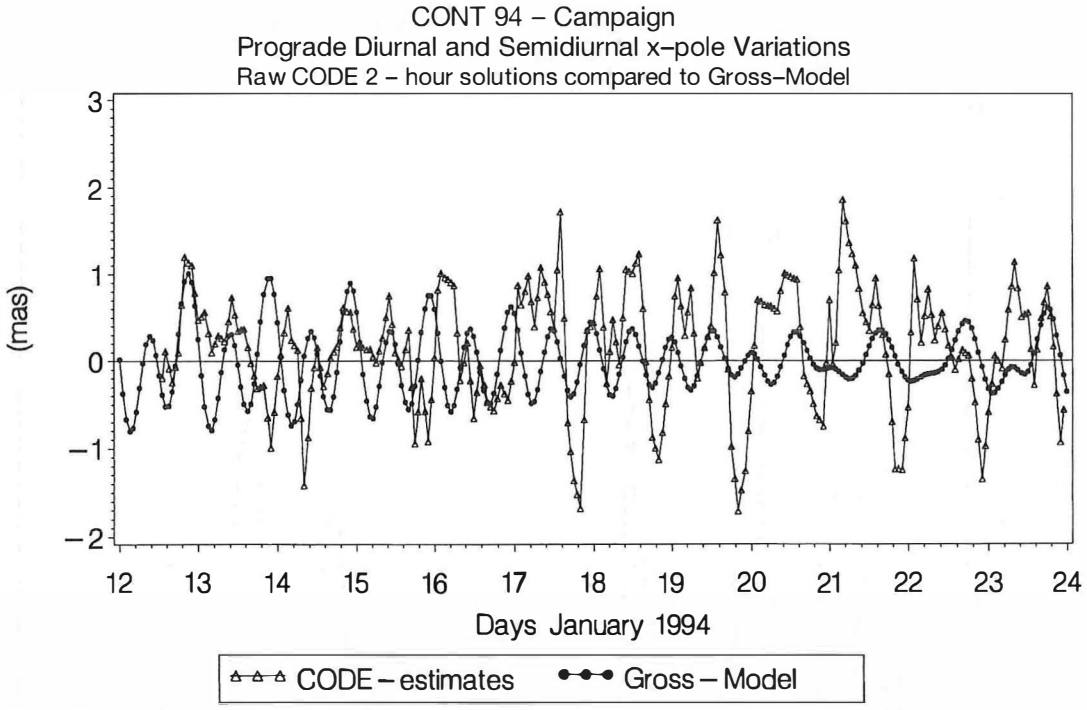


*Fig. 5: Estimated $x_p$ - variations compared to model predictions*

first one (Gross model) is based on the results of Seiler [11] for the axial component of the ocean tidal angular momentum. This model can be characterized as theoretical approach, but nevertheless the evaluated series fit our estimates quite well. The other one (Herring model) is based on 1085 VLBI experiments carried out between January 1984 and June 1992 [7]. This model describes amplitudes and phase angles of about 20 tidal constituents, particularly for the main tidal lines in the diurnal (K1, O1, P1, Q1) and the semidiurnal band (K2, S2, M2, N2). Recent investigations [3], dealing with predictions according to ocean tide models based on Topex/Poseidon observations, confirm the excellent quality of the Herring model. Sometimes the amplitudes of the CODE-series seem to be overestimated by a factor of two, which could be explained by modelling problems for particular satellites.

Due to the irregular geographic distribution of the world's oceans, oceanic current and sea-level height changes can also affect the non-axial components of the earth's rotation (polar motion). Additionally, we had to keep in mind that the polar coordinates $x_p$, $y_p$ specify the location of the celestial ephemeris pole (CEP) within the rotating, body-fixed terrestrial reference frame. Figure 5 outlines the estimated $x_p$ – variations in relation to the corresponding numbers computed by means of the Gross model. There is a fairly good correspondence in the first week but the remarkable amplitude differences in the second week are subject to further investigations.

Concerning figure 5 it must be emphasized that the retrograde diurnal polar motion was already constrained to zero within the actual estimation process. A retrograde diurnal polar motion (K1 ocean tide) is not observable, because it represents a constant offset of the CEP in space and is therefore absorbed into the definition of the CEP (Nutation).

## 4. Nutation Offset determination by means of GPS

The present theory of nutation adopted by the IAU is based on Kinoshita's rigid earth theory [8] and Wahr's non rigid theory [12] that uses the earth model 1066A. Wahr's theory deduces the ratio of nutation amplitudes for the non-rigid earth to that for a rigid model. Soon after the adoption of the IAU 1980 Theory of Nutation VLBI-observations showed deficiencies in this theory at the level of several milliarcseconds (mas). The motion of the celestial pole relative to the IAU 1980 Theory is expressed in the Ce-

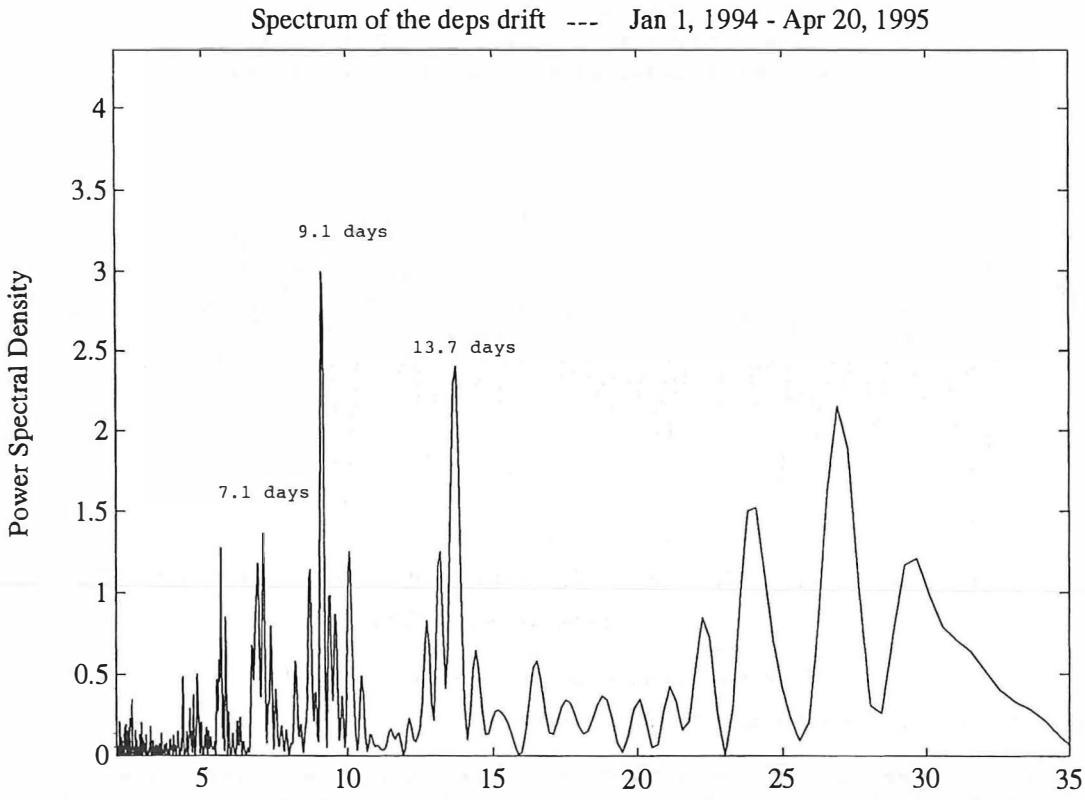


*Fig. 6: Frequency analysis of the drifts in $\delta\Delta\varepsilon$ as estimated by the CODE processing center*

lestial pole offset parameters $\Delta\varepsilon$ (Obliquity) and $\Delta\psi$ (Longitude), which complete in addition to the ERP the set of Earth Orientation Parameters (see chapter 2). Up to now VLBI was the only technique capable of measuring all EOP components simultaneously and accurately. In case of looking on long-period nutation this statement is also valid in the future, since VLBI is the technique with direct access to the Celestial Reference Frame. On the other hand satellite techniques should, similar to the monitoring of high-frequency variations of universal time, be able to make valuable contributions in the determination of celestial pole offset parameters, especially in the short period range. Therefore the CODE-Analysis center started (in February 1994) to derive celestial pole offset parameters based on GPS tracking data of the global IGS network. These estimates were thought to prove or reject the above mentioned idea that GPS, as a satellite technique, is able to locate the CEP in the celestial space fixed frame.

In the meantime, after a renewed computation of the January 1994 observation data, time series which cover more than 16 months, are available. Similar to LoD, there are correlations between the orbital elements (right ascension of the ascending node, inclination) and the nutation terms. Therefore only the first derivatives, the nutation offset rates in obliquity $\delta\Delta\varepsilon$ and longitude $\delta\Delta\psi$, are accessible to the GPS. The accuracy of these daily drifts is of the order of 0.3 mas/day. Ideally we should see essentially the same frequencies as VLBI in the spectrum of our estimated drifts and furthermore get the same order of magnitude when estimating the relevant terms. Figure 6 reflects the results of a spectral analysis of the $\Delta\varepsilon$ - rates.

The $\delta\Delta\varepsilon$ - spectrum shows the maxima roughly at the expected periods, in particular at 7.1 , 9.1 and 13.7 days. The corresponding curve for the nutation in longitude is somewhat less convincing, but will improve with a growing time base. Analizing the $\delta\Delta\varepsilon$- and $\delta\Delta\psi$- series enables us to estimate amplitude corrections for some of the short period nutation terms (periods up to 35 days) relative to the IAU 1980 model. The author is therefore convinced that the GPS is able to give essential contributions in the high frequency range in future.

**Acknowledgements**

I am very grateful to my colleagues in Berne for their support during my stay at the Astronomical Institute over the past two years. In particular I should like to thank the head of the Institute Prof. Dr. Gerhard Beutler and Dr. Markus Rothacher whose continued assistance was invaluable for the work presented above.

**References:**

[1] *Beutler G., Neilan R. (1995):* International GPS Service for Geodynamics, Resource Information, IGS Central Bureau, JPL, Pasadena.

[2] *Castrique L. (1995):* IERS Annual Report 1994, Central Bureau of IERS-Observatoire de Paris.

[3] *Chao B., Ray R., Egbert G. (1995):* Diurnal/semidiurnal oceanic tidal angular momentum: Topex/Poseidon models in comparison with Earth's rotation rate, Geophysical Research Letter, Vol.22, No.15, AGU-Publication.

[4] *Eubanks T.M. (1993):* Variations in the Orientation of the Earth. In: Contributions of Space Geodesy to Geodynamics: Earth Dynamics, Geodynamic Series, Volume 24, pp. 1–54, AGU-Publication.

[5] *Gipson J.M., C. Ma, T.M. Eubanks, A.P. Freedman (1994):* Diurnal and subdiurnal EOP variations during CONT94, Eos, Trans. Amer. Geophysical Union, Volume 75, No. 111.

[6] *Gross R.S. (1993):* The effect of ocean tides on the earth's rotation as predicted by the results of an ocean tide model, Geophysical Research Letter, Vol.20, No.4, AGU-Publication.

[7] *Herring T.A., Dong D. (1994):* Measurement of diurnal and semidiurnal rotational variations and tidal parameters from earth, Journal of Geophysical Research, Vol. 99, No. B9, pp. 18051–18071, AGU-Publication.

[8] *Kinoshita H. (1977):* Theory of the rotation of the rigid earth, Celestial Mechanics, Vol. 15, pp. 277–326, Kluwer Publishers

[9] *Moritz H., Mueller I. (1988):* Earth Rotation-Theory and Observation, Ungar Publishing Company, New York.

[10] *Rothacher M. et al. (1994):* Annual Report of the CODE Analysis Center of the IGS for 1993, IERS Technical Note 17, pp. P1–P14, Central Bureau of IERS – Observatoire de Paris.

[11] *Seiler U. (1991):* Periodic changes of the angular momentum budget due to the tides of the world ocean, Journal of Geophysical Research, Vol. 96, No. B6, pp. 10287–10300, AGU-Publication.

[12] *Wahr J. (1981):* The forced nutations of an elliptical, rotating, elastic and oceanless earth, Geophysical Journal Royal Astronomical Society, Vol. 64, pp. 705–727.

[13] *Weber R., Walter G., Klotz St. (1995):* GPS-relevante Koordinatensysteme und deren Bezug zum österreichischen Festpunktfeld, Österr. Zeitschrift f. Vermessung u. Geoinformation, Heft 4, 1995, Wien.

*Address of the author:*

Dipl.-Ing. Dr. Robert Weber, Institut f. Theoretische Geodäsie und Geophysik, Abteilung Theoretische Geodäsie, Technische Universität Wien, Gußhausstraße 27–29, A-1040 Wien.

# The Austrian Gravity Base Net 1995

*Diethard Ruess, Wolfgang Gold, Vienna*

**Abstract**

The Austrian Gravity Network is one of the tasks of the Federal Office of Metrology and Surveying (BEV) in Vienna. A revision of the old existing network were started 1981. New stations were established and relative measurements were made with LCR gravimeters only. The neighboring networks were connected with the Austrian network. Since 1987 the absolute gravity meter JILAG-6 has been used for observations on 28 stations of the 0. order. Two different national network adjustments and an European adjustment were calculated. The results were compared and contrasted with the absolute observations. The maximum difference is less then 30 μGal, the average difference is less than 1.5 μGal.

Repeated absolute measurements twice a year have been done on a station in the Central Alps of Austria to check the stability of the gravity values. The amplitude of these results is $8 \cdot 10^{-8}$ m/s$^2$ (8 μGal).

## 1. Introduction

The Federal Office of Metrology and Surveying in Vienna has a long tradition in determining the gravity. First observations were made 1878 in Vienna with a Repsold Pendulum by Theodor R. v. Oppolzer of the k. k. Gradmessungsbüro. Further measurements were made by Robert D. v. Sterneck. The Vienna Gravity System was established and valid until 1909 when the Potsdam Gravity System was decided by the IAG. In the 50$^{th}$ and 60$^{th}$ relative measurements were possible using the relative gravimeters Nørgaard and Worden. Therefore a base station network was established and derived from the European Calibration Line which crossed Austria between Kufstein and Brenner. At the end of the 70$^{th}$ a lot of these base stations were lost. In 1980 four new

absolute gravity stations were established in Austria, measured by I. Marson with the rise and fall apparatus IMGC of Italy [1]. New relative gravimeters were available and a lot of geophysical projects demanded a new homogeneous and practical gravity base network. Since 1987 the JILAG-6 free fall absolute gravimeter (figure 1) has been used for several new absolute stations in Austria [7]. The results of these observations have been introduced in the gravity network.

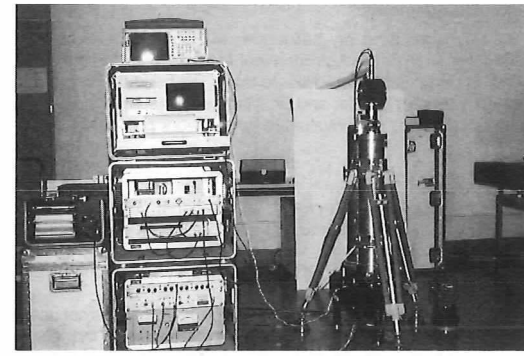

*Fig. 1: The absolute gravitymeter JILAG-6*

## 2. The Austrian Gravity Base Net (ÖSGN = Österreichisches Schwere-Grund-Netz)

A lot of different tasks in geodesy, geophysics and technical applications effect the necessity of a homogeneous distribution of gravity base stations with high accuracy. The mountainous area of Austria causes the number of 236 main stations of the order 0. – 2. The stations of the order Zero are defined as absolute stations. A primary network of further 20 stations (1. order) was established in the area of important junctions in 1981 – 1985 [6]. At least in the 2. order a distribution of one station on each page of the Austrian Map 1:50.000 (1 station/≈520 km$^2$) was aimed. The final distribution is shown in figure 2. One to three witness stations were established in the surrounding of each main station and somewhere points of 3. order complete the number of about 720 stations (table 1).

The most of the relative measurements were observed by the La Coste & Romberg gravity meters D-9, D-51, G-625. The ÖSGN is connected with the networks of the surrounding states (table 2).

## 3. Network Adjustments

A first homogeneous adjustment was presented at the XX. IUGG Assembly 1991. Further

| ÖSGN | | | | |
|---|---|---|---|---|
| order | stations | σ[μGal] | determination | instruments |
| 0 | 28 | 4–8 | absolutely | JILAG-6 |
| 1 | 139 | 5–10 | relatively, directly and jointly | 2–4 LCR |
| 2 | 446 | 5–15 | relatively, jointly | 1–3 LCR |
| 3 | 106 | 8–20 | relatively, directly | 1 LCR |
| 0–3 | 719 | 4–20 | summary | |

*Table 1: Station groups of the Austrian Gravity Base Network (June 1995) (σ [μGal]: adjusted error of the absolute g-value on a station)*

| Connection to the surrounding states | time | connections |
|---|---|---|
| Italy | 1985 | 2 |
| Switzerland / Liechtenstein | 1982–85, 1994 | 6 |
| Germany | 1982–85 | 19 |
| Czechia | 1991, 1995 | 34 |
| Slovakia | 1991 | 4 |
| Hungary | 1992 | 12 |
| Slovenia | 1995 | 11 |

*Table 2: Gravity network connections with surrounding countries*

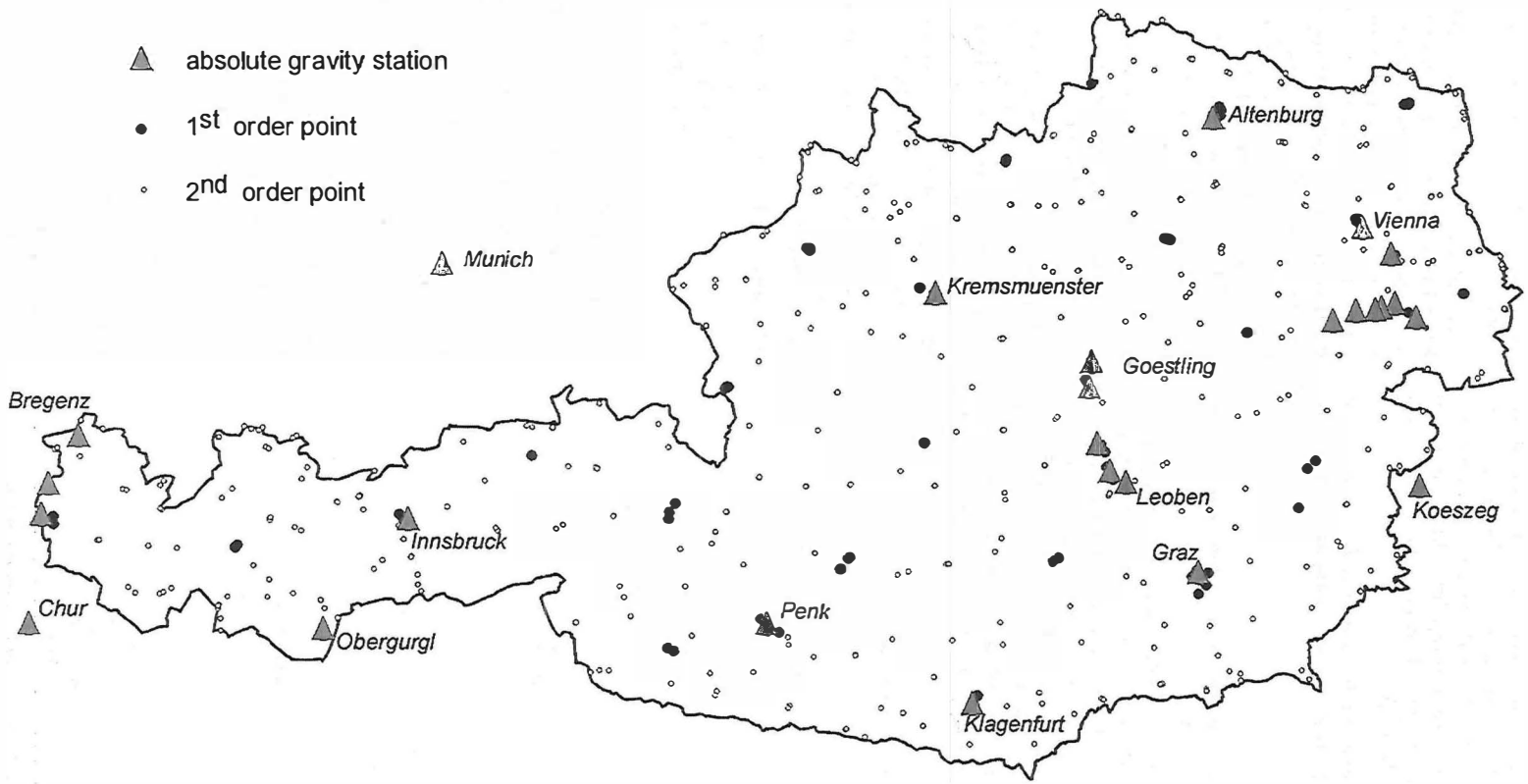


*Fig. 2: Distribution of network stations*

analyses were done and the main part of the Austrian gravity network is included in the new European Gravity Network. According to the accuracy of the absolute gravity values the mean error of the adjusted values is better than $8 \cdot 10^{-8}$ m/s$^2$ (8 μGal).

The solutions of the three different types of network adjustments are compared and presented.

### 3.1. *Iterative Solution of the Austrian Gravity-network (ISAG)*

At the same time when the measurements in the new gravity network were started the values of the base stations were needed for different other gravity projects. Therefore it was necessary to make a first partially network adjustment. The distribution of the measured network connections was very inhomogeneous until 1985. Therefore it was not possible to use modern adjustment computing models using matrix algorithms.

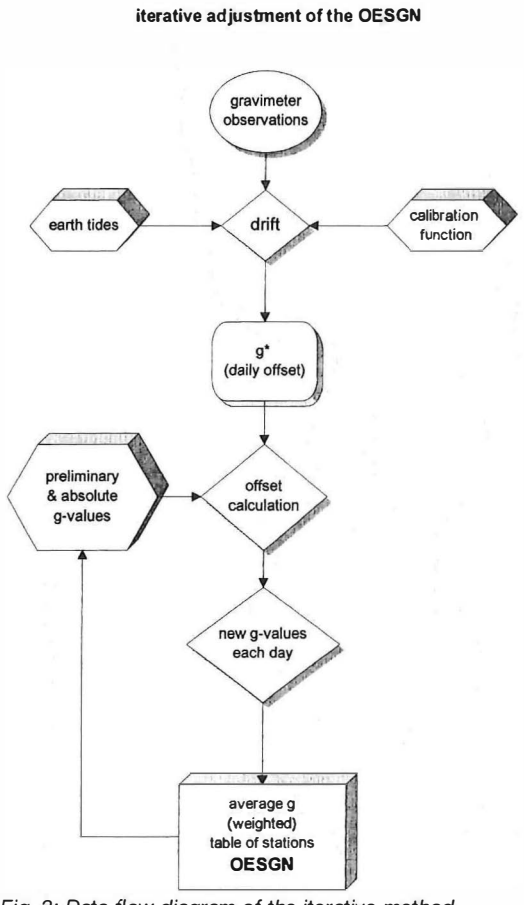


*Fig. 3: Data flow diagram of the iterative method*

Therefore a method was developed which allows to calculate new station values for each measuring cycle beginning on well known starting points. The Gaussian law of propagation of errors was used straight. The new values on each station were given by the weighted mean of the results of the certain cycles and then used for a new turn of calculation. This procedure is a modification of the technique of Anér and Lichte "The adjustment of a trigonometric elevation network" [12]. The data flow diagram is shown in figure 3.

The first step used was to calculate the g-values by the daily observation cycles, beginning at the absolute stations.

1) calculation of relative g-values using the calibration function of the certain instrument and correction of tidal and drift effects ⇒ g-values of each daily station + unknown offset
2) calculation of the unknown offsets by using absolute stations and preliminary values
3) recalculation of the station – values
4) computing the average value by using all results of 3)
5) back to 2)

Introduced data: 3826 relative observations
107 absolute observations which give the datum
27 foreign network values

### 3.2. *ANAG (ANalyse AusGleich)*

This adjustment system is a modified version of the 3D network adjustment program system ANAG which is used in the BEV to adjust control points [13]. The part of the adjustment of the heights was befitted for the gravity network adjustment.

The observation equation is given by:

$$v_{ij} = gd_j - gd_i + [(g_j - g_i) - \Delta g_{ij}]$$

$\Delta g_{ij}$ observations
$g_j, g_i$ preliminary g-values
$gd_j, gd_i$ unknowns

Used data in the adjustment: 2439 Δg values
769 stations

The Δg values were computed by using the adjustments of the daily observations (drift & tide corrected). It is the same data set as in 3.1. 1).

The absolute g-values are included by using the fixed g-values and a pseudo-difference of

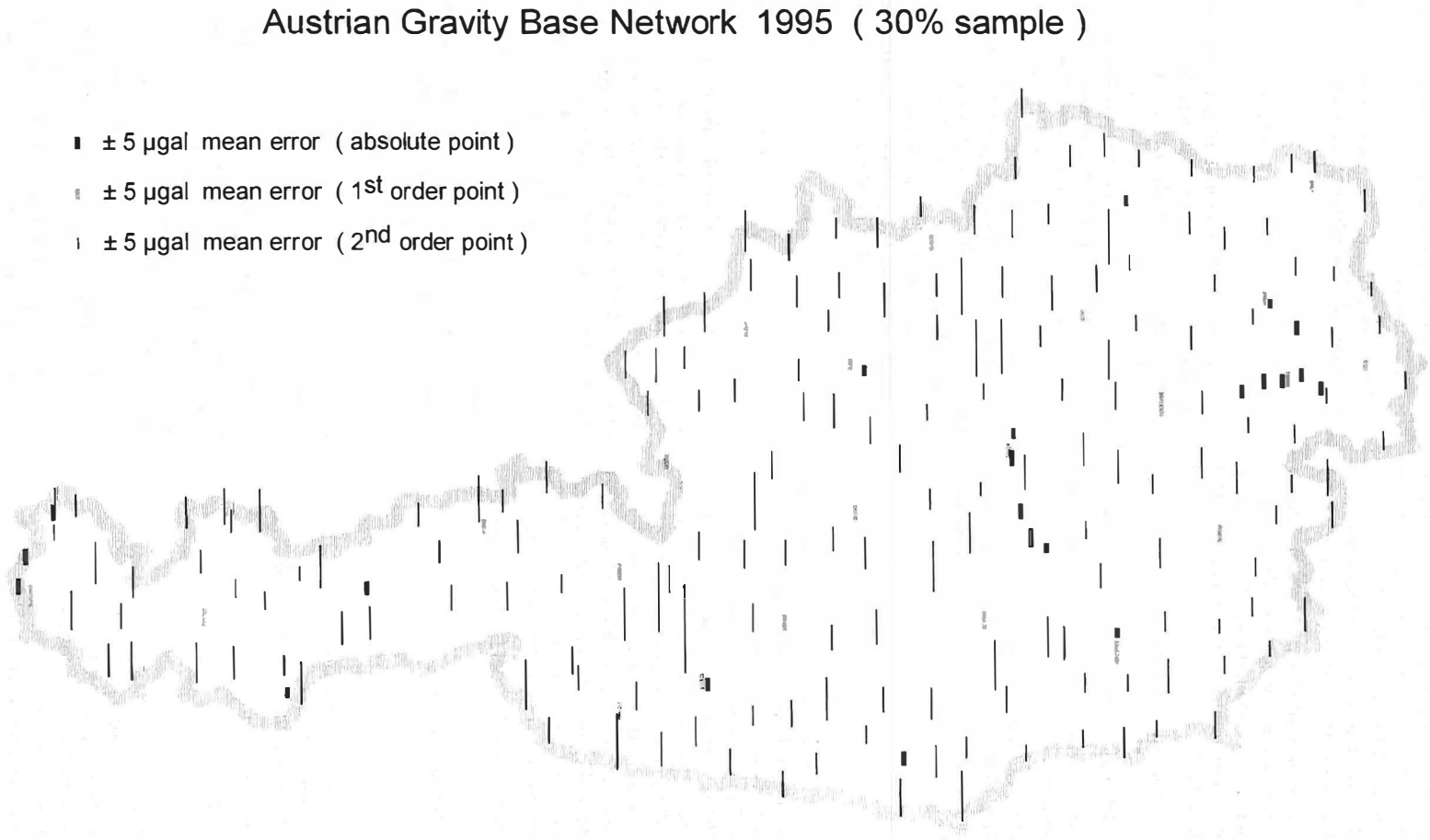


*Fig. 4: Error bars of results of ANAG*

zero to an identical relative station. The rectification's of these zero-differences corresponds to the rectification's of the absolute values. The accuracy of the absolute measurements are used for the weight of the pseudo-difference 0.

The errors of the preliminary (daily) adjustments are used for the weight of the g-differences by eliminating the extremes ($5 \leq \sigma \leq 30$). An error proportional to the g-differences (2 μGal / 100 mGal) is used.

Therefore the extremes of the errors are:

$$1.2 \leq \sigma \leq 8.5$$

and the used weights are: $0.0013 \leq p \leq 0.069$

The error bars of the results of the adjustment are shown in figure 4.

The absolute stations in Austria measured in 1987 – 1994 with the JILAG-6 give the datum of the adjustment, additionally the station Munich of the DSGN 80 was used.

### *3.3. UEGN*

The Austrian observations of the 0. and 1. order observations and some important parts of 2. order measurements are included in the adjustment of the Unified European Gravity Network UEGN [1]. All the superior parts of the most western European countries are included. For this adjustment all the row – data of the field observations were used. These data were evaluated using a unified algorithm of drift calculation and corrected with the newest earth tide model. Therefore inconsistencies due to different national computing algorithms were avoided.

The dispositions of the rectification equations are:

on absolute measurements:

$$v_i = g_j - g_i$$

with

$v_i$ *residuals of the observations*
$g_j$ *estimated station value*
$g_i$ *observed value (earth tide corrected)*

on relative measurements:

$$v_i = g_j + o_l + z_j f_g + t_j d_l + r_j$$

with

$v_i$, $g_j$ *as above*
$o_l$ *unknown offset of a measuring cycle*
$z_j$ *observed value (reading)*
$f_g$ *calibration factor of the instrument*
$t_j$ *time of observation*
$d_l$ *linear drift coefficient in a cycle*
$r_j$ *gravimeter reading # i, earth tide corrected, calibrated*

The datum of the adjustment corresponds to the 123 used absolute measurements.

## 4. Comparisons with the absolute stations

The results of the 3 different kinds of network adjustments were compared with the given absolute values (table 3). The mean errors are very close together. The higher mean value of the UEGN error – results is caused by a smaller number of used relative observations. Therefore the big difference of 44 μGal in the UEGN at Mannswörth is declared by only a few week relative connections to the other stations on one hand and by not using the absolute value on the other hand. Also further 5 absolute values are not introduced in the UEGN. The average residuals of the different adjustments lay between –1.7 (UEGN) and + 0.6 (ANAG). So a good agreement could be found in all three types of adjustments.

## 5. Comparisons with further network stations

The results of the different adjustment routines were compared on 47 significant base stations and presented in table 4. The extremes in the discrepancies are –27 and + 32 and will be found in the row UEGN – ANAG. The maximum discrepancies between ANAG and ISAG is –13 and +18. The reason of the smaller disagreements is caused be the greater number of used observations.

The gravity niveau of the UEGN fits very good to the results of ISAG (~ 0.5 μGal). The niveau of ANAG seems to be higher by about 1.5 μGal than the results of ISAG.

## 6. Checks on stability of absolute gravity observations

The long term stability of gravity can only be checked by repeated absolute observations. In Austria this was possible only on few stations. The most frequented absolute stations are Obergurgl and Vienna. Repeated measurements are also planned in geodynamic sensitive zones.

In Obergurgl (Ötztal in Tyrol) repeated absolute observations have been made twice a year since 1987 every spring and autumn with the JILAG-6 instrument [11]. The goal of these measurements

| Comparison between 3 different adjustments of the Austrian Gravity Base Net | | | | | | | | | | | | |
|---|---|---|---|---|---|---|---|---|---|---|---|---|
| ÖSGN UEGN | Name | ABS | ± | ISAG | ± | ANAG | ± | UEGN | ± | ISAG-ABS | ANAG-ABS | UEGN-ABS |
| 0-021-00 1764 | Altenburg-O | 867386 | 6 | 867383 | 5 | 867381 | 4.3 | 867371 | 5 | –3 | –5 | –15 |
| 0-021-01 1851* | Altenburg-W | 868930 | 5 | 868935 | 5 | 868929 | 4.9 | 868927 | 9 | 5 | –1 | –3 |
| 0-050-00 1769 | Kremsmünster | 741249 | 15 | 741259 | 5 | 741273 | 4.5 | 741260 | 5 | 10 | 24 | 11 |
| 0-059-00 1772 | Wien | 849543 | 2 | 549544 | 5 | 849544 | 3.9 | 849542 | 3 | 1 | 0 | –1 |
| 0-059-10 1863* | Mannswörth | 837769 | 7 | 837760 | 5 | 837756 | 5.9 | 837725 | 12 | –9 | –13 | –44 |
| 0-071-00 1775 | Göstling | 681846 | 6 | 681845 | 5 | 681852 | 4.4 | 681841 | 5 | –1 | 6 | –5 |
| 0-076-00 1778 | Hirtenberg | 813033 | 3 | 813033 | 5 | 813034 | 5.6 | 813036 | 6 | 0 | 1 | 3 |
| 0-076-01 1854* | Tattendorf | 810686 | 3 | 810686 | 5 | 810688 | 6.4 | 810694 | 9 | 0 | 2 | 8 |
| 0-077-00 1780 | Seibersdorf | 829677 | 5 | 829675 | 5 | 829675 | 5.5 | 829675 | 5 | –2 | –2 | –2 |
| 0-077-01 1857* | Unterwalters | 822607 | 4 | 822607 | 5 | 822604 | 6.4 | 822603 | 7 | 0 | –3 | –4 |
| 0-077-02 1859* | Ebreichsdorf | 818014 | 4 | 818015 | 5 | 818019 | 5.5 | 818024 | 8 | 1 | 5 | 10 |
| 0-078-00 1784 | Kaisereiche | 795426 | 4 | 795430 | 5 | 795435 | 5.8 | 795429 | 7 | 4 | 9 | 3 |
| 0-082-10 1785 | Bregenz | 650100 | 7 | 650104 | 5 | 650103 | 6.4 | 650111 | 7 | 4 | 3 | 11 |
| 0-101-00 1789 | Hochkar | 484653 | 4 | 484652 | 5 | 484657 | 6.5 | 484646 | 8 | –1 | 4 | –7 |
| 0-101-50 1790 | Präbichl | 513094 | 9 | 513096 | 6 | 513097 | 6.3 | 513095 | 6 | 2 | 3 | 1 |
| 0-111-10 1861* | Koblach | 612425 | 6 | 612418 | 5 | 612414 | 6.4 | 612396 | 15 | –7 | –11 | –29 |
| 0-118-00 1796 | Innsbruck | 546559 | 6 | 546570 | 5 | 546568 | 5.7 | 564580 | 7 | 11 | 9 | 21 |
| 0-132-10 1800 | Trofaiach | 616484 | 8 | 616483 | 5 | 616482 | 7.5 | 616482 | 8 | –1 | –2 | –2 |
| 0-133-10 1802 | Leoben | 648195 | 8 | 648190 | 5 | 648191 | 3.9 | 648203 | 6 | –5 | –4 | 8 |
| 0-140-00 1805 | Tisis | 588321 | 7 | 588331 | 11 | 588335 | 6.4 | 588323 | 7 | 10 | 14 | 2 |
| 0-164-00 1813 | Graz | 715514 | 4 | 715511 | 5 | 714513 | 4.1 | 714512 | 8 | –3 | –1 | –2 |
| 0-173-00 1814 | Obergurgl 1 | 239926 | 4 | 239923 | 5 | 239922 | 4.5 | 239922 | 5 | –3 | –4 | –4 |
| 0-173-01 1815 | Obergurgl 2 | 239890 | 2 | 239891 | 5 | 239892 | 3.9 | 239892 | 3 | 1 | 2 | 2 |
| 0-181-00 1819 | Penk | 467787 | 8 | 467780 | 5 | 467782 | 5.5 | 467796 | 6 | –7 | –5 | 9 |
| 0-202-00 1822 | Klagenfurt | 620236 | 9 | 620229 | 6 | 620234 | 6.0 | 620227 | 9 | –7 | –2 | –9 |
| 0D18/0 1243 | München | 723137 | 7 | 723109 | 9 | 723124 | 7.3 | 723131 | 4 | –28 | –13 | –6 |
| 0U KOESZ 1837 | Köszeg | 784708 | 5 | 784706 | 5 | — | — | 784705 | 15 | –2 | | –3 |
| | mean values | | 5.8 | | 5.4 | | 5.5 | | 7.2 | –1.1 | 0,6 | –1.7 |
| 1851* | absolute value not used in UEGN | | | | | | | | | | | |

*Table 3: Comparisons of 27 used absolute stations and the different adjustment results*

| **Results of adjustments** (main stations) 980 ... ... [µGal] | | | | | | | differences | | |
|---|---|---|---|---|---|---|---|---|---|
| ÖSGN Number | ISAG | σ | ANAG | σ | UEGN | σ | ANAG-ISAG | UEGN-ISAG | UEGN-ANAG |
| 1-016-00 | 776.237 | 5 | 776.243 | 7 | 776.232 | 8 | 5 | –5 | –11 |
| 1-025-00 | 882.229 | 5 | 882.236 | 5 | 882.221 | 8 | 7 | –8 | –15 |
| 1-047-00 | 740.110 | 5 | 740.118 | 6 | 740.118 | 7 | 8 | 8 | 0 |
| 1-050-02 | 740.394 | 5 | 740.402 | 6 | 740.406 | 7 | 8 | 12 | 4 |
| 1-054-00 | 855.361 | 5 | 855.374 | 6 | 855.365 | 7 | 13 | 4 | –9 |
| 1-055-01 | 861.618 | 5 | 861.625 | 8 | 861.615 | 9 | 7 | –3 | –10 |
| 1-059-00 | 849.546 | 5 | 849.550 | 4 | 849.539 | 5 | 4 | –7 | –11 |
| 1-059-10 | 837.662 | 7 | 837.665 | 6 | 837.641 | 12 | 3 | –21 | –24 |
| 1-061-00 | 851.691 | 5 | 851.700 | 5 | 851.686 | 8 | 9 | –5 | –14 |
| 1-071-00 | 683.147 | 5 | 683.154 | 4 | 683.142 | 5 | 7 | –5 | –12 |
| 1-074-00 | 711.440 | 5 | 711.449 | 10 | 711.425 | 8 | 9 | –15 | –24 |
| 1-076-00 | 812.618 | 5 | 812.620 | 5 | 812.625 | 6 | 2 | 7 | 5 |
| 1-076-01 | 810.347 | 5 | 810.350 | 5 | 810.352 | 7 | 3 | 5 | 2 |
| 1-077-00 | 829.410 | 5 | 829.413 | 8 | 829.414 | 7 | 3 | 4 | 1 |
| 1-077-10 | 837.967 | 5 | 837.976 | 5 | 837.970 | 7 | 9 | 3 | –6 |
| 1-082-10 | 650.190 | 5 | 650.186 | 7 | 650.183 | 13 | –4 | –7 | –3 |
| 1-093-00 | 670.597 | 5 | 670.603 | 6 | 670.609 | 6 | 6 | 12 | 6 |
| 1-097-00 | 570.794 | 5 | 570.797 | 7 | 570.808 | 9 | 3 | 14 | 11 |
| 1-101-10 | 641.992 | 5 | 642.010 | 6 | 642.007 | 9 | 18 | 15 | –3 |
| 1-101-30 | 484.808 | 5 | 484.818 | 7 | 484.813 | 12 | 10 | 5 | –5 |
| 1-111-10 | 612.404 | 5 | 612.398 | 7 | 612.381 | 13 | –6 | –23 | –17 |
| 1-118-00 | 546.254 | 5 | 546.249 | 6 | 546.265 | 7 | –5 | 11 | 16 |
| 1-120-00 | 608.969 | 5 | 608.972 | 7 | 608.968 | 8 | 3 | –1 | –4 |
| 1-123-00 | 523.939 | 5 | 523.945 | 7 | 523.944 | 9 | 6 | 5 | –1 |
| 1-132-10 | 616.462 | 10 | 616.463 | 9 | 616.436 | 7 | 1 | –26 | –27 |
| 1-133-10 | 647.553 | 5 | 647.556 | 4 | 647.560 | 8 | 3 | 7 | 4 |
| 1-136-00 | 711.940 | 5 | 711.937 | 8 | 711.936 | 8 | –3 | –4 | –1 |
| 1-140-00 | 588.184 | 5 | 588.176 | 7 | 588.172 | 6 | –8 | –12 | –4 |
| 1-141-00 | 489.751 | 5 | 489.738 | 10 | 489.760 | 8 | –13 | 9 | 22 |
| 1-144-00 | 476.672 | 5 | 476.667 | 8 | 476.685 | 6 | –5 | 13 | 18 |
| 1-157-00 | 466.156 | 5 | 466.167 | 7 | 466.171 | 10 | 11 | 15 | 4 |
| 1-161-00 | 581.868 | 5 | 581.868 | 8 | 581.875 | 8 | 0 | 7 | 7 |
| 1-173-00 | 239.914 | 5 | 239.916 | 5 | 239.910 | 6 | 2 | –4 | –6 |
| 1-179-00 | 522.487 | 5 | 522.483 | 7 | 522.490 | 11 | –4 | 3 | 7 |
| 1-190-08 | 707.132 | 8 | 707.142 | 8 | 707.124 | 12 | –12 | –8 | –18 |
| 1-202-01 | 622.405 | 5 | 622.403 | 6 | 622.404 | 10 | –2 | –1 | 1 |
| 2-001-00 | 825.997 | 5 | 825.987 | 2 | 825.978 | 9 | –10 | –19 | –9 |
| 2-005-00 | 818.525 | 5 | 818.520 | 9 | 818.503 | 17 | –5 | –22 | –17 |
| 2-100-00 | 643.555 | 5 | 643.569 | 5 | 643.560 | 8 | 14 | 5 | –9 |
| 2-107-00 | 776.278 | 5 | 776.276 | 7 | 776.276 | 10 | –2 | –2 | 0 |
| 2-111-00 | 623.737 | 5 | 623.734 | 7 | 623.740 | 9 | –3 | 3 | 6 |
| 2-116-10 | 562.679 | 5 | 562.676 | 6 | 562.693 | 11 | –3 | 14 | 17 |
| 2-145-00 | 516.210 | 5 | 516.203 | 8 | 516.235 | 6 | –7 | 25 | 32 |
| 2-146-00 | 490.001 | 5 | 489.992 | 8 | 490.007 | 7 | –9 | 6 | 15 |
| 2-173-00 | 344.982 | 5 | 344.974 | 9 | 344.970 | 8 | –8 | –12 | –4 |
| 2-201-00 | 577.692 | 5 | 577.685 | 9 | 577.693 | 6 | –7 | 1 | 8 |
| 2-205-00 | 647.433 | 5 | 647.434 | 7 | 647.440 | 12 | 1 | 7 | 6 |
| mean values | | 5 | | 7 | | 9 | 1,3 | 0,4 | –1,1 |

*Table 4: Comparisons on a sample of 47 main base stations of the ÖSGN*

is the investigation in slow changing gravity in the area of the Central Alps. Possible reasons are the changing of the air pressure in wide surroundings and the seasonal changing in the hydrological equilibrium. This effects will also cause different loading of the earthcrust and its response in deformations [14]. The graph of the observation – series is shown in figure 5. An evidence of a correlation to the effects mentioned above is not yet produced. Also the uplift of the Alps (1mm/y) calculated with levelling data [3] does not expect increasing of the gravity. Possible explanations may be found in changing of the water budget in this area. Further investigations will be done.

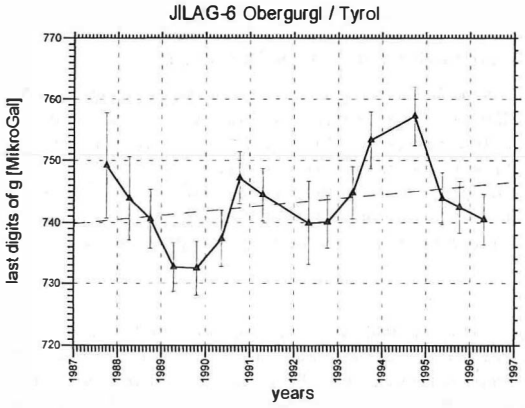


*Fig. 5: Repeated absolute gravity measurements in the Central Alps.*

## 7. Conclusion

It was shown that three different methods of adjustments of the Austrian Gravity Base Network (ÖSGN) give the same results within the accuracy of the adjusted values. The accuracy of gravity at the stations is better than $8 \cdot 10^{-8}$ m/s$^2$ (8 μGal). Therefore a high precision base network is available in Austria for all tasks in Gravity.

**References:**


[1] *Boedecker G., Marson I., Wenzel H.G., 1994:* The Adjustment of the Unified European Gravity Network 1994 (UEGN 94). Gravity and Geoid, IAG Symposium 113, Graz, Springer.

[2] *Csapó G., Meurers B., Ruess D., Szatmári G., 1993:* Interconnecting Gravity Measurements between the Austrian and the Hungarian Network. Geophysical Transactions, Vol.38, No.4, 251–259.

[3] *Höggerl N., 1989:* Rezente Höhenänderungen in Österreich abgeleitet aus Präzisionsnivellement – Messungen. Tagungsber. 5. Int. Alpengrav. Kolloquium Graz 1989. Österr. Beiträge zu Meteorologie und Geophysik, Heft2, Wien.

[4] *Marson I., Steinhauser P., 1981:* Absolute Gravity Measurements in Austria. EOS, Trans. Am. Geoph. Un., Vol. 62, 258.

[5] *Ruess D., 1985:* Aufbau des Österreichischen Schweregrundnetzes. Tagungsber. 3. Int. Alpengravimetrie- Kolloquium. Leoben 1983. Berichte über den Tiefbau der Ostalpen, 17–28, Wien.

[6] *Ruess D., 1988:* Stand des Österr. Schweregrundnetzes und des digitalen Geländemodelles. Tagungsbericht über das 4. Int. Alpengravimetrie- Kolloquium, Wien 1986. Berichte über den Tiefbau der Ostalpen, 159–164, Wien.

[7] *Ruess D., Steinhauser P., Jeram G., Faller J., 1989:* Neue Absolutschweremessungen in Österreich. Tagungsber. 5. Int. Alpengravimetrie-Kolloquium Graz 1989, Österr. Beitr. zu Meteorol. u. Geophysik, 2, 95–110, Wien.

[8] *Ruess D., 1993:* Schwerevariationen im Alpinen Raum. Tagungsber. 6. int. Alpengravimetrie-Kolloquium Leoben 1993, Österr. Beitr. zu Meteorol. u. Geophysik, Heft 8, 113–126, Wien.

[9] *Ruess D., Gold W., 1995:* The Austrian Gravity Base Net 1995 stabilised by Absolute Gravity Measurements and Connected to the European Network Adjustment. Posterpresentation, XXI. IUGG general meeting, Boulder, Colorado, USA.

[10] *Ruess D., 1995:* Das Österreichische Schweregrundnetz. EVM Nr. 80, Wien.

[11] *Ruess D., 1995:* Die Absolutschwerestation Obergurgl. Institut für Hochgebirgsforschung der Leopold-Franzens-Universität Innsbruck, Jahresbericht 1995, 57–60.

[12] *Reißmann, 1976:* Die Ausgleichungsrechnung. VEB, Berlin.

[13] *Stanek H., 1990:* Analyseausgleichung zur Interpretation geodätischer Netze. Geowiss. Mitt. d. TU-Wien, Bd.36, Wien.

[14] *Van Dam T.M., Wahr J.M., 1987:* Displacements of the Earth's Surface Due to Atmospheric Loading: Effects on Gravity and Baseline Measurements. J. Geoph. Res., Vol. 92, No. B2, 1281–1286.



*Adress of the Authors:*

Dr. Diethard Ruess, Dipl.-Ing. Wolfgang Gold, Federal Institute of Metrology and Surveying, Schiffamtsgasse 1–3, A-1025 Wien.



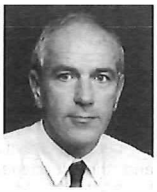

# Calibration of Digital Levelling Systems

*A. Reithofer, B. Hochhauser, F.K. Brunner, Graz*

**Abstract**

Since the introduction of the first digital level by Leica in 1990, this type of equipment is rapidly gaining acceptance in high precision levelling. A digital levelling system consists of the following main components: coded invar staff, illumination of staff, atmospheric propagation path, optics of the level, automatic compensator and electro-optical linear array. Therefore the complete system needs to be calibrated in order to assess its accuracy performance over a wide range of conditions.

A new vertical comparator has been developed for the calibration of digital levelling systems. The coded invar staff can be positioned vertically to better than 2 μm using a laser interferometer. The digital level can be positioned anywhere between 5 to 30 m from the staff. The true errors of the height differences can be determined as a function of distance from the difference between the vertical comparator and the digital level readings.

The performance of two digital levelling systems has been investigated in great detail. In the Leica NA 3000/3 results a clear periodic effect was discovered. The periods of this effect are distance dependent and range between 1 and 3 mm with amplitudes of up to 0.2 mm. The periodic nature of this effect raises the question of the correct choice of the sampling interval of the vertical comparator which is addressed. The specified RMS of double run levelling can be confirmed for the NA 3003, however, the accuracy of single height measurements is affected by the periodic effect. The results of the calibration of the Zeiss DiNi10 equipment do not exhibit any periodic effect. In conclusion, the calibration of digital levelling systems is recommended as part of the required quality control.

**Zusammenfassung**

Das Digitalnivellier und die dazugehörigen Invarcodelatten bilden jeweils das zu prüfende Meßsystem. Dazu wurde ein neuer Vertikalkomparator entwickelt, mit dem die lotrecht gestellten Codelatten um beliebige Intervalle mit Hilfe des Laserinterferometers automatisch positioniert werden können. Das Digitalnivellier ist meßgerecht in einer frei wählbaren Entfernung zwischen 5 m und 30 m aufgestellt. Die Beleuchtung der Latten wurde durch die Messung der Spektralverteilung optimiert.

Die Genauigkeiten der Digitalnivelliere LEICA NA3000/3 und ZEISS DiNi10 wurden unter Meßlaborbedingungen bei konstantem Klima untersucht. Bei den Typen NA3000/3 wurde eine Grundschwingung der Abweichungen von den Sollwerten, deren entfernungsabhängige Perioden zwischen 1 und 3 mm liegen, festgestellt. Die korrekte Wahl der Abtastung der Höhenablesung für die Kalibrierung bei Vorliegen eines periodischen Effektes wird geklärt. Bei einer Zielweite von 14,97 m tritt ein Maximum eines Überlagerungseffektes auf, der die Amplituden bis 0,5 mm vergrößert. An der Reduktion dieses Effektes wird bereits intensiv gearbeitet. Es sind bei Zielweiten zwischen 20 und 25 m maximale Amplituden von 0,2 mm der Abweichungen vorhanden, sodaß unter Berücksichtigung einer annähernden Gleichverteilung der mittlere Kilometerfehler eines Doppelnivellements – nach Herstellerangaben von 0,4 mm/km – eingehalten werden kann. Die Spezifikation des mittleren Fehlers einer Einzelmessung von $\pm$ 0.03 mm kann nicht bestätigt werden. Die ersten Untersuchungen des Digitalnivelliers Zeiss DiNi10 ergaben eine sehr hohe Genauigkeit unabhängig von der Distanz und es sind keinerlei periodische Effekte erkennbar. Diese Untersuchungen werden fortgeführt.

Schließlich wurde festgestellt, daß es zwischen den einzelnen Typen der Nivelliersysteme erhebliche Genauigkeitsunterschiede gibt, sodaß eine Kalibrierung jedes Meßsystems im Sinne einer Qualitätskontrolle der Meßmittel zu empfehlen ist.

## 1. Introduction

Since the introduction of the first digital level by Leica in 1990, [1], [2], this type of equipment is rapidly gaining acceptance in high precision levelling. A digital levelling system consists of a coded invar staff and an automatic level with an electronic eye piece in order to achieve an automatic horizontal height reading of the staff.

A new calibration facility has been developed for digital levelling systems using a vertical comparator in the measurement laboratory of the TU Graz. The performance of two digital levelling systems (Leica and Zeiss) has been investigated in great detail using this new vertical comparator. The results of these calibration tests are presented as functions of the sight length and the height reading on the staff.

## 2. Measurement System

The complete measurement system of a digital level consists of several basic elements (Fig.1). The first basic element is the staff with a known code of the sequence of black and white fields. Naturally, the staff has to be illuminated. Next, the coded information propagates through the atmosphere which causes refraction and scintillation of the staff image. Then the staff image passes through the optics and the automatic compensator of the level. A beam splitter directs the staff image on a linear CCD array. Finally the staff reading can be computed using the image and known code information. This process depends on the design of the levelling system. In the case of the Leica level the correlation between the staff image and the known staff code is calculated which will depend on the distance and on the height reading.

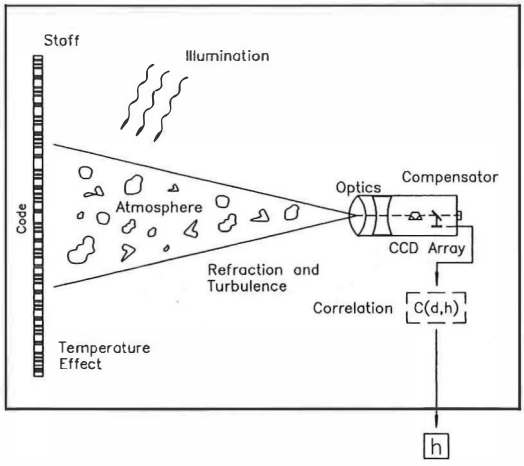


*Fig. 1: Measurement system of a digital level*

It would be a formidable task to calibrate each of these basic elements. Therefore it is of advantage to calibrate the measurement system as a whole, varying the height of the staff and the distance of the staff to the level. Since this calibration yields relative height information only, the standard level test continues to be mandatory for field work.

## 3. Vertical Comparator

The TU Graz is the owner of a temperature controlled (20°C $\pm$ 0,5°C) measurement laboratory [3] with a range of calibration facilities. During the past two years a vertical comparator for digital levelling systems has been developed

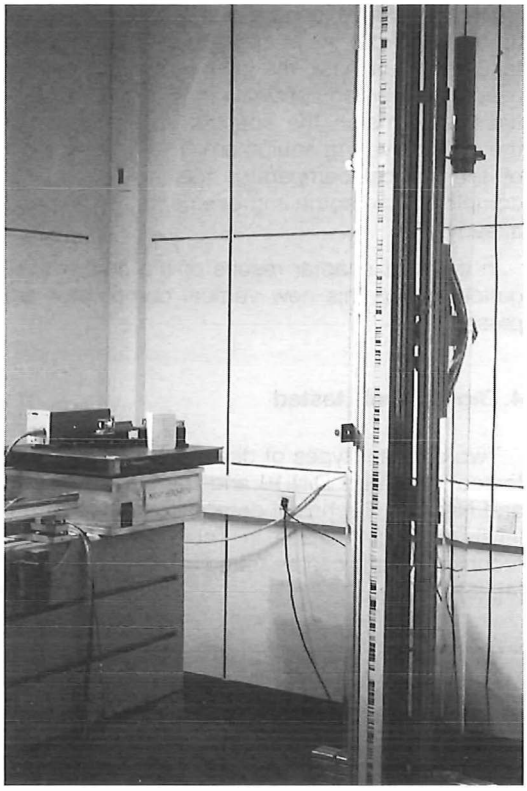

*Fig. 2: Vertical comparator and laser interferometer*

(Fig. 2). A special shaft was built in order to move the staff up und down by $\pm$ 3 m using 3 m long standard invar staffs. The staff is attached to a vertical rail system on which the staff can be moved vertically. The motion is controlled by the laser interferometer. The vertical comparator design adheres to the Abbé principle (Fig. 3). Using a feed-back control system it is possible to position the staff with an accuracy of 2 $\mu$m.

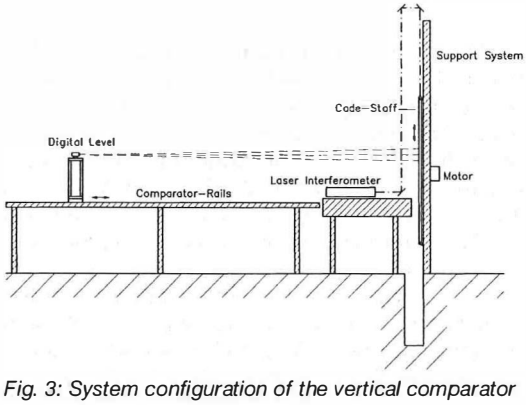


*Fig. 3: System configuration of the vertical comparator*

The digital level can be positioned in distance up to 30 m from the staff. Special care has been taken to illuminate the staff. Four lamps are used with a broad spectral range which was optimised to match the spectral requirements of the digital levelling equipment. The development of the vertical comparator has not been fully completed and some improvements are planned already.

In the next chapter results of the first investigations using this new vertical comparator are presented.

## 4. Digital levels tested

Two different types of digital levels have been tested: the Zeiss DiNi10 and the Leica NA3000 and NA3003. Technical details of the two digital levels are summarised in Table 1, and further technical details can be found in the publications [4], [5] and [6].

| | ZEISS DiNi10 | LEICA NA3003 |
|---|---|---|
| Code field | 0,3 m | 2° |
| Measuring range | 1,5 – 100 m | 1,8 – 60 m |
| Setting accuracy of Compensator | 0,2″ | 0,3″ |
| RMS of 1 km double run levelling | 0,3 mm | 0,4 mm |
| RMS of single pointing, good atmospheric conditions | | 5 m : < 0,01 mm<br>10 m : 0,01 mm<br>20 m : 0,03 mm<br>30 m : 0,05 mm |

*Table 1: Specifications of the digital levels tested*

There are several important differences between the two levelling systems which were tested. The code field measured by the Zeiss level is 30 cm independent of the distance, whilst the Leica level uses an angle of two degrees. For the fine measurements the Zeiss level uses 15 black and white intervals, however, the Leica level uses for this purpose a correlation function. This correlation function depends on two variables: the distance to determine the scale of the staff image and the staff reading for obtaining the required codeshift. Another important difference is that the basic interval of the Zeiss code is 20 mm, with some coded elements in it, whilst the basic chip length of the Leica code is 2.025 mm.

## 5. Results

The final result of a calibration test is the variation of height deviations which are calculated as the differences between the vertical comparator readings and the digital level results. These deviations can be considered true measurement errors of the digital levelling system.

The Zeiss DiNi10 was analysed with a 2 m staff, and distances between 10 and 25 m were used. Fig. 4 shows the true deviations of these test runs. The range of the true deviations is less than 0.1 mm with a very uniform pattern at all distances used. The staff readings were sampled with an interval of 10 cm. The RMS is calculated for each of the distances and the overall RMS is about 0.02 mm.

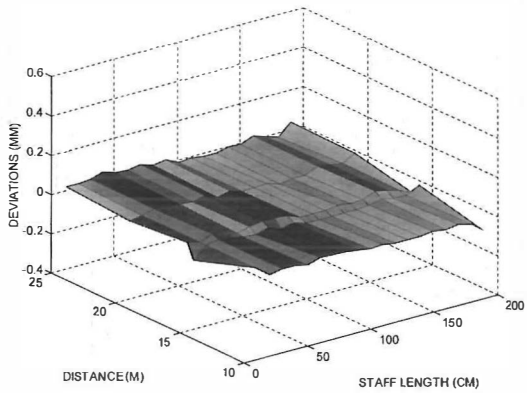


*Fig. 4: Deviations of DiNi10 level readings*

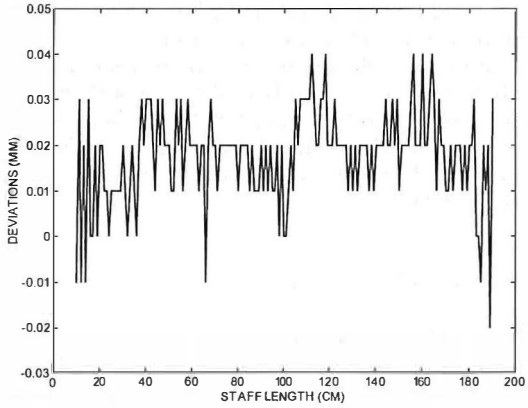


*Fig. 5: Deviations of DiNi10 results at a distance of 20 m and sampling interval of 10 mm*

It is of some concern that the staff readings were sampled at the rather arbitrary interval of 10 cm, and therefore larger but undetected deviations could still be hidden inside the 10 cm intervals. Thus the measurements were repeated with a 10 mm interval (Fig. 5). Additionally an interval of 0.5 mm was used which means that the staff is shifted after every measurement by 0.5 mm. This result shows a range of 0.06 mm for the true measurement errors and there is no pattern apparent in these results. In summary, the calibration tests fully confirmed the specification of the Zeiss DiNi10.

The Leica levels NA3000 and NA3003 were tested using a 3 m invar staff and again a distance range from 10 to 25 m at certain intervals. The results (Fig. 6) show a rather large deviation at a distance of 14.97 m. This effect was already discussed in a previous publication [7]. The reason for this effect is that at the distance of 15 m the picture of the code chip length of 2.025 mm is very close to the pixel length of 25 µm of the linear array. Therefore a problem occurs at that particular distance. The "sharpness" of this effect is of practical interest and therefore tests were carried out at several distances between 14.9 and 15.1 m. The effect disappears rather rapidly by moving away from the 14.97 m distance value. This is shown as the rather "flat area" before the "15 m effect" in Fig. 6. Larger deviations also occurred at a staff height of 2 m whose origin could not be clarified at the time of writing this paper.

The results shown above were sampled using a 10 cm interval, which used to be the "standard sampling rate" at the time of these tests. However, as already mentioned above, it has been decided to sample at much shorter intervals because the 10 cm sampling interval may not reveal the full "picture". The fundamental Shannon's sampling theorem states that the full information of a signal can only be obtained if the signal is sampled faster than twice the highest frequency of the signal. Fig. 7 shows the result of the 2 mm sampling of the height deviations at the distance of 19 m. An enlargement of this figure revealed a clear periodic oscillation. Of course the sampling rate of 2 mm might still not be the correct value, because there could be an aliasing effect present. Therefore it was decided to sample at intervals of 0.7 mm and 0.25 mm. Fig. 8 shows the results of both measurements which demonstrate clearly that the results are independent of these two sampling rates. Therefore the smallest period of this periodic oscillation of the true deviations was found to be

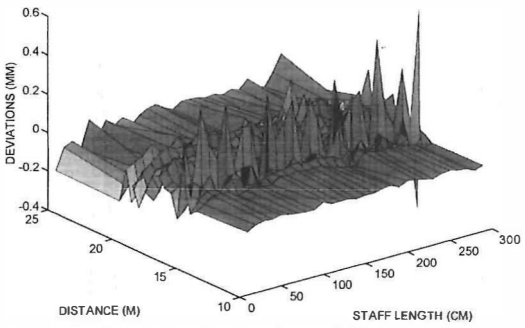


*Fig. 6: Deviations of NA3000/3 readings*

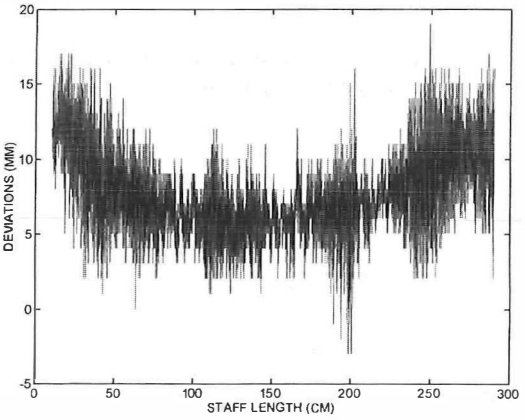


*Fig. 7: Deviations of NA3000/3 results at a distance of 19 m and sampling interval of 2 mm*

2.5 mm with an amplitude of 0.15 mm. The power spectrum shows (Fig. 9) a definite peak for this particular measurement result.

Fig. 10 summarises the power spectra measured at different distances which show significant periods of 1 mm to 3 mm. The amplitudes

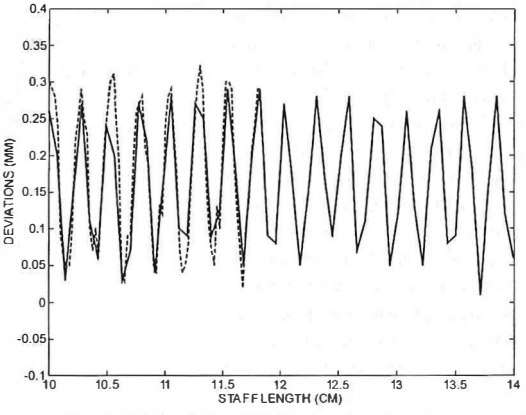


*Fig. 8: Deviations of NA3000/3 results at a distance of 19 m and sampling interval of 0.7 mm and 0.25 mm*

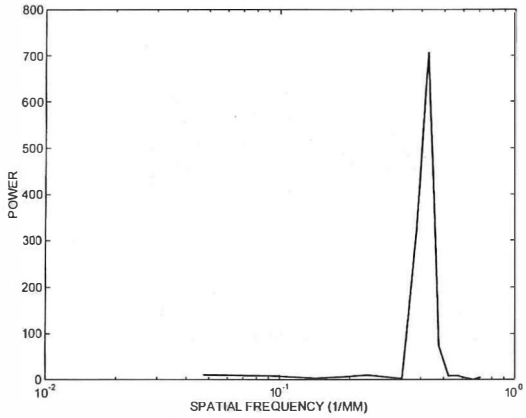


*Fig. 9: Power spectrum of NA3000 results at a distance of 19 m and sampling interval of 0.7 mm*

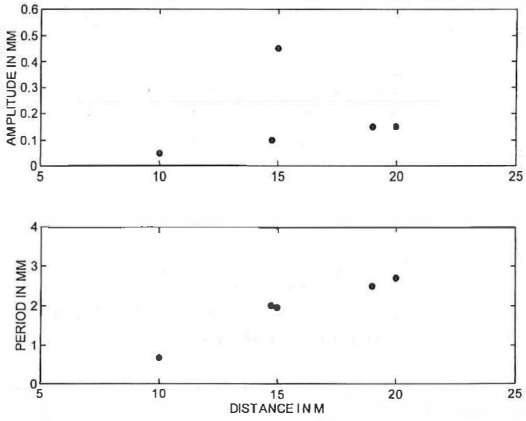


*Fig. 10: Summary of power spectra for the NA3000/3 results*

of these periodic oscillations are below 0.2 mm except at a distance of 15 m.

The important question is what causes such periodic oscillations in the results. There is a certain agreement of the 2.025 mm code chip length and the pixel size of the linear array. Therefore by forming the correlation function of the image and the code a new periodic function might be created. It has been suggested (H. Ingensand, personal communications) that by working in the open air this effect disappears because atmospheric turbulence randomises the effect. In order to test this explanation an experiment was carried out in the open air. The results of this experiment (Fig.11) show that the periodic pattern which was detected in the measurement laboratory also occurred using an open air propagation path.

## 6. Discussion

For the sight length of 20 m and a staff length of 2 m the calibration results under laboratory conditions yielded a RMS of $\pm$ 0.017 mm for the Zeiss DiNi10 levelling system and a RMS of $\pm$ 0.032 mm for the Leica NA3000 levelling system. These values are to be considered preliminary results as only one (Zeiss) and two (Leica) instruments have been tested so far.

A periodic oscillation of the true deviations of NA3000/3 levelling system was discovered. The amplitudes and periods of this periodic effect are distance dependent. Fig.10 shows maximum values of 0.2 mm for the amplitudes of this periodic effect if the values at the distance of 14.97 m are excluded. In view of this result, it appears necessary to explain the RMS of double run levellings as quoted in Table 1. Considering the periodic nature of the deviations, the RMS in a single staff reading, $\sigma_i$, needs to be calculated using an uniform probability density distribution. Using an amplitude of 0.2 mm, $\sigma_i$ is calculated as $\sigma_i = 0.2/\sqrt{12} = 0.06$ mm. For an average sight length of 25 m, the RMS of 1 km double run levelling is calculated as $0.06\sqrt{20} = 0.27$ mm. This

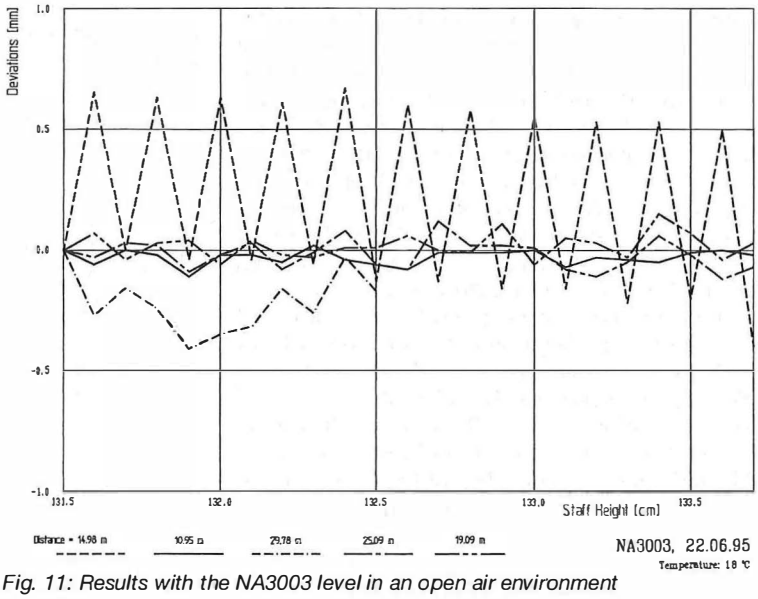


*Fig. 11: Results with the NA3003 level in an open air environment*

result is in agreement with the appropriate specification of line levelling as shown in Table 1 for the NA3003, which have been fully confirmed by all known practical measurements, e.g. [2]. However, the specifications for individual staff readings (Table 1) could not be confirmed by the calibration tests due to the periodic effect present in the true deviations of the NA3000/3 results. These results are summarised in Fig. 10. Therefore the accurate measurement of small height changes as frequently required in industrial applications would be affected by this periodic effect.

The periodic effect of the NA3000/3 equipment which was discovered by the present investigation raises also the fundamental question about the choice of the proper sampling interval for the calibration of a digital levelling system. Shannon's sampling theorem requires the sampling period to be shorter than half the shortest period of the signal which is represented by the true deviations of the height reading in the present case. Fig.10 also allows to determine the required sampling period using the appropriate periods of the periodic effect as a function of distance.

**Acknowledgements**

The calibration facility was developed under the guidance of Professor Dr. G. Schelling. Most of the measurements were carried out by B. Mölg and his help is gratefully acknowledged.

**References**

[1] *Ingensand H, (1990)* Das WILD NA2000, Das erste Digitalnivellier der Welt, Allgemeine Vermessungsnachrichten 97

[2] *Schauerte W, (1991)* Untersuchungen zur Leistungsfähigkeit des Digitalnivelliers WILD NA2000, Vermessungswesen und Raumordnung 53

[3] *Reithofer A, Schlauf S, (1992)* Geodäsie – Meßlabor der TU Graz, Ingenieurvermessung 1992, Ferd. Dümmler-Verlag, Bonn

[4] *Feist W, Gürtler K, Marold T, Rosenkranz H, (1995)* Die neuen Digitalnivelliere DiNi10 und DiNi20, Vermessungswesen und Raumordnung 57

[5] *Ingensand H, (1995)* Neue digitale Nivelliertechniken und ihre Anwendungen, Vermessung, Photogrammetrie, Kulturtechnik 93

[6] *Schauerte W, (1995) Erste Untersuchungsergebnisse zum neuen DiNi10 – Digitalnivellier der Fa. Carl Zeiß, Vermessungswesen und Raumordnung 57*

[7] *Reithofer A, (1993)* Überprüfung des Digitalnivelliersystems WILD NA3000/GPCL, Festschrift Prof. Schelling, Mitteilungen der geodätischen Institute der TU Graz, Folge 78

*Address of the authors:*

A. Reithofer, B. Hochhauser and F.K. Brunner, Department of Engineering Geodesy, TU Graz, Steyrergasse 30, A-8010 Graz.




# Austrian Geoid 2000

*Erhard Erker, Vienna;*
*Bernhard Hofmann-Wellenhof,*
*Helmut Moritz, Hans Sünkel, Graz*

**Abstract**

By the impact of the relative GPS accuracy of 1 ppm to 0.1 ppm (for longer baselines), the Austrian geoid with its present mean accuracy of about 1 ppm is no longer considered to be sufficiently consistent. For this reason, a new computation of the Austrian geoid was initiated with the objective to obtain a relative accuracy of at least 0.5 ppm throughout the country. The project is denoted as Austrian Geoid 2000 to indicate that the resulting product is intended to survive the turn of the century.

The new computation of the Austrian geoid will be performed by three approaches, (1) the conventional least squares collocation method, (2) the fast collocation method which implies gridded input data and a symmetric block Toeplitz matrix for the covariance function, and (3) the gravimetric solution by the Fast Fourier Transform based on either a planar approximation or a spherical approach for the kernel functions.

As far as Austria is concerned, the data input consists of a 50 × 50 m digital terrain model, some 30.000 gravity data, about 700 deflections of the vertical, and GPS derived points. From the neighboring countries, gravity and height information is available in different quality and density.

## 1. Least squares collocation today

Slightly more than a quarter of a century ago, the estimation of linear functionals of the anomalous potential based on heterogeneous and noisy gravity data, one of the key problems in physical geodesy, was not yet solved. The mathematical solution of this problem was given by [6] and extensively elaborated by [8] and other scientists and is known as "least squares collocation" (LSC).

The theoretical beauty of LSC has one practical drawback: the processing quickly exceeds the computational capacity of the computer because the solution time increases with the third power of the size of the data set. Therefore, numerous efforts have been made in tuning LSC to manage large data sets.

Among the various methods, the following techniques have been applied frequently and are capable of reducing the LSC computational effort:

a) The LSC patchwork method. The area under consideration is subdivided into a number of overlapping subareas. For each subarea, the LSC solution is performed. The solution for the whole area is obtained by "glueing" together (in a mathematical sense) the subarea solutions.
b) LSC with finite covariance functions. The correlation of data decreases with the separation of the data points. Data with a large spatial separation are almost uncorrelated. Therefore, using a covariance function with finite support produces a band-structured covariance matrix which significantly reduces the computational effort for LSC processing of large areas.
c) Local LSC solutions. Data interpolation and differentiation are mainly affected by the local data environment; the effect of remote data is often negligible. Based on this principle, local LSC solutions with only a small data set can be obtained very efficiently by updating the inverse covariance matrix and the solution vector when the prediction point is moved over the prediction area.
d) Fast Fourier Transform (FFT) solution. For planar gridded homogeneous data sets with homogeneous noise and a covariance function depending on the planar distance, the covariance matrix is a block Toeplitz matrix consisting of symmetric Toeplitz blocks. This specific situation offers the transformation of the LSC solution into the frequency domain by means of the FFT algorithms, cf. Eren [2]. However, errors due to edge effects caused by the finite grid must be carefully considered.
e) Fast collocation. For homogeneous data with homogeneous data noise on a geographical grid and a covariance function depending on the spherical distance, the covariance matrix, due to the convergence of meridians, has no longer the block Toeplitz structure of symmetric Toeplitz blocks. The symmetric Toeplitz structure of each block is preserved, but the block Toeplitz structure is lost. This fact can be overcome as outlined below (Sect. 2.2).

## 2. The Austrian Geoid 2000

Due to the steadily increasing accuracy requirements, a new effort will be made to recompute the Austrian geoid. For reasons of comparison, three groups will compute independently three different methods: (1) the conventional least squares collocation, (2) the fast collocation, and (3) a gravimetric solution by using the FFT. Some brief explanations of the typical characteristics of these methods are given.

### *2.1. Conventional least squares collocation*

The main input source for the geoid used so far in Austria are deflections of the vertical. The new solution will use heterogeneous data, i.e., gravity data and deflections of the vertical. In addition, GPS data will be used to account for the datum problem.

Details on the solution as realized in the GRAVSOFT program package are given by [14]. This program uses stepwise least squares collocation. The method requires data sets with known standard deviations and, in addition, isotropic covariance functions being specified by a set of empirical anomaly degree-variances. For the input of observations, the GRAVSOFT program package allows potential coefficients, mean or point gravity anomalies, height anomalies, deflections of the vertical, gravity gradients, and density contrasts.

### *2.2 Fast collocation*

Among the previously described methods, the favorite candidate is fast collocation because it is both extremely efficient and provides at the same time an exact solution on the sphere (in contrast to the planar FFT approach). The idea of fast collocation is simple: for a small area on the sphere, a planar grid may be used as a good approximation for a geographical grid. As a consequence, the block Toeplitz structure of the covariance matrix for the planar case may be used as a good approximation for the non-block Toeplitz structure of the covariance matrix for the geographical case.

Following [1], the covariance matrix $C$ may be split into

$$C = \tilde{C} + \delta C \qquad (1)$$

where $\tilde{C}$ represents the block Toeplitz matrix of symmetric Toeplitz blocks, and the matrix $\delta C$ accounts for the deviation of the spherical from the planar case. The diagonal elements of each block correspond to the covariances between

data on the same meridian. Therefore, $\delta C$ has zeroes on each block diagonal. The size of the off-diagonal elements in each block depends on the grid size and can reach about 10% of the diagonal elements of $C$ for solutions such as the one considered here.

This small deviation suggests the application of an iterative solution with $\tilde{C}$ as the zero-order approximation of the covariance matrix. Denoting the data vector by $y$ and the solution vector by $x$, the iterative solution is accomplished by

$$\tilde{C}\, x_{n+1} = y - \delta C\, x_n. \qquad (2)$$

It is important to note that the product $\delta C x_n$ can be computed very rapidly if advantage of the structure of $\delta C$ is taken: by properly arranging the elements of $\delta C$ in a vector, the product $\delta C x_n$ can be transformed into a circulant convolution of two vectors which can be computed very efficiently by the Fast Hartley Transform (FHT) by taking into account the convolution theorem.

The convergence rate of Eq. (2) can be improved dramatically by a skillful preconditioning. Two conflicting requirements must be fulfilled by a preconditioner: first, it should be as simple as possible, and, second, it should be as close as possible to the inverse of the operator. The second requirement is certainly achieved by $\tilde{C}^{-1}$ as preconditioner. Therefore, the proposed collocation solution for the Austrian geoid project will focus on a preconditioned conjugate gradient method with incorporated FHT.

The proposed LSC solution will be supplemented by the usual data reduction due to residual terrain and a high resolution geopotential model. Gridded residual gravity data for Austria and all neighboring countries, at least 100 km beyond the Austrian border, will be used.

According to feasibility studies which have been conducted recently, a relative geoid accuracy of about 0.2 – 0.3 ppm may be expected for the entire country.

### 2.3. Gravimetric geoid by FFT techniques

The classical formula to determine the geoid from gravity data is the Stokes formula

$$N = \frac{R}{4\pi\gamma} \iint_{\sigma} \Delta g\, S(\psi)\, d\sigma \qquad (3)$$

where $N$ denotes the geoidal undulation, $R$ is the radius of a sphere, $\gamma$ is a mean value of gravity, $\sigma$ indicates the unit sphere, $\Delta g$ are the gravity anomalies, and $S(\psi)$ is the Stokes function. The gravity anomalies $\Delta g$ refer to the geoid. Thus, measured surface gravity data must be reduced to the geoid by a terrain reduction using height data (digital terrain model) and further reduced by the global geopotential model. The reduced data is used to generate the residual part of the geoid by means of (3). The final geoidal undulation results from the residual part, the reference undulation computed by the geopotential model, and the indirect effect (which may be derived from the height data).

The solution of the gravimetric method may be carried out conventionally (e.g., by numerical integration) or by the FFT technique. Several approaches for the FFT were developed: the planar approximation, see [10], the spherical approach, see [11], and other methods.

The principle of the planar approximation is expressed by the following equation

$$N(x_P, y_P) = \frac{1}{2\gamma} \iint_E \frac{\Delta g(x, y)}{\sqrt{(x_P - x)^2 + (y_P - y)^2}}\, dx\, dy \qquad (4)$$

where the geoidal height at $x_P$, $y_P$ is computed from $\Delta g$ in an area $E$. This approximation is now a two-dimensional convolution integral. The application of a two-dimensional FFT is straightforward. The error inherent in the planar approximation will grow with the integration area.

The drawback of the planar approximation may be circumvented by the spherical approach where the Stokes integral is transformed to a two-dimensional convolution integral by a modification of the Stokes function. The evaluation is performed on the sphere which causes the superiority compared to the planar approximation. However, [11] introduces also an approximation by using a mean latitude for each grid mesh. The geoid undulations for all grid points can simultaneously be computed by applying a two-dimensional FFT accordingly.

The Stokes function may also be expressed as a convolution in east-west direction (along a parallel), because the Stokes function is constant for all computation points on one parallel, cf. [7]. Applying a one-dimensional FFT, the simultaneous computation of geoid undulations on a parallel is possible without approximation as far as the Stokes function is concerned. This approach was proposed by [5].

Detailed formulas of these and other approaches may be found e.g. in [7] and in [9].

### 2.4. Available data sets

*Gravity data*

For Austria, some 32.400 gravity data is available at the Section of Physical Geodesy of the

Technical University Graz. This data was provided from several institutions: Institute of Meteorology and Geophysics of the University Vienna, Institute of Geophysics of the University Leoben, Austrian Petroleum Industry, Institute of Geophysics of the Technical University Clausthal, and the Federal Office of Metrology and Surveying. The data refer to the Austrian gravity network which is compatible with the international system IGSN71. The position parameters referring to the gravity data are related to the datum of the former Military Geographical Institute (MGI), i.e., a local datum associated with the Bessel ellipsoid. Using a grid with a mesh size of 2 x 2 km, the gravity data set may be reduced to 14.255 data for Austria.

*Deflections of the vertical*

At 683 homogeneously distributed points in Austria, deflections of the vertical are available. The data refers to the same local datum as the gravity data (datum of MGI associated with the Bessel ellipsoid). This data was the primary source of the previously computed Austrian astrogeodetic geoids, cf. [3], [4], [12], [13].

*GPS data*

From several campaigns, GPS data is ready to be used all over Austria. The main purpose of the introduction of GPS data is the possibility of an accurate datum relation. The GPS data refers to a geocentric system, e.g., the World Geodetic System 1984 (WGS-84). The most important Austrian campaigns since 1990 are the "Austrian Geodynamic Reference" campaigns AGREF90, AGREF92, and AGREF94. Some 75 GPS points established by these campaigns are located on Austrian territory.

*Digital terrain model*

The Federal Office of Metrology and Surveying provides a high resolution 50 x 50 m digital terrain model for Austria. The positions of the grid points are expressed in geographical coordinates $\varphi$, $\lambda$. The heights refer to the official Austrian height system consisting of normalorthometric heights associated with the datum point Molo Sartorio in Trieste, Italy.

*Surface density model*

The two-dimensional surface density model, cf. [15], was derived from a geological map of Austria comprising 40 regions and twelve different densities between 2000 and 2850 kg/m$^3$.

*Global earth model*

For the low to medium frequency part of the gravity field of the earth, a global geopotential model (e.g., OSU81 or the model being currently developed by DMA) will be used.

*Data of neighboring countries*

Gravity and DTM data of all neighboring countries, i.e., Germany (Bavaria and Baden-Württemberg), Czech Republic, Slovakia, Hungary, Slovenia, Italy, Switzerland, are available. The gridding of the data is different. However, all data will be transformed to mean values in a 3′ x 3′ grid. The densification of data is performed by prediction and interpolation, thinning is achieved by averaging data.

## 3. Conclusion

The three approaches, (1) the conventional least squares collocation method, (2) the fast collocation method, and (3) the gravimetric solution by the FFT will be computed independently from three different groups. After a comparison of the results, the Austrian geoid 2000 will be established. It is almost unnecessary to say that the fast collocation method will yield this Austrian geoid 2000. The reasons are the computational efficiency compared to the conventional least squares collocation method and the superiority with respect to input data compared to the purely gravimetric solution.

**Acknowledgment**

The authors express their sincere thanks to Konrad Rautz (Graz), Herbert Lichtenegger (Graz), Josef Graf (Vienna), and Volker Sturm (Vienna) for valuable support.

**References**

[1] *Bottoni GP, Barzaghi R (1993):* Fast collocation. Bulletin Geodesique, 67(2): 119–126.

[2] *Eren K (1982):* Toeplitz matrices and frequency domain collocation. Manuscripta geodaetica, 7: 85–116.

[3] *Erker E (1983):* Das Geoid in Österreich; Berechnungen des Bundesamtes für Eich- und Vermessungswesen. In: Österreichische Kommission für die Internationale Erdmessung (ed): Das Geoid in Österreich. Geodätische Arbeiten Österreichs für die Internationale Erdmessung, Neue Folge, Vol III: 89–115.

[4] *Grasegger J, Wotruba M (1983):* Geoidbestimmung; Berechnungen an der TU Graz, 1. Teil. In: Österreichische Kommission für die Internationale Erdmessung (ed): Das Geoid in Österreich. Geodätische Arbeiten Österreichs für die Internationale Erdmessung, Neue Folge, Vol III: 117–124.

[5] *Haagmans R, de Min E, van Gelderen M (1993):* Fast evaluation of convolution integrals on the sphere using 1D FFT, and a comparison with existing methods for Stokes' integral. Manuscripta geodaetica, 18: 227–241.

[6] *Krarup T (1969):* A contribution to the mathematical foundation of physical geodesy. Danish Geodetic Institute, Copenhagen, vol 44.
[7] *Li YC (1993):* Optimized spectral geoid determination. Reports of the Department of Geomatics Engineering of the University of Calgary, vol 20050.
[8] *Moritz H (1980):* Advanced physical geodesy. Wichmann, Karlsruhe.
[9] *She BB (1993):* A PC-based unified geoid for Canada. Reports of the Department of Geomatics Engineering of the University of Calgary, vol 20051.
[10] *Sideris MG, Schwarz KP (1985):* Computation of geoidal undulations and deflections of the vertical for Alberta. Alberta Bureau of Surveying and Mapping Contract Report No 84004, Edmonton, Alberta, Canada.
[11] *Strang van Hees G (1990):* Stokes formula using fast Fourier techniques. Manuscripta geodaetica, 15: 235–239.
[12] *Sünkel H (1983):* Geoidbestimmung; Berechnungen an der TU Graz, 2. Teil. In: Österreichische Kommission für die Internationale Erdmessung (ed): Das Geoid in Österreich. Geodätische Arbeiten Österreichs für die Internationale Erdmessung, Neue Folge, Vol III: 125–143.
[13] *Sünkel H, Bartelme N, Fuchs H, Hanafy M, Schuh W-D, Wieser M (1987):* The gravity field in Austria. In: Austrian Geodetic Commission (ed): The gravity field in Austria. Geodätische Arbeiten Österreichs für die Internationale Erdmessung, Neue Folge, vol IV: 47–75.
[14] *Tscherning CC, Forsberg R, Knudsen P (1992):* The GRAVSOFT package for geoid determination. In: Holota P, Vermeer M (eds): Proceedings of the First Continental Workshop on the Geoid in Europe, Prague, Czech Republic, May 11–14, 327–334.
[15] *Walach G (1987):* A digital model of surface rock densities of Austria and the Alpine realm. In: Austrian Geodetic Commission (ed): The gravity field in Austria. Geodätische Arbeiten Österreichs für die Internationale Erdmessung, Neue Folge, vol IV: 3–9.

*Addresses of the authors:*

Erhard Erker, Federal Office of Metrology and Surveying Schiffamtsgasse 1–3, A-1025 Vienna, Austria;
Bernhard Hofmann-Wellenhof, Helmut Moritz, Hans Sünkel, Technical University Graz, Steyrergasse 30, A-8010 Graz, Austria.




# The Austrian Geodynamic Reference Frame (AGREF) Motivation and Results

*Erhard Erker, Günter Stangl, Peter Pesec, Hans Sünkel, Vienna/Graz*

**Abstract**

A summary of the works on AGREF is presented and a review of the accuracy of the results is given. Some prospects of future related activities are mentioned.

**Zusammenfassung**

Die Arbeiten an AGREF werden zusammengefaßt, die Resultate in Hinblick auf ihre Genauigkeit durchleuchtet und die Zukunftsaussichten betrachtet.

## 1. Preliminary Remarks

This contribution presents the complementary written summary to a poster presented at the IUGG XXI General Assembly, Boulder, July 2–14, 1995. A special monograph which will contain details of the AGREF activities, including the final coordinates and station documentations, will be published in the course of 1996.

## 2. Objectives

The objectives remained the same as mentioned in [1], namely to establish a 3D homogeneous reference frame with a total r.m.s. of better than $\pm 1.5$ cm, to support the Austrian Geoid at the cm-level, to monitor regional crustal movements, and to link national and international networks.

In future AGREF may also be used for further objectives, like to provide base stations for DGPS and other real time applications.

## 3. Realization

### *3.1 Concept*

During the last years the accuracy of GPS-coordinates derived from continuous observation periods of some days could be improved in such a way that it competes with SLR/VLBI methods, without however replacing them for

global control and special applications like determination of geocentric coordinates and polar motion. Cheap permanently observing GPS-stations are under way to replace fundamental stations, equipped with all kinds of measurement devices, at least for geodynamical applications. The installation of the International GPS Geodynamic Service (IGS) and of the Central Europe Geodynamic Reference Network (CEGRN) was a logical consequence. Austria, presently, contributes with two permanent AGREF GPS-stations (Graz, Hafelekar/Innsbruck) to IGS and CEGRN and, temporarily, operates the AGREF stations Reisseck and Hutbigl for CEGRN.

This development led to a revision of the initial concept of AGREF to use only fundamental stations for linking AGREF to international and global networks by introducing a hierarchic structure. A subset of seven AGREF points (including Graz and Innsbruck) is planned to operate permanently, thus fulfilling all objectives of AGREF mentioned above. A further subset will be monitored periodically (about one week/year) mainly for geodynamic investigations. The remaining bulk of points should serve for national surveying objectives. It is well distributed over the whole national area with a spacing of about 50 km. Except for the improvement of accuracy of some "bad" points and the restitution of lost points no further activity is intended for the moment. Furthermore, a dense network (distances about 20 km) has been installed in a special area of tectonic movements (Carinthia-Friuli-Slovenia). There, measurements will be repeated periodically. Figure 1 presents the state of the art distribution of all Austrian and associated AGREF points.

### *3.2 Monumentation*

Based on the fact that most of the measurement errors are introduced by the definition of the reference point and eccentricity problems of the antennas special brass bolts were used as a cheap and reliable monumentation, which allows for a plain re-occupation without using tripods. All bolts were founded in bedrock, pillars or old buildings obeying the usual criteria for GPS-observations. Only very few points had to be observed at eccenters. Presently the distribution is as follows:

Austria: 81 points (bedrock 48, pillars 12, others 21)
Croatia: 11 points (bedrock 2, pillars 6, others 3)
Italy: 17 points (bedrock 8, pillars 4, others 5)
Slovenia: 20 points (bedrock 14, pillars 4, others 2)

These numbers are temporarily changing due to the inclusion of of new areas of interest.

### *3.3. Measurements*

During the years 1990–1995 99% of these points have been measured at least twice during several campaigns. Starting with Ashtech receivers, Trimble and Rogue receivers have been used during the last 3 years. The occupation time could be extended from six hours in 1990 to 24 hours in 1994, mainly due to the upgrading of the GPS space segment. All data were stored at the Graz observatory. During the 1992 campaign 25% of the Croatian and German receivers showed malfunctions in L2. Since, unfortunately, the bulk of points was observed during that campaign, this was a major setback for determining an accurate solution of AGREF.

## 4. Results

### *4.1 Adjustment*

The computations were carried out using the Bernese Software in its various versions (mainly 3.4), adopting ITRF92 at epoch 1988.0 as the reference frame. The results of the campaigns prior to 1992 were transformed to this solution via identical points. The main complications were introduced by the 1992 data, which had to be processed at least twice to get reasonable results for most of the points.

All sessions were computed independently. The final coordinates and their r.m.s errors were computed from those daily solutions. All important session products have been stored at the Graz observatory.

### *4.2 Results*

During the last years the update of the satellite constellation and the availability of precise orbits and clocks provided by IGS led to a considerable increase of the accuracy of GPS-derived coordinates which is demonstrated by the following statistics:

46% of all points have an r.m.s. of below $\pm 1$ cm;
27% of all points have an r.m.s. of between $\pm 1$ and $\pm 2$ cm;
27% of all points fail the required accuracy requirements and need additional measurements.

All points failing the required accuracy were determined during 1990 or 1992. The main problem concerns the height component, because 69% of all points have horizontal r.m.s. of below

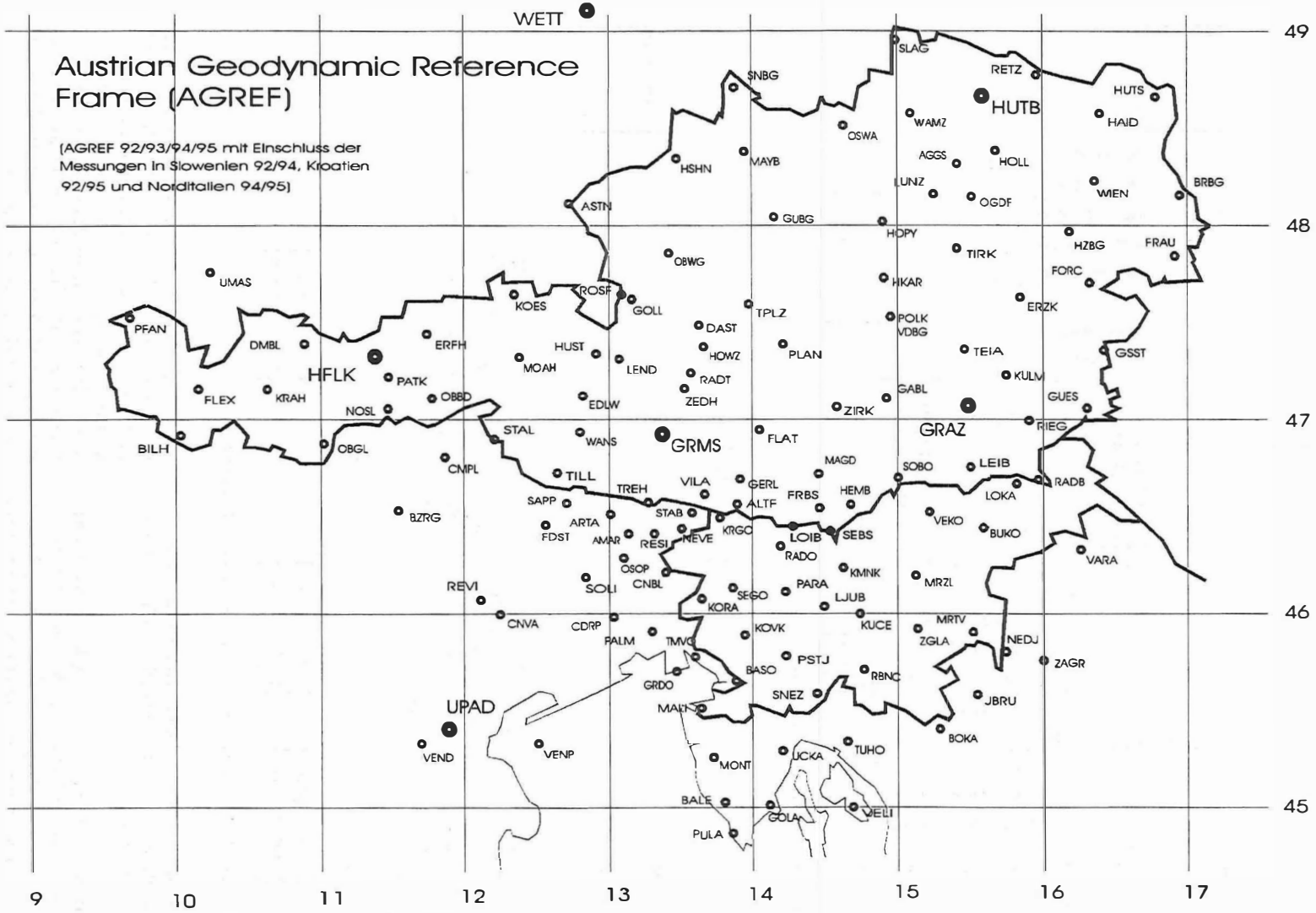


*Fig. 1 : Distribution of AGREF points; status end of 1995.*

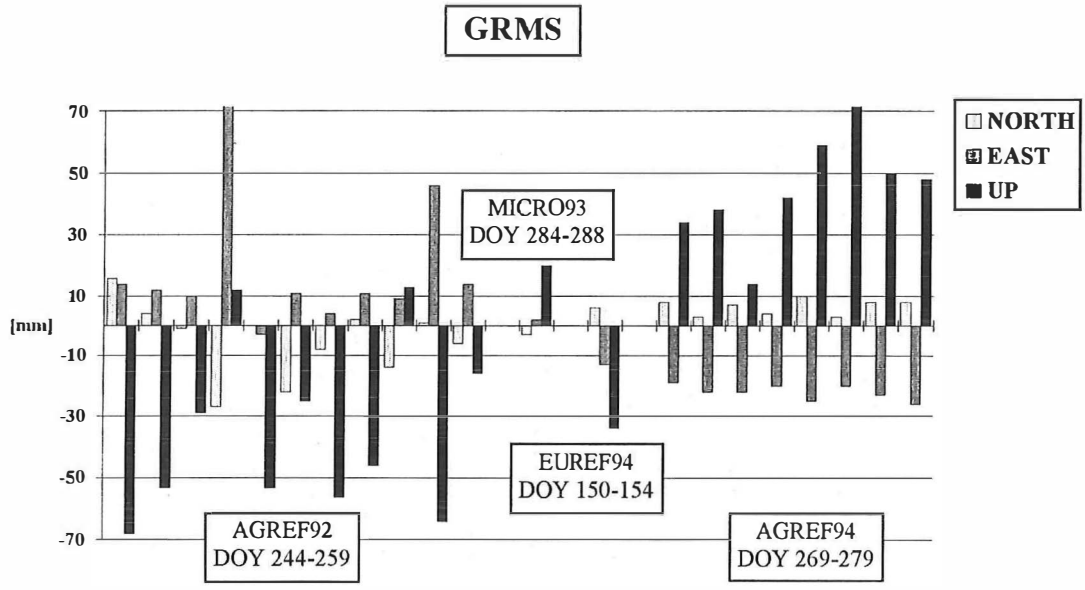


*Fig. 2 : AGREF Session Differences (Bad Example)*

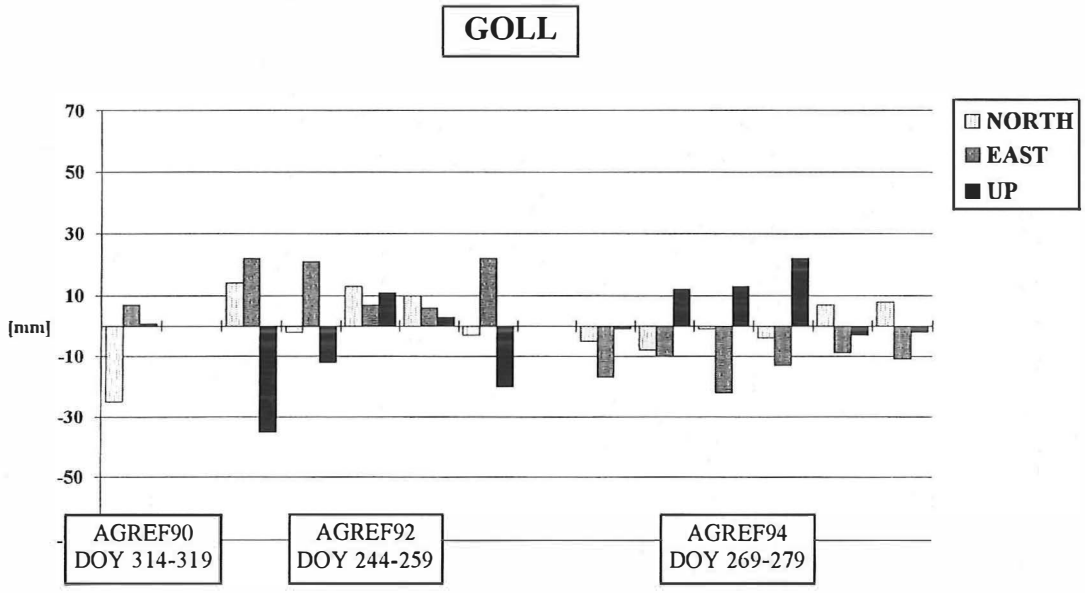


*Fig. 3 : AGREF Session Differences (Representative Example)*

$\pm 1$ cm and only 27% horizontal r.m.s. between $\pm 1$ cm and $\pm 2$ cm, leaving 4% with unsufficient horizontal accuracy.

Figure 2 shows a bad example, the site GRMS. During 1990 to 1993 unstable horizontal components are joined by considerable height differences. The earlier data did not allow for reasonable tropospheric zenith delay estimations, which proved fatal for this point with an altitude of 2300 meters. Since 1994 the horizontal components remained stable, the height still showing some offshots of more than three centimeters. During 1995 (not shown in the figure) the situation improved to a resulting maximum height difference of below two centimeters.

| STATION | RMS[MM] | | | | STATION | RMS[MM] | | | |
|---|---|---|---|---|---|---|---|---|---|
| | X | Y | Z | | | X | Y | Z | |
| AGGS | 0 | 0 | 2 | 1) | GSST | 7 | 1 | 9 | |
| ALTF | 4 | 6 | 23 | | GUBG | 3 | 0 | 1 | 1) |
| ARTA | 4 | 3 | 8 | | GUES | 20 | 9 | 1 | |
| ASTN | 672 | 848 | 1090 | 2) | GURS | 18 | 11 | 9 | |
| BALE | 9 | 3 | 11 | | HAID | 4 | 5 | 5 | |
| BASO | 4 | 2 | 5 | | HEMB | 7 | 0 | 1 | |
| BILH | 13 | 4 | 3 | | HFLK | 4 | 1 | 3 | |
| BRBG | 69 | 18 | 77 | 1) | HKAR | 12 | 0 | 12 | |
| BRSK | 19 | 7 | 15 | | HOLL | 2 | 4 | 7 | 1) |
| BUKO | 39 | 6 | 4 | | HOPY | 5 | 3 | 7 | |
| BZRG | 3 | 2 | 3 | | HOWZ | 5 | 8 | 27 | |
| CDRP | 1 | 1 | 4 | | HSHN | 3 | 5 | 15 | 1) |
| CMPL | 8 | 1 | 8 | | HUST | 5 | 3 | 1 | |
| CNBL | 3 | 1 | 4 | | HUTB | 6 | 2 | 6 | |
| CNVA | 1 | 0 | 0 | | HUTS | 6 | 7 | 8 | 1) |
| DAST | 11 | 7 | 5 | | HZBG | 25 | 9 | 27 | 1) |
| DMBL | 4 | 2 | 4 | | JOZE | 3 | 1 | 3 | |
| EDLW | 8 | 3 | 3 | | KMNK | 1 | 0 | 0 | |
| ERFH | 17 | 13 | 14 | | KOES | 5 | 6 | 6 | |
| ERZK | 5 | 7 | 5 | | KORA | 2 | 1 | 1 | |
| FLAT | 2 | 8 | 10 | | KOVK | 4 | 5 | 2 | |
| FLEX | 4 | 8 | 8 | | KRAH | 4 | 1 | 3 | 2) |
| FORC | 7 | 2 | 0 | | KRAH94 | 3 | 0 | 0 | 2) |
| FRAU | 66 | 70 | 36 | | KRGO | 18 | 8 | 19 | |
| FRBS | 25 | 8 | 2 | | KUCE | 4 | 2 | 4 | |
| GABL | 1 | 9 | 4 | | KULM | 9 | 9 | 9 | |
| GERL | 3 | 3 | 2 | 2) | LEIB | 4 | 0 | 14 | |
| GERP | 7 | 0 | 0 | 2) | LEND | 16 | 9 | 15 | |
| GOLA | 6 | 4 | 11 | | LJUB | 5 | 2 | 2 | |
| GOLL | 4 | 3 | 3 | | LOIB | 0 | 0 | 1 | |
| GRAZ | 3 | 1 | 3 | | LOKA | 10 | 7 | 10 | |
| GRDO | 5 | 3 | 0 | | LUNZ | 19 | 5 | 21 | 1) |
| GRMS | 5 | 2 | 5 | | | | | | |

| STATION | RMS[MM] | | | | STATION | RMS[MM] | | | |
|---|---|---|---|---|---|---|---|---|---|
| | X | Y | Z | | | X | Y | Z | |
| MAGD | 4 | 0 | 12 | | ROSF | 12 | 15 | 25 | |
| MALI | 2 | 1 | 2 | 2) | SEBS | 1 | 1 | 0 | |
| MALI92 | 1 | 13 | 2 | 2) | SEGO | 0 | 0 | 2 | |
| MATE | 5 | 3 | 5 | | SEXT | 20 | 7 | 3 | |
| MAYB | 5 | 2 | 7 | | SLAG | 7 | 1 | 8 | 1) |
| MEDI | 624 | 122 | 629 | 2) | SNBG | 16 | 17 | 25 | 1) |
| MOAH | 17 | 9 | 7 | | SNEZ | 10 | 7 | 8 | |
| MONT | 10 | 7 | 3 | | SOBO | 8 | 2 | 7 | |
| MRTV | 29 | 12 | 6 | | SOLI | 5 | 2 | 2 | |
| MRZL | 5 | 5 | 4 | | STAL | 12 | 9 | 3 | |
| NEDJ | 2 | 4 | 13 | | TEIA | 10 | 5 | 11 | |
| NEVE | 1 | 3 | 4 | | TILL | 4 | 6 | 3 | |
| NOSL | 23 | 10 | 10 | | TIRK | 1 | 3 | 3 | |
| OBBD | 6 | 2 | 4 | | TMVO | 1 | 1 | 1 | |
| OBGL | 1 | 7 | 11 | | TPLZ | 3 | 3 | 6 | |
| OBWG | 7 | 12 | 1 | | TREH | 2 | 1 | 4 | |
| OGDF | 20 | 2 | 17 | 1) | TUHO | 15 | 2 | 10 | |
| OSWA | 2 | 2 | 2 | | UCKA | 42 | 16 | 53 | |
| PALM | 3 | 2 | 4 | | UMAS | 19 | 14 | 20 | |
| PARA | 1 | 0 | 2 | | UPAD | 3 | 1 | 3 | |
| PFAN | 3 | 4 | 3 | | VARA | 8 | 5 | 2 | |
| PLAN | 4 | 3 | 4 | | VDBG | 4 | 6 | 2 | |
| POLK | 44 | 31 | 48 | | VEKO | 17 | 2 | 2 | |
| PSTJ | 3 | 2 | 0 | | VELI | 24 | 3 | 16 | |
| PULA | 3 | 3 | 7 | | VILA | 1 | 1 | 3 | |
| RADB | 12 | 10 | 21 | | WAMZ | 18 | 6 | 8 | 1) |
| RADO | 7 | 7 | 1 | | WANS | 7 | 12 | 8 | |
| RADS | 6 | 1 | 1 | | WETT | 2 | 2 | 4 | |
| RBNC | 2 | 2 | 1 | | ZAGR | 3 | 4 | 5 | |
| RETZ | 20 | 3 | 14 | 1) | ZGLA | 3 | 5 | 6 | |
| REVI | 14 | 6 | 32 | | ZIMM | 2 | 3 | 2 | |
| RIEG | 7 | 8 | 10 | | ZIRK | 9 | 19 | 13 | |

1) Station values from Helmert Transformation (no external check)
2) Eccenter Determination Pending

*Fig. 4 : AGREF Stations : RMS of Mean Values X,Y,Z (ITRF92)*

Figure 3 presents the normal case (except the abundance of sessions) at the site GOLL. The differences are much less, but still, until 1994, all components show an unstable behaviour.

Figure 4 gives an overview of the accuracy of AGREF based on data up to end of 1994. Gross errors have been omitted, where possible. Considerable improvements have been attained in some regions since that time. It seems quite logical that each forthcoming well designed campaign may improve the values of some points.

## 5. Conclusions

The coordinates of AGREF are available now, but yet still unpublished. The horizontal components show a repeatability of below 10 mm with an r.m.s. of the mean tending well below 5 mm. The height can now repeated within 20 mm, the r.m.s. of the mean already remaining below 10 mm. Only points with occupations older than 1994 show worse accuracies. Therefore, the results of AGREF can now be used for several objectives.

AGREF provides a pretty good national representation of the international reference frame. It can be used for purposes of national surveying very well. It also can support geoid computations, but still an improvement in height determination would be desirable. This is even more demanding for geodynamic investigations. Having small tectonic movements in Austria the present accuracy will be the minimum for their fast and precise determination.

The next targets should be the replacements of older results by more precise ones. Additionally, the combination of measured values of the troposphere with its conventional estimation should be investigated to improve the determination of the height component.

**References:**

[1] *G. Stangl, Hofmann-Wellenhof B., Pesec P., Sünkel, H.:* Austrian GPS Reference Network – Concept, Realization, and First Results. XX General Assembly of IUGG in Vienna, Austria, August 11–24, 1991.

*Adresses of the authors:*

Dipl.-Ing. Dr. Erhard Erker, Abteilung K2, Bundesamt für Eich- und Vermessungswesen, Schiffamtsgasse 1-3, A-1025 Wien.

Mag. Dipl.-Ing. Günter Stangl, Abteilung K2, Bundesamt für Eich- und Vermessungswesen, Lustbühelstraße 46, A-8042 Graz.

Dr. Peter Pesec, o.Univ.-Prof. Dipl.-Ing. Dr. Hans Sünkel, Abteilung Satellitengeodäsie, Institut für Weltraumforschung der ÖAW, Lustbühelstraße 46, A-8042 Graz.

# Veranstaltungskalender

**Datenqualität und Metainformation in Geo-Informationssystemen**
**7.–8. Oktober 1996 in Rostock**
*Informationen:* Institut für Geodäsie und Geoinformatik, Fachbereich Landeskultur und Umweltschutz, Universität Rostock, Justs-von-Liebig-Weg 6, 18051 Rostock, Fax: 0381/4982188

**33. Sitzung der Arbeitsgruppe „Automation in der Kartographie"**
**8.–9. Oktober 1996 in Bonn-Bad Godesberg, Landesvermessungsamt Nordrhein-Westfalen**

**SYMPOSIUM ÜBER GEOGRAPHISCHE NAMEN**
**10. Oktober 1996 in Wien**
*Informationen:* Österreichisches Statistisches Zentralamt, Hintere Zollamtstraße 2b, A-1033 Wien, Tel.: 0043/1/71128/7393, Fax: 0043/1/71128/7088.

**VI National Congress on Topography and Cartography**
**14.–18. Oktober 1996 in Madrid, Spanien**
*Informationen:* Organising Committee TOP-CART '96, Avda. Reina Victoria, 66, 2C, 28003 Madrid, Spanien, Tel.: 34 (1) 553 8965, Fax.: 34 (1) 533 4632.

**GIS/LIS FOR SUSTAINABLE DEVELOPMENT GIS/LIS AND THE FUTURE**
**FIG Commission 3**
**28.–30. Oktober 1996 in Kopenhagen, Dänemark**
*Informationen:* FIG-COMMISSION 3, Jes Ryttersgaard, National Survey and Cadastre, Denmark, Bjerggade 6, DK 6200 Aabenraa, Dänemark

**MIS/UDMS '96**
**2nd International Conference on Municipal Information Systems and Urban Data Management**
**18.–21. November 1996 in Prag, Tschechische Republik**
*Informationen:* Secretariat of MIS/UDMS '96, Institut městské informatlky hl. M. Prahy, Zatecka 2, 11001 Praha 1, Tschechische Republik, Tel.: +42 2 24485201, +42 2 24485301, Fax: +42 2 2481 1902, E-Mail: pragimlp@imip.anst.cz

**Remote Topographic Mapping for Geoscience**
**16.–17. Dezember 1996 in Nottingham, England**
*Informationen:* Dr. S.H. Marsh, British Geological Survey, Keyworth, Nottingham, NG12 5GG, UK, Tel.: + 44

(0) 115 936 3452, Fax: + 44 (0) 115 936 3474, E-mail: s.marsh@bgs.ac.uk

**9. Internationale Geodätische Woche**
**16.–22. Februar 1997 in Obergurgl, Tirol**
*Informationen:* Institut für Geodäsie der Universität Innsbruck, Technikerstraße 13, A-6020 Innsbruck, Tel. +43 512 507 6751, Fax +43 512 507 2910.

**JEC'97 – Joint European Conference and Exhibition on Geographic Information**
**15.–18. April 1997 in Wien**
*Informationen:* Dipl.-Ing. Erich Wilmersdorf, Magistrat der Stadt Wien, MA 14 ADV, Grafische Datenverarbeitung, Rathausstraße 1, A-1082 Wien, Tel.: +43 222 4000/91301, Fax: +43 222 4000/7141, E-Mail: wil@adv.magwien.gv.at

**The 64th FIG PC Meeting and INTERNATIONAL SYMPOSIUM**
**11.–16. Mai 1997 in Singapore**
*Informationen:* Singapore Institute of Surveyors & Valuers, 20 Maxwell Road #10-09B Maxwell House, Singapore 069113, Tel.: (065) 222-3030, Fax: (065) 225-2453.

**geotechnica**
**13.–16. Mai 1997 in Kölln**
*Informationen:* Tel.: 49 (221) 8210

**6. Österreichischer Geodätentag 1997**
**4.–7. Juni 1997 in Villach**
*Informationen:* Örtlicher Vorbereitungsausschuß (ÖVA), Dipl.-Ing. Andreas Kubec, A-9500 Villach, Jakob Ghon Allee 4, Tel. (04242) 37 466-63, Fax-73.

**ICC '97 – 18th International Cartographic Conference**
**22.–28. Juni 1997 Stockholm, Schweden**
*Informationen:* Swedish Cartographic Society, c/o National Land Survey, S-801 82 Gävle, Schweden, Tel.: 46 (26) 153 000, Fax.: 46 (26) 653 160.

**9. Symposium für Angewandte Geographische Informationsverarbeitung – AGIT '97**
**2.–4. Juli 1997 in Salzburg**
*Informationen:* AGIT'97 – Zentrum für Geographische Informationsverarbeitung am Institut für Geographie der Universität Salzburg (ZGIS), Hellbrunnerstrasse 34, A-5020 Salzburg, Tel.: +43 (0) 662 8044-5224, Fax: DW-525, E-Mail: agit@geo.sbg.ac.at, WWW: http://www.sbg.ac.at/geo/agit/agit.htm

**IAMAS/IAPSO 1997**
**1.–9. Juli 1997 in Melbourne, Australien**
*Informationen:* IAMAS/IAPSO Secretariat Convention Network, 224 Rouse Street, Port Melbourne, Victoria 3207, Australien, Tel.: +61 3 9646 4122, Fax: + 61 3 9646 7737, E-mail: mscarlett@peg.apc.org

**46. Photogrammetrische Woche**
**22.–26. September 1997 in Stuttgart**
*Informationen:* Institut für Photogrammetrie der Universität Stuttgart, Keplerstraße 11, D-70174 Stuttgart, Tel. 49711/121-3201, Fax 49711/121-3297.

**Optical 3-D Measurement Techniques**
**29. September bis 2. Oktober 1997 in Zürich, Schweiz**
*Informationen:* Institut für Geodäsie und Photogrammetrie, ETH Hönggerberg, CH-8093 Zürich, Schweiz, Tel.: +41-1-633 31 57, Fax: +41-1-633 11 01, E-mail: steinbrueckner@geod.ethz.ch

**CIPA INTERNATIONAL SYMPOSIUM 1997**
**1.–3. Oktober 1997 in Göteborg, Schweden**
*Informationen:* Institute of Conservation, Göteborg University, Bastionsplatsen 2, S-411 08 Göteborg, Schweden, Tel. +46 31 7734700, Fax: +46 31 7734703, Email: conservation@icug.gu.se

*Selbstverständlich steht für alle Mitglieder auch das Sekretariat der Österreichischen Gesellschaft für Vermessung und Geoinformation jederzeit für Auskünfte und nähere Informationen zu den angeführten Veranstaltungen, soweit vorhanden, zur Verfügung.*

# Redaktionsschluß

für die nächste Ausgabe der VGI (Heft 4/1996) ist

# Dienstag, der 12. November 1996

## Impressum

**Herausgeber und Medieninhaber:** Österreichische Gesellschaft für Vermessung und Geoinformation (ÖVG), Austrian Society for Surveying and Geoinformation (ASG), Schiffamtsgasse 1-3, A-1025 Wien zur Gänze. Bankverbindung: Österreichische Postsparkasse BLZ 60000, Kontonummer PSK 1190933.

**Präsident der Gesellschaft:** Dipl.-Ing. August Hochwartner, Schiffamtsgasse 1-3, A-1025 Wien, Tel. (0222) 21176-3603, Fax (0222) 2161062.

**Sekretariat der Gesellschaft:** Dipl.-Ing. Gert Steinkellner, Schiffamtsgasse 1-3, A-1025 Wien, Tel. (0222) 21176-4604, Fax (0222) 2161062.

**Schriftleitung:** Dipl.-Ing. Reinhard Gissing, Schiffamtsgasse 1-3, A-1025 Wien, Tel. (0222) 21176-3401, Fax (0222) 2161062, Dipl.-Ing. Wolfgang Gold, Schiffamtsgasse 1-3, A-1025 Wien, Tel. (0222)21176-2315, Fax (0222) 2161062, Dipl.-Ing. Bernhard Jüptner, Krotenthallergasse 3, 1080 Wien, Tel. (0222) 40146-432, Fax (0222) 4069992.

**Redaktionsbeirat:** O.Univ.-Prof. Dr. K. Bretterbauer, o.Univ.-Prof. Dr. K. Kraus, o.Univ.-Prof. Dr. W. Pillewizer, alle Technische Universität Wien, Gußhausstraße 27-29, 1040 Wien, o.Univ.-Prof. Dr. G. Brandstätter, o.Univ.-Prof. Dr. H. Moritz, alle Technische Universität Graz, Steyrer Gasse 30, 8010 Graz, HR Dr. J. Bernhard, BEV, Krotenthallergasse 3, 1080 Wien, Dipl.-Ing. M. Eckharter, Friedrichstraße 6, 1010 Wien, HR Dipl.-Ing. K. Haas, Lothringerstraße 14, 1030 Wien, Präsident i.R. Dipl.-Ing. F. Hrbek, BEV, Schiffamtsgasse 1-3, 1025 Wien.

**Manuskripte:** Bitte direkt an die Schriftleitung senden. Es wird dringend ersucht, alle Beiträge in digitaler Form auf Diskette zu übersenden. Genaue Angaben über die Form der Abfassung des Textteiles sowie der Abbildungen (Autoren-Richtlinien) können bei der Schriftleitung angefordert werden. Beiträge können in Deutsch oder Englisch abgefaßt sein; Hauptartikel bitte mit einer deutschsprachigen Zusammenfassung und einem englischen Abstract einsenden. Namentlich gezeichnete Beiträge geben die Meinung des Autors wieder, die sich nicht mit der des Herausgebers decken muß. Die Verantwortung für den Inhalt des einzelnen Artikels liegt daher beim Autor. Mit der Annahme des Manuskriptes sowie der Veröffentlichung geht das alleinige Recht der Vervielfältigung und Wiedergabe auf den Herausgeber über.



**Anzeigenbearbeitung und -beratung:** Dipl.-Ing. Wolfgang Gold, Schiffamtsgasse 1-3, A-1025 Wien, Tel. (0222) 21176-2315. Unterlagen über Preise und technische Details werden auf Anfrage gerne zugesendet.

**Erscheinungsweise:** Vierteljährlich in zwangloser Reihenfolge (1 Jahrgang = 4 Hefte). Auflage: 2700 Stück.

**Abonnement:** Nur jahrgangsweise möglich. Ein Abonnement gilt automatisch um ein Jahr verlängert, sofern nicht bis zum 1.12. des laufenden Jahres eine Kündigung erfolgt. Die Bearbeitung von Abonnementangelegenheiten erfolgt durch das Sekretariat. Adreßänderungen sind an das Sekretariat zu richten.

**Verkaufspreise:** Einzelheft ÖS 170.- (Inland), ÖS 190.- (Ausland), Abonnement ÖS 600.- (Inland), ÖS 700.- (Ausland); alle Preise beinhalten die Versandspesen, die für das Inland auch 10% MWSt.

**Satz und Druck:** Druckerei Berger, A-3580 Horn, Wiener Straße 80.

**Grundlegende Richtung der Zeitschrift:** Wahrnehmung und Vertretung der fachlichen Belange aller Bereiche der Vermessung und Geoinformation, der Photogrammetrie und Fernerkundung sowie Information und Weiterbildung der Mitglieder der Gesellschaft hinsichtlich dieser Fachgebiete.

# 6. Österreichischer Geodätentag '97

## VILLACH

**Vermessung ohne Grenzen**

Die

**Österreichische Gesellschaft**

für

**Vermessung und Geoinformation**

veranstaltet

**vom 4. bis 7. Juni 1997**

den

**6. Österreichischen Geodätentag 1997 in Villach.**

Unter dem Motto "Vermessung ohne Grenzen" werden u.a. Themenkreise betreffend die technischen Möglichkeiten der grenzübergreifenden Meß- und Informationstechnologie und die Öffnung der politischen sowie wirtschaftlichen Grenzen nach Süden und Osten behandelt werden.

*Informationen:*
*Örtlicher Vorbereitungsausschuß (ÖVA)*
*Dipl.-Ing. Andreas Kubec*
*A-9500 Villach, Jakob Ghon Allee 4*
*Tel.: (+43 4242) 04242 / 37 466 - 63*
*Fax.: (+43 4242) 04242 / 37 466 - 73*
*email: gt97.villach@online.edvg.co.at*